BIOKINEMATIC ANALYSIS OF HUMAN BODY

A Thesis Submitted to
the Graduate School of Engineering and Sciences of
İzmir Institute of Technology
in Partial Fulfillment of the Requirements for the Degree of

DOCTOR OF PHILOSOPHY

in Mechanical Engineering

by
Erkin GEZGİN

March 2011

İZMİR

We approve the thesis of **Erkin GEZGİN**

_____
Prof. Dr.Sc. Rasim ALİZADE
Supervisor

_____
Prof. Dr.Sc. Rafail ALİZADE
Committee Member

_____
Assist. Prof. Dr. H. Seçil ARTEM
Committee Member

_____
Assist. Prof. Dr. M. İ. Can DEDE
Committee Member

_____
Assist. Prof. Dr. Fatih Cemal CAN
Committee Member

25 March 2011

_____   _____
Prof. Dr. Metin TANOĞLU   **Prof. Dr. Durmuş Ali DEMİR**
Head of the Department of   Dean of the Graduate School of
Mechanical Engineering   Engineering and Sciences

Anyone who has never made a mistake

has never tried anything new…

<u>Albert Einstein</u>

ACKNOWLEDMENTS

ABSTRACT

BIOKINEMATIC ANALYSIS OF HUMAN BODY

This thesis concentrates on the development of rigid body geometries by using method of intersections, where simple geometric shapes representing revolute (R) and prismatic (P) joint motions are intersected by means of desired space or subspace requirements to create specific rigid body geometries in predefined octahedral fixed frame. Using the methodical approach, space and subspace motions are clearly visualized by the help of resulting geometrical entities that have physical constraints with respect to the fixed working volume. Also, this work focuses on one of the main areas of the fundamental mechanism and machine science, which is the structural synthesis of robot manipulators by inserting recurrent screws into the theory. After the transformation unit screw equations are presented, physical representations and kinematic representations of kinematic pairs with recurrent screws are given and the new universal mobility formulations for mechanisms and manipulators are introduced. Moreover the study deals with the synthesis of mechanisms by using quaternion and dual quaternion algebra to derive the objective function. Three different methods as interpolation approximation, least squares approximation and Chebyshev approximation is introduced in the function generation synthesis procedures of spherical four bar mechanism in six precision points. Separate examples are given for each section and the results are tabulated. Comparisons between the methods are also given. As an application part of the thesis, the most important elements of the human body and skeletal system is investigated by means of their kinematic structures and degrees of freedom. At the end of each section, an example is given as a mechanism or manipulator that can represent the behavior of the related element in the human body.

ÖZET

İNSAN VÜCUDUNUN BİYOKİNEMATİK ANALİZİ

Tezin ilk aşamasında, döner (R) ve doğrusal (P) mafsal hareketlerini temsil eden basit geometrik şekillerin, önceden belirlenmiş sabit hacim içerisinde özel katı cisim geometrilerinin oluşturulması için, istenen uzay ve altuzay gereksinimleri göz önüne alınarak kesiştirildiği kesişimler metoduna yoğunlaşılmıştır. Sistematik yaklaşım kullanılarak, oluşturulan sabit çalışma hacmine göre fiziksel sınırlamalara sahip geometrik cisimlerin yardımıyla uzay ve altuzay hareketleri açık olarak canlandırılmıştır. Ayrıca, bu çalışma, makinalar ve mekanizmalar bilimdalının en önemli dallarından biri olan robot manipülatörlerin yapısal sentezi konusunda çalışmalar içermektedir. Çalışma içerisinde kinematik mafsallar ve vida teorisi üzerine odaklanılmıştır. Her bir kinematik mafsalın ardışık vidalar ile hem fiziksel hem de kinematik gösterimleri verildikten sonra robot manipülatörler için yeni genel serbestlik derecesi formülü belirtilmiştir. Tezin ileriki aşamalarında "quaternion" ve "dual quaternion" cebiri kullanılarak mekanizmaların sentezlenmesi üzerine çalışılmıştır. Interpolasyon yaklaşımı, en küçük kareler yaklaşımı ve Chebyshev yaklaşımı olmak üzere üç farklı teknik kullanılarak küresel dört çubuk mekanizmasının altı dizayn noktasında fonksyon üretme sentezi yapılmış, her bölüm için farklı örnekler verilmiş ve sonuçlar tablolarda gösterilmiştir. Çalışma içerisinde kullanılan metodların karşılaştırılmaları ayrıca yapılmıştır. Tezin son bölümlerinde insan vücudu ve iskelet sisteminde bulunan önemli elemanlar kinematik yapıları ve serbestlik derecelerine göre incelenmiş, her bölümün sonunda incelenen elemanın davranışını gösterebilecek mekanizma veya manipülatör örnekleri verilmiştir.

TABLE OF CONTENTS

LIST OF FIGURES

LIST OF TABLES

CHAPTER 1

INTRODUCTION

Although the thesis title just indicates the *"Biokinematic Analysis of Human Body"*, the studies that will be introduced throughout this study are interrelated but are not solely limited to the cover name. During the following chapters, both theoretical and practical aspects will be given along with illustrations and examples on the fundamental area of mechanism and machine science, especially for the design of mechanisms and robot manipulators.

1.1. Research Statement

During the first chapters of the study different mathematical tools such as quaternion algebra, biquaternion algebra and screw theory are introduced as they are used throughout the study for various purposes. The reason behind the usage of multiple models is the fact that each of them has unique characteristics in different cases that simplifies the overall problem. For instance, quaternions can be easily used to carry out the calculations of solely rotational sequences, while the biquaternions can be used in the cases, where translational sequences exist as well as rotational ones. On the screw theory side, both rotational and translational components can be introduced in only one screw, where they can be used to represent the displacements, velocities, forces and torques in three dimensional space.

One of the important studies of this thesis concentrates on the development of rigid body geometries by using method of intersections, where simple geometric shapes representing revolute (R) and prismatic (P) joint motions are intersected by means of desired space or subspace requirements to create specific rigid body geometries in predefined octahedral fixed frame. Using the methodical approach, space and subspace motions can be clearly visualized by the help of resulting geometrical entities that have physical constraints with respect to the fixed working volume. Also, using the same idea, one degrees of freedom (DoF) mechanism with variable general constraint one is created and illustrated along with its design procedure for further references.

Afterwards, the thesis focuses on one of the main areas of the fundamental mechanism and machine science, which is the structural synthesis of robot manipulators by inserting recurrent screws, screws that have directions intersected one another in series, into the theory and focusing on the smallest elements of the robot manipulators, kinematic pairs. Brief information about the screws along with illustrations is presented. Physical representations and kinematic representations of both lower and higher kinematic pairs with recurrent screws are directly given. New universal mobility formulations are introduced for both kinematic pairs and robot manipulators. Examples are given throughout the related chapters to clarify the idea behind the subject and the method is applied to the existing robot manipulators in previous structural synthesis studies of the same author.

Also the thesis deals with the function generation synthesis of spherical four bar mechanism for the six precision points in order to design six construction parameters $\varphi_0, \psi_0, \alpha_1, \alpha_2, \alpha_3$, and α_4. Quaternion algebra is used as a mathematical tool to derive the objective function. Three different methods as interpolation approximation, least squares approximation and Chebyshev approximation are used for synthesis procedure. Separate examples are given for each section and the results are tabulated. Comparisons between the used methods are given at the end of the related chapter.

Another interesting and challenging point in the study is using dual quaternions in the process of kinematic synthesis to compute the objective function of mechanisms that are desired to be synthesized. Before introducing the algebra, a mixed method of quaternion and vector algebra is used to show the limitations of quaternions and to verify the results of the dual quaternion algebra in the synthesis procedure. One degree of freedom mechanism from subspace five is used as an example and RP serial robot manipulator is used for the calculations. A new approach is proposed in the synthesis of subspace five mechanism by integrating both function generation and body guidance synthesis.

Following the theoretically rich sections, as its title clearly implies, this thesis starts to investigate the kinematics of human body. All the important sections of the human skeletal system and body including human eyes, arm, hand, leg, foot, skull and vertebral column are introduced in terms of their kinematical structure and DoF with their possible mechanism or manipulator counterparts. The importance of the study is to extract all possible information about the biokinematics of human body into one

reference that can be used for further studies in the area of medicine to design advanced prosthetics and robotics to design advanced humanoid robots for various tasks.

1.2. Literature Survey

Quaternions, and biquaternions are being used continuously in the area of computational kinematics. First application of quaternions is found in the description of motion of the rigid body (Hamilton, 1866). The topological geometry in spatial kinematics is discussed by Porteous (1921), where the representation of spherical displacements and motions are described by the rotation group of unit quaternions. Nixravesh et al. (1985) introduced the method which is based on a sequence of matrix computation, and identities for relating a representation of spherical motion with their corresponding velocity and acceleration vectors. Angeles (1988) introduced the theory of vector and scalar invariants of a rotation tensor as a function of time of a spherical motion. Chevallier (1991) discussed about dual quaternions in kinematics. Collins et al. (1998) studied the workspace and singular configurations of the 3-RPR parallel manipulator, where they also used quaternions. Larochelle (2000) used planar quaternions to create synthesis equations for planar robots, and created a virtual reality environment that could promote the design of spherical manipulators. Martinez et al. (2000) presented quaternion operators for describing the position, angular velocity and angular acceleration for a spherical motion of a rigid body with respect to the reference frame. McCarthy et al. (2006) used Clifford algebra exponentials in the kinematic synthesis. Dai (2006) reviewed theoretical development of rigid body displacements, where he also mentions about quaternions and biquaternions. Roy et al. (2008) used quaternion interpolation in the finite element approximation of geometrically exact beam. Zupan (2009) tried to implement rotational quaternions into the geometrically exact three dimensional beam theory. In the study, novel finite element formulation was proposed. Pennestri et al. (2009) used dual quaternions for the analysis of rigid body motions and tries to apply them to the kinematic modeling of the human joints. Cellodoni et al. (2010) investigated an elastic model of rod and carried out the group of rotations by using quaternions. Banavar et al. (2010) developed an analytical model of a novel spherical robot by using quaternion algebra. Liao et al. (2010) used biquaternions in the inverse kinematic analysis of general 6R serial manipulators.

In accordance with the mathematical tools, investigation of rigid body motions in space and constrained subspaces is another fundamental tool for designing different new kinds of mechanisms in the area of mechanism and machine science. Although there are not so many studies that are solely concentrated on rigid body movements and subspaces, the idea is indirectly found in the works that involve mechanism designs and mobility calculation criterions.

Herve (1999) introduced the lie group of rigid body displacements as an important tool for mechanism design. Gogu (2005) proposed a new mobility calculation formulation for parallel mechanisms with elementary legs. In his formulation, the independent motion parameters of the platform and the legs must be observed with respect to the fixed frame. Zhao et al. (2006) pointed out in the beginning of their study that, determination of the independent motions of the end effectors is the main problem in mechanism analysis. Müller (2008) mentioned in one part of his study about the mobility criteria that are based on motion groups, where the main idea is to identify the group of rigid body motions. Alizade et al. (2007) presented the history of structural formulations, where space or subspace number λ was introduced in many works of different authors. Also in their papers (2004-2008), they proposed new mobility and end effector motion formulations by taking into account subspace of the platforms, leg loops, branch loops and legs. Using these formulations along with the design procedures, they created different kinds of manipulators. Throughout the presented studies in the literature, it is apparent that the visualization of the end effector motions and determination of the space or subspace number λ have vital importance. Multiple kinds of manipulators are designed or analyzed after these sequences are fulfilled.

During the last century, research conducted in the area of structural synthesis of robot manipulators have continuously increased. Due to this rapid increase in research, many investigations on the subject are discussed in literature by using different tools and methodologies. Among those investigations, new mobility formulations as well as new procedures to use or follow in the structural design of robot manipulators are proposed. Thanks to its versatility, screw theory can be classified as one of the most prominent tools used in the mentioned researches.

In their studies Huang and Li (2002-2003) proposed a screw theory based method for the type synthesis of parallel manipulators. A new method is introduced to find constraints given to the end effector from limbs by using reciprocal screws and the motion of the platform is decided. Three-, four-, and five-DoF non-constrained and

overconstrained manipulators are also revealed in their researches. Similarly, by using theory of reciprocal screws, Fang and Tsai (2002-2004) investigated four-, and five-DoF parallel manipulators with identical limb structures and three-DoF translational and rotational non-constrained and overconstrained manipulators. Kong and Gosselin (2001-2007) proposed a way for the type synthesis of parallel manipulators that is composed of screw theory and virtual chain approach. Jin et al. (2004) investigated the structural synthesis of parallel manipulators based on the selective actuation by using screw algebra. His study resulted in developing three-DoF spherical motions, three-DoF translational motions, three-DoF hybrid motions and six-DoF spatial motions depending on the types of the actuation.

Being the main components of mechanisms and robot manipulators, kinematic pairs have also vital importance in structural synthesis. Designers should decide and select which kinematic pairs to be used from a variety of choices in their designs with respect to the given constraints, such as workspace limitations, subspace conditions, and mobility requirements. Many researchers are used kinematic pairs in their proposed mobility calculations and structural synthesis procedures. Those procedures can be examined briefly in the detailed review about kinematic structure of mechanisms that has been introduced by Mruthyunjaya (2003), and in the studies of Alizade et al. (2007) that have reviewed the history of DoF analysis and structural synthesis formulations in a table including the names of authors, publication dates and commentaries. The updated table is presented in this study and can be seen in Table 1.1.

As additional information, in the design process of mechanisms, the importance of the kinematic synthesis problem cannot be neglected. After the selection of the mechanism that will be used for a specific task, its construction parameters must be designed with respect to the given or desired constraint conditions. There are different types of synthesis for different tasks. Function generation is one kind of synthesis, where mentioned constraint conditions are related with some function between the input and output links. It is important to note that the whole calculation process can become complicated especially when the number of design parameters is increased. Thus, different methods throughout the literature have been developed and examined in various mechanisms to overcome this difficulty.

Table 1.1. Formulas for structural analysis and synthesis (revisited).

	Equations	*Authors*	*Commentary*
1	$L = j - l + 1$ *l is the* number of links; j is the number of joints	L. Euler, 1752	L is the number of independent loops;
2	$3l_m - 2j - 1 = 0$ $0 < j - j_m < 1 + \frac{1}{2}l$ $j_m > l - 3 \qquad l_m = n = l - 1$	P. L. Chebyshev, 1869	Eq. for planar mech. with 1 DoF j_m is the number of moving joints l_m = n is the number of moving links
3	$3l - 2j - 4 = 0$ $j = n - 1$	J. J. Sylvester, 1874	Eq. for planar mech. with 1 DoF
4	a) $M = 3l - 2j - 3$ b) $3l - 2j - 4 + q = 0$ c) $2l - j - 3 = 0$ d) $3l - 2j - 4 + q - C = 0$ e) $5H - 6l + 7 = 0$ or $M = 6(l-1) - 5p_1$ q is the number of overclosing constraints p_1 is the one mobility joints C is the number of cam pairs H is the number of helical joints	M. Grübler, 1883, 1885	M is mobility of mechanisms. DoF depends from the rank of functional determinant (r=3, 2) a) DoF for planar mech. b) Eq. for kinematic chains with revolute R and prismatic P pairs c) Eq. for plane mech. just with prismatic P pairs d) Eq. for kinematic chains with revolute, prismatic and cam pairs e) DoF of spatial mech. with helical joints
5	a) $l - (\lambda - 1)(\nu + 1) = 2$ b) $l + q + \sum K_u - (\lambda - 1)(\nu + 1) = 2$ c) $M = (l-1) + \sum f_i - j - 5L + q$ $l = 5\nu + 7, \quad \lambda = 6, \quad \nu = L - 1,$ $\sum K_u = j_p - 1$ j_p is the passive mobilities in the joints f_i is the mobility of kinematic pairs	P.O. Somov, 1887	a) Eq. for plane (λ=3) and spatial (λ=6) mech. (M=1) b) Eq. for plane and spatial mech. (M=1) c) Somov's universal structural formula λ is the number of independent parameters describing the position of rigid body (general constraint parameter)
6	a) $\lambda(l-1) - S = 1$ $S = \sum (\lambda - i) f_i$ is the total number of independent joint constraints b) $\sum f_i - \lambda L = 1$ c) $\lambda(j - L) - S = 1$	Kh. I. Gokhman, 1889	a) Eq. for plane and spatial mech. (M=1) b) Loop mobility criterion (M=1) c) Eq for mech. (M=1) Eqs. (a) and (c) gives Euler's equation
7	$M = 6n - S$	G. Koeings, 1905	Mobility Eq. for spatial mech. (similar to Gokhman Eq.)
8	$3n - 2j = 0$	L. V. Assur, 1916	Eq. for simple structural groups
9	$(\lambda - 1)S_s - \lambda l + (\lambda + 1) = 0$ $M = \lambda n - (\lambda - 1)S_s$ S_s is the number of screw pairs	R. Muller, 1920	Eq. for kinematic chains with screw pairs (Similar to M. Grubler Eq.)

(cont. on next page)

Table 1.1. (cont.)

	Equations	*Authors*	*Commentary*
10	$$M = 6(l-1) - \sum_{i=1}^{5} i p_i + q - n_v$$ p_i is the kinematic pairs with i class i = number of joint constraint	A. P. Malushev, 1923	Universal Somov-Malushev's mobility Eq. n_v is the number of links with variable length
11	$$M = \lambda(l-j-1) + \sum_{i=1}^{j} f_i$$ $$M = \lambda(l-1) + \sum_{i=1}^{j} (\lambda - i) f_i$$	K. Kutzbach, 1929	Other form of universal mobility Eq.
12	$$M = 3(l-1) - 2(P+R+K) - p_2$$ P is the number of prismatic pairs R is the number of revolute pairs	N. I. Kolchin, 1932-1934	Structural formula for planar mechanisms. K is the number of higher pairs with pure roll or pure slippage p_2 is the number of higher pair with rolling and slipping
13	$$M = 6n - \sum_{i=1}^{j} S_j + \sum_{K=1}^{L} d_K + q$$ $d_K = 6 - \lambda_K$ is the family of the elementary closed loop or the number of independent constraints in the loops	I. I. Artobolevskii, 1935	Other form of universal mobility Eq. First time in mobility Eq., it is used variable general constraint as variable number of independent close loops family. λ_K is the variable general constraint
14	$$M = \lambda n - \sum_{i=1}^{\lambda-1} (\lambda - i) p_i + q$$ $\lambda = 2, ..., 6$	V. V. Dobrovolskii, 1939	Other form of universal structural formula
15	$a) M = \sum_{i} i p_i - r$ $b) M = \sum_{i} i p_i - \sum_{\lambda} \lambda L_\lambda$ $i = 1, ..., 5 \quad \lambda = 2, ..., 6$ $c) L = j - n$	U. F. Moroshkin, 1958	a) Structural Eq. of system with the integrable joining b) Eq. of the DoF with variable general constraint c) Number of independent close loops $r = \lambda$ is the rank of linear independent loop
16	$$M = \sum_{i=1}^{j} f_i - \sum_{K=1}^{L} r_K - j_p$$ $\sum_{i=1}^{j} f_i$ is the total number DoF of joints with revolute, prismatic and helical joints;	R. Voinea and M. Atanasiu, 1959	Mobility Eq of a complex mechanisms $1 \le r_K \le 6$ is the rank of screw system
17	$L = j - l + 1$	B. Paul, 1960	Using formula #1, it was created topological condition of criterion for the degree of constraint of plane kinematic chains
18	$$M = \sum_{i=1}^{j} f_i - 6(j - l + 1)$$	W. Rössner, 1961	The mobility Eq. taking into consideration Euler's formula # 1

(cont. on next page)

7

Table 1.1. (cont.)

	Equations	*Authors*	*Commentary*
19	$M = \sum\limits_{i=1}^{j} f_i - 6(j-l+1) - 3(j-l+1)$	H. Boden, 1962	Mobility Eq., consisting from the planar and the spatial loops
20	$a)\ M = \sum\limits_{i=1}^{j} f_i - 6L + q$ $b)\ M = \sum\limits_{i=1}^{j} f_i - 3L + q$ $c)\ M = 2(l-1) - j + q$ $d)\ M = j - 2L + q$	O. G. Ozol, 1962	a), b), and c) mobility Eq.s for variable general constraint, as λ=6, 3, 2 with excessive constraints d) mobility Eq. for cylindirical mechanisms (λ=2)
21	$M = F - r$ F is the relative freedom between links	K. J. Waldron, 1966	Mobility Eq of closed loop r is the order of the equivalent screw system of the closed loop
22	$M = \sum\limits_{i=r+1}^{5} (6-i)p_i - (6-d)L$	N. Manolescu, 1968	Mobility Eq. with the parameter of the family of the elementary closed loop.
23	$M = 6(l-1) - \sum\limits_{i=1}^{5}(6-i)f_i + \sum\limits_{K=1}^{L} d_K +$ $+ \sum q - \sum j_p$	C. Bagci, 1971	Mobility Eq. to calculate DoF of motion in a mechanism similar to Eq. # 13 by adding parameter j_p
24	$M = (6 - d_a)(l-1) - \sum\limits_{i=1}^{5}(i - d_a)p_i$	P. Antonescu, 1973	Mobility formulas with different values for the motion coefficient λ (formula #14)
25	$a)\ M = \sum\limits_{i=1}^{E} m_i - \sum\limits_{K=1}^{L} \lambda_K$ $b)\ M = \sum\limits_{i=1}^{j} f_i - \sum\limits_{K=1}^{L} \lambda_K$ $c)\ M = \sum\limits_{i=1}^{E} m_i - \lambda L$ $d)\ M = \sum\limits_{i=1}^{j} f_i - \lambda L$ $\lambda = 2, 3, 4, 5, 6$ E is the total number of independent displacement variable m_i is the relative displacements of the joints f_i is the relative joint motion when m_i correspond in 1:1 with DoF in joints	F. Freudenstein, R. I. Alizade, 1975	Mobility Eq.s without exception a) and b) mobility Eq.s are used for mechanisms which contain mixed independent loops with variable general constraint. c) and d) Mobility equations of mechanisms with the same number of independent, scalar loop closure equations in each independent loop. λ_K is the number of independent, scalar, differential loop closure equations λ is the DoF of space where the mechanism operates
26	$M = \lambda(l - j - 1) + \sum\limits_{i=1}^{j} f_i$	K. H. Hunt, 1978	Mobility Eq. coming from Eq. 25d using Eq 1

(cont. on next page)

Table 1.1. (cont.)

	Equations	*Authors*	*Commentary*
27	$$M = \lambda(l-1) - \sum_{i=1}^{j}(\lambda - f_i)$$	J. M. Herve, 1978	Mobility formula based on the algebraic group structure of the displacement set
28	$$M = \sum \lambda_K - \sum_{K=1}^{L-1}\sum_{j=K+1}^{L} F_{Kj}$$ F_{Kj} is the mobility of the joints that is common between any two loops K and j, and the mobility of the joints in the L loops can be counted once or twice	A. Gronowicz, 1981	Mobility Eq. for multi loop kinematic chains
29	$$M = \sum_{i=1}^{j} f_i - r$$	T. H. Davies, 1981	Mobility equations similar to Eq. # 15a r is the rank of the coefficient matrix of constraint equations
30	$$M = \sum_{K=1}^{L}\lambda_K - \sum_{K=1}^{L-1}\sum_{j=K+1}^{L} F_{Kj} + \sum_{i=1}^{N_1}\frac{1}{2}(\tilde{n}_i^2 + \tilde{n}_i - 2)F_{\tilde{n}i} +$$ $$+ \sum_{i=1}^{N_2}\frac{1}{2}(n_i^2 - 3n_i + 2)F_{ni}$$	V. P. Agrawal, J. S. Rao, 1987	Mobility Eq. to any general mechanism with constant or variable general constraints with simple or multiple joints N_1, N_2 is the total number of internal and external multiple joints respectively $\tilde{n}_i$, $F_{\tilde{n}i}$; n_i, F_{ni} is the number of links and the mobility of simple joints forming the i th internal and external multiple joints respectively.
31	*a)* $M = \sum_{i=1}^{j} f_i^e - \sum_{K=1}^{L} \lambda_K^e$ *b)* $M = \sum_{K=1}^{L} \lambda_K - \sum_{j}(L_{comj} - 1)f_{comj}^e$ L_{comj} is the number of loops with common joint j f_{comj}^e is the active degree of mobility of the j th common joint	F. Dudita, D. Diaconescu, 1987	Eq. of a elementary or a complex (multi loop) mechanisms f_i^e is the active mobilities in i th joint λ_K^e is the dimension of the active motion space
32	$M = nullity(J)$ $nullity(J) = d(v) - r(J)$ J is the Jacobian matrix; r(J) is the rank of the Jacobin matrix; d(v) is the finite dimensional vector space v	J. Angeles, C. Gosselin, 1988	The mobility Eq. by using the Jacobian matrix of a simple or multi loop closed kinematic chain without exception

(cont. on next page)

Table 1.1. (cont.)

	Equations	Authors	Commentary
33	a) $L = j_B - B - c_b$ b) $M = \sum\limits_{i=1}^{E} m_i - \lambda(j_B - B - c_b) + q - j_p$ c) $M = \sum\limits_{i=1}^{j} f_i - \lambda(j_B - B - c_b) + q - j_p$ d) $\sum\limits_{i=1}^{j} f_i = \lambda(j_B - B - c_b)$ B is the number of mobile platform; j_B is the total number of joints on the mobile platforms	R. I. Alizade, 1988	a) A new formula of number of independent loops b) and c) are structural formulas as a function of number of branches, platforms and sum of mobility of kinematic pairs and other parameters d) Eq. for simple structural groups (λ=6,5,4,3,2) c_b is the total number of branches between mobile platforms
34	$M = \lambda - \sum\limits_{i=1}^{c_l} (\lambda - f_i)$ $(\lambda - f_i)$ is the degree of constraint of the platform	J. M. McCarthy, 2000	Mobility Eq. of a parallel manipulator
35	$M = (6-d)(l-j-1) + \sum\limits_{i=1}^{j} f_i + q$	Z. Huang, Q .C. Li, 2003	Structural formula for parallel mechanisms
36	a) $M = \sum\limits_{i=1}^{j} f_i - \lambda(c - B)$ b) $\sum\limits_{i=1}^{j} f_i = \lambda(c - B)$ c) $L = c - B$, $c = c_l + c_b$, $c_l = j_B - 2c_b$	Rasim Alizade, Cagdas Bayram, 2003	a) MobilityEq. of mechanisms b) Eq.'s for simple structural groups. c) New formula of the number of independent loops c is the sum of legs and branches, c_l is the total number of legs, connecting mobile platforms to ground
37	$M = \sum\limits_{i=1}^{j} f_i - \sum\limits_{j=1}^{l} S_j + S_p$ S_p and S_j are spatialities of mobile platform and legs respectively	Grigore Gogu, 2005	Mobility Eq. for parallel mechanisms

(cont. on next page)

Table 1.1. (cont.)

	Equations	Authors	Commentary
38	a) $M = (B-c)\lambda + \sum_{i=1}^{j} f_i + q - j_p$ b) $M = (\lambda+3) + \sum_{l=1}^{c_l}(d_l - D) + \sum_{l=1}^{c_l}(f_l - \lambda_l) + q - j_p$ $c = c_l + c_b + c_h$ D is number of dimensions of vectors in Cartesian space d_i is number of dimensions of vectors in Subspace	Rasim Alizade, Cagdas Bayram, Erkin Gezgin, 2005	a) Mobility Eq. for robotic systems with independent loops with variable general constraint b)A new structural formula of mobility loop-legs equation for parallel Cartesian platform manipulators. λ is the general constraint parameters of simple structural group c_h is the number of hinges
39	a) $M = \lambda + j_h + \sum_{L=1}^{n}(f_L - \lambda_L) + \sum_{l=1}^{c_l}(f_l - \lambda_l)$ b) $m = \lambda + j_h + c_l + \sum_{L=1}^{n}(f_L - \lambda_L) + \sum_{l=1}^{c_l}(d_l - D)$	Rasim Alizade, Fatih Cemal Can, Erkin Gezgin, 2008	Mobility (M) and motion (m) Eq. for serial parallel Euclidean robot manipulators with variable general constraints that include, several hinges, legs and branch-loops.
40	a) $M_k = \$ + s - \Gamma, \ \Gamma = T + 1$ b) $M = \$ + s - 2l - \sum_{i=1}^{l}(N_i - 2) - \sum_{j=2}^{3}(j-1)T_j - \sum_{k=1}^{L}\lambda_k$ T stands for the type number of the kinematic pair Γ is the contact origin of the kinematic pair \$ represents the total number of screws s is the number of screws with variable pitch	Rasim Alizade, Erkin Gezgin, 2010	Mobility equation of the kinematic pairs (M_k) and the general mobility equation (M) for the mechanisms and manipulators

As spherical mechanisms hold a transition position between the planar and spatial linkages, they attract many authors for synthesis purposes. Being the smallest member of close loop spherical mechanisms, function generation synthesis of four bar spherical linkage can be seen in many studies. Denavit and Hartenberg (1964) presented the synthesis procedure for three precision points in the function generation of spherical four bar mechanism, where a logarithmic function is decided to be generated. Zimmerman (1967) proposed an algorithm for the same mechanism for four precision points. Polynomial approximation is used for three, four and five precision points in the works of Alizade (1994), Alizade et al. (2005), Farhang et al. (1988, 1999), Rao et al. (1973), and Murray et al. (1995) for the spherical four bar mechanism. Also in the paper of Alizade et al. (2005), effects of the locations of the precision points are considered and a graphical method in CAD environment is shown to verify the solutions of the construction parameters. Sancribrian et al. (2007) proposed a synthesis method that uses a dimensional synthesis technique and local optimization. Cervantes-Sanchez et al. (2009) introduced a new approach for three and four precision points exact kinematic synthesis, where several examples for the spherical four-bar mechanism are given. Also, Kazerounian et al. (1993) and Gupta et al. (1998) presented additional conditions as rotability, branch and circuit defect elimination etc. that can be controlled after the synthesis problem.

On the biokinematics side, many authors has studied the various elements of the human body in terms of their moving capabilities, structures and functions. Jenkin et al. (1993) presented the hardware and software designs of the stereo robotic head system "*TRISH*" with torsional eye movements. Haslwanter (1994) studied the mathematics of the three-DoF human eye rotations by using rotational matrices and the quaternions. Gosselin et al. (1994) represented the agile eye that is an optimized parallel spherical manipulator with the capability to orient a camera within a workspace larger than the human eye. Moeslund et al. (2001) dealt with the pose estimation of the human arm by using kinematic constraints. In their work, the main concern was on the visual motion capture of the human arm. Koolstra (2002) reviewed the dynamics of human masticatory system. In the study, the movement characteristics of the human masticatory system are discussed. Breazeal (2003), dealt with the role of emotion and expressive behaviour between the humans and expressive antromorphic robots. Ludewig et al. (2004) studied three dimensional clavicular motions during arm elevation. Admiraal et al. (2004) modelled the dynamics and kinematics of the human

arm movements. In their work, the relation between the dynamics and kinematics is studied. Pileicikiene et al. (2004) reviewed the human masticatory system from a biomechanical perspective. Oswald et al. (2004) tried to integrate an anthropomorphic robot hand into a humanoid robot. Wu et al. (2005) placed recommendations for the various joint coordinate axes of human body. Peck et al. (2007) accomplished the modeling of human jaw and its muscles. Benjelloun et al. (2007) conducted the vertebral mobility analysis by using faces contours detection and anterior faces detection. In their work, X-ray images of the spinal column in various positions are used. Zhang et al. (2008) proposed three-DoF humanoid eye that is actuated by using artificial pneumatic muscles. Barshan et al. (2009) classified the human leg motions by using two low-cost piezoelectric gyroscopes that are placed on the legs. Raabe et al. (2009) introduced a new dynamic jaw simulator based on the kinematics of human jaw. In their work, six-DoF Steward-Gough Platform is used as a manipulator. Buschmann et al. (2009), introduced a walking humanoid robot, LOLA, to reach fast and human like walking.

As the presented literature review related with this thesis study shows the development of the subjects throughout the century, it is clear that there will be more advanced future studies by the help of rapidly evolving technology and new theoretical methods.

CHAPTER 2

QUATERNION AND DUAL QUATERNION ALGEBRA

William Rowan Hamilton searched for thirteen years for a system for the analysis of three-dimensional space. This search came to end in 1843 in four-dimensional space with his discovery of hyper-complex numbers of rank 4, named quaternions, one of the main systems of the vector analysis.

In general, quaternions are four dimensional numbers that have one scalar and one vector part. The vector part is obtained by adding the elements $\boldsymbol{i}$, $\boldsymbol{j}$ and $\boldsymbol{k}$ to the real numbers which satisfy the following relations:

$$\boldsymbol{i}^2 = \boldsymbol{j}^2 = \boldsymbol{k}^2 = \boldsymbol{ijk} = -1 \tag{2.1}$$

Equation (2.1) shows the main rule of Hamilton for dealing operations on the vector part of the quaternions. All of his concepts and ideas were developed in the light of this rule.

2.1. Quaternion Preliminaries

Quaternions can be represented mainly by two alternative ways. As the name already suggests, they can be considered as the row of four real numbers that can be represented by;

$$q = (q_0, q_1, q_2, q_3) \tag{2.2}$$

where, q_0, q_1, q_2 and q_3 are simply real numbers or scalars. Also, they can be denoted by scalar and vector parts as,

$$q = q_0 + \boldsymbol{q} \tag{2.3}$$

where, q_0 is some scalar and $\boldsymbol{q}$ is an ordinary vector in R^3. Equation (2.3) can be extended to,

$$q = q_0 + \boldsymbol{i}q_1 + \boldsymbol{j}q_2 + \boldsymbol{k}q_3 \qquad (2.4)$$

As seen in Equations (2.3 & 2.4), quaternions can be represented as the sum of scalar and vector, which is not defined in ordinary linear algebra. So that, it is important to express the operation procedures of the quaternions.

2.2. Quaternion Addition and Equality

Let us take two quaternions $q = q_0 + \boldsymbol{i}q_1 + \boldsymbol{j}q_2 + \boldsymbol{k}q_3$ and $p = p_0 + \boldsymbol{i}p_1 + \boldsymbol{j}p_2 + \boldsymbol{k}p_3$. These quaternions are equal if and only if they have exactly the same components, that is;

$$p = q \iff \begin{cases} p_0 = q_0 \\ p_1 = q_1 \\ p_2 = q_2 \\ p_3 = q_3 \end{cases} \qquad (2.5)$$

In the addition case, the sum of two quaternions $p + q$ is described by adding the corresponding components of both quaternions, Equation (2.6).

$$p + q = (p_0 + q_0) + \boldsymbol{i}(p_1 + q_1) + \boldsymbol{j}(p_2 + q_2) + \boldsymbol{k}(p_3 + q_3) \qquad (2.6)$$

Due to the fact that there is no difference between the addition of quaternions and the row of four real numbers, quaternion addition satisfies the field properties that are applied to the addition.

The addition of two quaternions is again a new quaternion, so the set of quaternions are closed under addition, Equation (2.7).

$$p + q = r$$
$$r = r_0 + \boldsymbol{i}r_1 + \boldsymbol{j}r_2 + \boldsymbol{k}r_3 \tag{2.7}$$

Also each quaternion has a negative or additive inverse where each component of the corresponding quaternion is negative, Equation (2.8).

$$-r = -r_0 - \boldsymbol{i}r_1 - \boldsymbol{j}r_2 - \boldsymbol{k}r_3 \tag{2.8}$$

Moreover, there exists a zero quaternion, in which each component of the quaternion is "0", and the sum of any quaternion with the zero quaternion is again itself, Equation (2.9).

$$p = 0 \Leftrightarrow \begin{Bmatrix} p_0 = 0 \\ p_1 = 0 \\ p_2 = 0 \\ p_3 = 0 \end{Bmatrix} \tag{2.9}$$
$$r + p = r$$

Finally, note that, the quaternion addition is commutative and associative, Equation (2.10).

$$p + q = q + p$$
$$(p + q) + r = p + (q + r) \tag{2.10}$$

2.3. Quaternion Multiplication

When compared with the addition, quaternion multiplication is more complicated, except the multiplication by a scalar. Similar to the addition, multiplication of a quaternion by a scalar quantity is described by a quaternion, in which components of the corresponding quaternion is multiplied by the scalar Equation (2.11).

$$Aq = p$$
$$p = Ap_0 + \boldsymbol{i}Ap_1 + \boldsymbol{j}Ap_2 + \boldsymbol{k}Ap_3 \tag{2.11}$$

On the other hand, if a quaternion is multiplied by another quaternion, more detailed procedure should be followed.

In the product of two quaternions, the fundamental rule of Hamilton, Equation (2.1), should be satisfied. Equation (2.1) can be opened as:

$$
\begin{aligned}
&i^2 = j^2 = k^2 = -1 \\
&ij = k = -ji \\
&jk = i = -kj \\
&ki = j = -ik
\end{aligned}
\tag{2.12}
$$

and the product of two quaternions will be,

$$
\begin{aligned}
pq &= (p_0 + ip_1 + jp_2 + kp_3)(q_0 + iq_1 + jq_2 + kq_3) \\
&= p_0q_0 + ip_0q_1 + jp_0q_2 + kp_0q_3 + ip_1q_0 + i^2p_1q_1 \\
&\quad + ijp_1q_2 + ikp_1q_3 + jp_2q_0 + jip_2q_1 + j^2p_2q_2 \\
&\quad + jkp_2q_3 + kp_3q_0 + kip_3q_1 + kjp_3q_2 + k^2p_3q_3
\end{aligned}
\tag{2.13}
$$

When Equation (2.12) and (2.13) are combined,

$$
\begin{aligned}
pq &= p_0q_0 + ip_0q_1 + jp_0q_2 + kp_0q_3 \\
&\quad + ip_1q_0 - p_1q_1 + kp_1q_2 - jp_1q_3 \\
&\quad + jp_2q_0 - kp_2q_1 - p_2q_2 + ip_2q_3 \\
&\quad + kp_3q_0 + jp_3q_1 - ip_3q_2 - p_3q_3
\end{aligned}
\tag{2.14}
$$

and Equation (2.14) is regrouped, the product of two quaternions will become,

$$
\begin{aligned}
pq &= p_0q_0 - (p_1q_1 + p_2q_2 + p_3q_3) \\
&\quad + p_0(iq_1 + jq_2 + kq_3) + q_0(ip_1 + jp_2 + kp_3) \\
&\quad + i(p_2q_3 - p_3q_2) + j(p_3q_1 - p_1q_3) + k(p_1q_2 - p_2q_1)
\end{aligned}
\tag{2.15}
$$

From this point, the cross and dot product of two vectors in three dimensional space should be recalled. Let us take two vectors $a = (a_1, a_2, a_3)$ and $b = (b_1, b_2, b_3)$, then the dot product of two vectors will be,

$$\boldsymbol{a.b} = (a_1b_1, a_2b_2, a_3b_3) \tag{2.16}$$

and the cross product will be,

$$\begin{aligned}
\boldsymbol{a} \times \boldsymbol{b} &= \begin{vmatrix} \boldsymbol{i} & \boldsymbol{j} & \boldsymbol{k} \\ a_1 & a_2 & a_3 \\ b_1 & b_2 & b_3 \end{vmatrix} \\
&= \boldsymbol{i}(a_2b_3 - a_3b_2) \\
&+ \boldsymbol{j}(a_3b_1 - a_1b_3) \\
&+ \boldsymbol{k}(a_1b_2 - a_2b_1)
\end{aligned} \tag{2.17}$$

Using Equations (2.15, 2.16 & 2.17) the product of two quaternions becomes,

$$pq = p_0q_0 - \boldsymbol{p.q} + p_0\boldsymbol{q} + q_0\boldsymbol{p} + \boldsymbol{p} \times \boldsymbol{q} \tag{2.18}$$

where, $\boldsymbol{p}$ and $\boldsymbol{q}$ are the vector parts of the quaternions consecutively.

As it can be easily seen from above equations, multiplication results of quaternions are still quaternions, and the fundamental rule of Hamilton violate the commutative rule. As a result, it can be said that, quaternions are closed under the multiplication and the product of quaternions are non commutative, Equation (2.19).

$$\left. \begin{cases} Ap = q \\ qr = s \end{cases} \right\} \Rightarrow \left\{ \begin{aligned} q &= q_0 + iq_1 + jq_2 + kq_3 \\ s &= s_0 + is_1 + js_2 + ks_3 \end{aligned} \right\} \tag{2.19}$$
$$qr \neq rq$$

Also quaternion product is associative and distributive over addition, Equation (2.20).

$$\begin{aligned}
(pq)r &= p(qr) \\
p(q+r) &= pq + pr \\
(p+q)r &= pr + qr
\end{aligned} \tag{2.20}$$

Note that the identity for quaternion multiplication is a quaternion that has real part "1" and vector part "0", and the product of any quaternion with the identity is again itself, Equation (2.21).

$$pq = q \Leftrightarrow \begin{Bmatrix} p_0 = 1 \\ p_1 = 0 \\ p_2 = 0 \\ p_3 = 0 \end{Bmatrix} \tag{2.21}$$

2.4. Conjugate of the Quaternion

Although it is simple, conjugate is a very important algebraic concept of the quaternions. The conjugate of quaternion q is usually denoted by $K(q)$, and it is given by,

$$\begin{aligned} K(q) &= q_0 - \boldsymbol{q} \\ &= q_0 - \boldsymbol{i}q_1 - \boldsymbol{j}q_2 - \boldsymbol{k}q_3 \end{aligned} \tag{2.22}$$

Due to the fact that, the vector parts of a quaternion and its conjugate differ only in sign, product and sum of the quaternion and its conjugate result in scalar quantity, Equation (2.23).

$$\begin{Bmatrix} qK(q) = K(q)q \\ \quad = q_0{}^2 + q_1{}^2 + q_2{}^2 + q_3{}^2 \end{Bmatrix} \\ \begin{Bmatrix} q + K(q) = K(q) + q \\ \quad = 2q_0 \end{Bmatrix} \tag{2.23}$$

As additional information, conjugate of the product of two quaternions is equal to the product of the individual conjugates in reverse order Equation (2.24).

$$K(pq) = K(q)K(p) \tag{2.24}$$

2.5. Norm of the Quaternion

.

The norm of a quaternion is usually denoted by $N(q)$ or $|q|$ and can be referred as the length of q. The norm is defined as,

$$N(q) = \sqrt{K(q)q} \tag{2.25}$$

Using Equation (2.18), Equation (2.25) can be extended to,

$$\begin{aligned}
N^2(q) &= (q_0 - \boldsymbol{q})(q_0 + \boldsymbol{q}) \\
&= q_0 q_0 - (-\boldsymbol{q}) . \boldsymbol{q} + q_0 \boldsymbol{q} + (-\boldsymbol{q})q_0 + (-\boldsymbol{q}) \times \boldsymbol{q} \\
&= q_0^2 + \boldsymbol{q}.\boldsymbol{q} \\
&= q_0^2 + q_1^2 + q_2^2 + q_3^2 \\
&= |q|^2
\end{aligned} \tag{2.26}$$

As additional information, norm of the product of two quaternions is equal to the product of the individual norms, Equation (2.27).

$$N(pq) = N(p)N(q) \tag{2.27}$$

Also note that, if the norm of a quaternion is unity, the components of the corresponding quaternions must have absolute values less than or equal to 1. Such quaternions are called as unit quaternions.

2.6. Inverse of the Quaternion

Dealing with the conjugate and the norm concepts, now it can be showed that every non-zero quaternion have a multiplicative inverse. The inverse of a quaternion usually denoted by q^{-1} and by the definition of inverse, product of a quaternion with its inverse should result in unity, Equation (2.28).

$$q^{-1}q = qq^{-1} = 1 \tag{2.28}$$

If it is multiplied with $K(q)$ by post and pre multiplication, Equation (2.28) becomes,

$$q^{-1}qK(q) = K(q)qq^{-1} = K(q) \tag{2.29}$$

Since $qK(q) = K(q)q = N^2(q)$ the inverse quaternion can be denoted as:

$$q^{-1} = \frac{K(q)}{N^2(q)} \tag{2.30}$$

Note that if q is a unit quaternion ($N(q) = 1$), than the inverse of the quaternion will be its conjugate as:

$$N(q) = 1 \Leftrightarrow q^{-1} = K(q) \tag{2.31}$$

2.7. Dual Quaternion Preliminaries

In fact dual quaternions are constructed in the same way as the quaternions; however, dual quaternions use dual numbers instead of real numbers as coefficients. In the light of the definition, a dual quaternion can be represented as,

$$Q = (a + \varepsilon e, \; b + \varepsilon f, \; c + \varepsilon g, \; d + \varepsilon h) \tag{2.31}$$

where ε is the dual unit $\varepsilon^2 = 0$. If the Equation (2.31) is opened in the vector form, dual quaternion representation will become,

$$\begin{aligned}
Q &= (a + \varepsilon e) + (b + \varepsilon f)\mathbf{i} + (c + \varepsilon g)\mathbf{j} + (d + \varepsilon h)\mathbf{k} \\
Q &= a + b\mathbf{i} + c\mathbf{j} + d\mathbf{k} + \varepsilon e + \varepsilon f\mathbf{i} + \varepsilon g\mathbf{j} + \varepsilon h\mathbf{k} \\
Q &= r + \varepsilon d
\end{aligned} \tag{2.32}$$

where "r" and "d" are quaternions individually. Looking at Eq. (2.32), it can be easily seen that dual quaternions have eight components, where four of them represent real part and the remaining represent the dual part.

2.8. Dual Quaternion Multiplication

The multiplication of a dual quaternion with a scalar quantity has the same procedure with the quaternion multiplication. On the other hand if the dual quaternion is to be multiplied by another dual quaternion, dual quaternion multiplication should be used (Table 2.1).

Table 2.1. Dual quaternion multiplications.

$Q_1 Q_2$	Q_2	$Q_2 i$	$Q_2 j$	$Q_2 k$	$Q_2 \varepsilon$	$Q_2 \varepsilon i$	$Q_2 \varepsilon j$	$Q_2 \varepsilon k$
Q_1	1	i	j	k	ε	εi	εj	εk
$Q_1 i$	i	-1	k	$-j$	εi	$-\varepsilon$	$-\varepsilon k$	εj
$Q_1 j$	j	$-k$	-1	i	εj	εk	$-\varepsilon$	$-\varepsilon i$
$Q_1 k$	k	j	$-i$	-1	εk	$-\varepsilon j$	εi	$-\varepsilon$
$Q_1 \varepsilon$	ε	$-\varepsilon i$	$-\varepsilon j$	$-\varepsilon k$	0	0	0	0
$Q_1 \varepsilon i$	εi	$-\varepsilon$	$-\varepsilon k$	εj	0	0	0	0
$Q_1 \varepsilon j$	εj	εk	$-\varepsilon$	$-\varepsilon i$	0	0	0	0
$Q_1 \varepsilon k$	εk	$-\varepsilon j$	εi	$-\varepsilon$	0	0	0	0

2.9. Conjugate of the Dual Quaternion

Unlike the quaternions, dual quaternions has three kinds of conjugates. If the ith conjugate of the dual quaternion is $K_i(Q)$ $(i = 1, 2, 3)$, it can be defined as,

$$
\begin{aligned}
Q &= r + \varepsilon d \\
K_1(Q) &= K(r) + \varepsilon K(d) \\
K_2(Q) &= r - \varepsilon d \\
K_3(Q) &= K(r) - \varepsilon K(d)
\end{aligned}
\tag{2.33}
$$

where $K(r)$ and $K(d)$ are the conjugates of the quaternions "r" and "d" individually.

2.10. Norm of the Dual Quaternion

Similar to the quaternions, the norm of a dual quaternion $N(Q)$ can be denoted as,

$$N(Q) = \sqrt{K_1(Q)Q} \qquad (2.34)$$

It should also be added that, the norm property of quaternions (Equation 2.27) is valid for the dual quaternions as $N(Q_1 Q_2) = N(Q_1)N(Q_2)$.

2.11. Inverse of the Dual Quaternion

The inverse of the dual quaternions Q^{-1} can be taken by using the same procedure of quaternion inverse as,

$$Q^{-1} = \frac{K_1(Q)}{N^2(Q)} \qquad (2.35)$$

Note that if Q is a unit dual quaternion ($N(Q) = 1$), than the inverse of the dual quaternion will be its first conjugate as,

$$N(Q) = 1 \Leftrightarrow Q^{-1} = K_1(Q) \qquad (2.36)$$

CHAPTER 3

SCREW THEORY

This chapter is presented to briefly describe the screw theory that was developed by Sir Robert Stawell Ball in 1876. As a mathematical tool, screw theory is mostly used in the rigid body dynamics, where it can represent the displacements, velocities, forces and torques in three dimensional space by using individual screws including both rotational and translational components.

3.1. Introduction to Screws

Screw can be described as a six component displacement vector, $\$ = (\mathbf{s}, \mathbf{u})$, which might also be either a twist or a wrench, with an axis $L(t) = \mathbf{r} + t\mathbf{s}$ (Figure 3.1). The angular velocity $\mathbf{w} = [w_x, w_y, w_z]^T$ and the linear velocity $\mathbf{V} = [V_x, V_y, V_z]^T$ of any moving rigid body are three dimensional vectors and can form a twist $\mathbf{T} = [\mathbf{w}, \mathbf{V} + \mathbf{q} \times \mathbf{w}]^T$, while the other three dimensional vectors as resultant force $\mathbf{F} = [F_x, F_y, F_z]^T$ acting at a point on the moving rigid body and resultant torque $\boldsymbol{\tau} = [\tau_x, \tau_y, \tau_z]^T$ applied to that body can form a wrench $\mathbf{W} = [\mathbf{F}, \mathbf{p} \times \mathbf{F} + \tau]^T$.
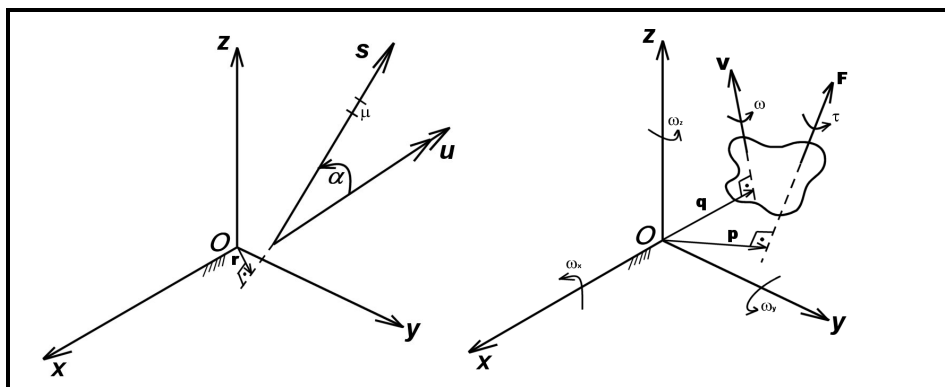
Figure 3.1. Screw, wrench and twist.

The displacement of a rigid body can be described in terms of unit vector $\mathbf{s} = [l, m, n]^T$ and moment $\mathbf{u} = [P + \mu l, \; Q + \mu m, \; R + \mu n]^T$, where (l, m, n, P, Q, R) are the Plucker coordinates of screw axis. The parameter μ is called the pitch of the screw, that is the ratio of the magnitude of the component "$\mathbf{u}$" in the direction of "$\mathbf{s}$" to the magnitude of "$\mathbf{s}$" (Hao 1998). Six independent components (l, m, P, Q, R, μ) of two vectors $(\mathbf{s}, \mathbf{u})$ are also three dimensional vectors and called displacement of screw $\$ = [\mathbf{s}, \mathbf{r} \times \mathbf{s} + \mu \mathbf{s}]^T$. Note that as $\mathbf{s} = [l, m, n]^T$ is a unit vector with the condition $\mathbf{s} \cdot \mathbf{s} = 1$, and one of its components is dependent on the other two.

3.2. Motor Screw

Before defining the motor screw, sliding vectors should be discussed. Sliding vector can be described as a vector with known length, direction, position and zero pitch $\mu = 0$. Consider that arbitrary number of sliding vectors is given in space $\{\mathbf{s}_i\}_1^n$ as shown in Figure 3.2. The resultant vector of sliding vectors in space will be the main vector $\mathbf{s} = \sum_{i=1}^{n} \mathbf{s}_i$ while the main moment with respect to an arbitrary point M in space will be $\mathbf{u}_M = \sum_{i=1}^{n} (\boldsymbol{\rho}_i \times \mathbf{s}_i)$. Changing the arbitrary point to a new one N, the main moment will become $\mathbf{u}_n = \sum_{i=1}^{n} (\boldsymbol{\rho} + \boldsymbol{\rho}_i) \times \mathbf{s}_i = \mathbf{u}_m + \boldsymbol{\rho} \times \mathbf{s}$, where "$\boldsymbol{\rho}$" is the shortest distance from the point N to the resultant main vector. The system of main vector and main moment is called motor screw.
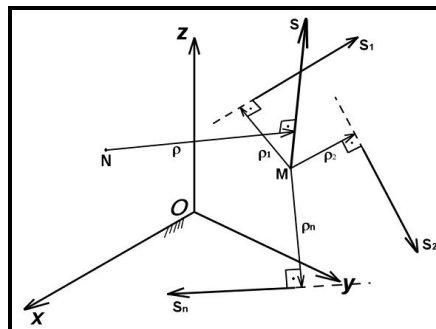
Figure 3.2. Sliding vectors, and motor screw.

In the general case the main vector and main moment form some angle α. Assume that the main vector "$\mathbf{s}$" is placed to an arbitrary point M and the main moment "$\mathbf{u}$" is calculated with respect to another arbitrary point N (Figure 3.3). The main moment "$\mathbf{u}$" can be assembled into two component vectors $\mathbf{u}'$ and $\mathbf{u}''$ where $\mathbf{u}' // \mathbf{s}$ and $\mathbf{u}'' \perp \mathbf{s}$. If the moments are said to be taken from some arbitrary point N than $\mathbf{u}''$ will be
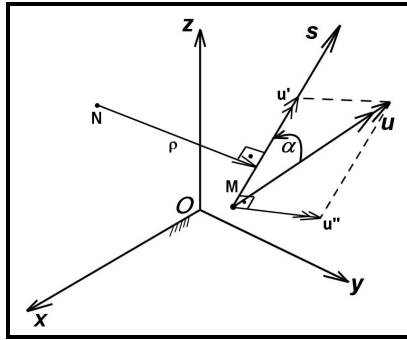
Figure 3.3. Main vector and main moment.

equal to $\mathbf{u}'' = \mathbf{\rho} \times \mathbf{s}$, where "$\mathbf{\rho}$" is the shortest distance from point N to the vector "$\mathbf{s}$". In order to find "$\mathbf{\rho}$" in terms of the main vector and main moment following algebraic procedure can be introduced as,

$$\mathbf{u}'' = \mathbf{\rho} \times \mathbf{s} = |\mathbf{\rho}||\mathbf{s}|\,Sin(\frac{\pi}{2}); \quad |\mathbf{\rho}| = \frac{|\mathbf{u}''|}{|\mathbf{s}|} = \frac{|\mathbf{u}|\,Sin(\alpha)}{|\mathbf{s}|} = \frac{|\mathbf{s}||\mathbf{u}|\,Sin(\alpha)}{|\mathbf{s}||\mathbf{s}|}; \quad \mathbf{\rho} = \frac{\mathbf{s} \times \mathbf{u}}{\mathbf{s} \cdot \mathbf{s}}$$

3.3. Particular Cases

Although screws are defined in their most general forms, there also exist some special cases. If the screw is lack of pitch μ that is also called zero screw, it forms a line that can be described as $\mathbf{L} = (\mathbf{s}, \mathbf{r} \times \mathbf{s})$, this particular line is called Plucker vector and can be shown in dual form as $\$ = \mathbf{e} + w\mathbf{e}°$ or $\$ = (\mathbf{e}, \mathbf{e}°)$. Note that Plucker vector will be formed by two vectors (main vector and moment vector) that are perpendicular to each other. The other situation is valid when the main vector and the main moment are directed in the same direction or the opposite directions. These special types of screws are called right and left screws respectively (Figure 4.4). Also, it can be easily seen from Figure 3.4 that, to form a right or left screw, the direction of the main vector

"**s**" should be passing from the point where the moment is considered to be taken, origin "O" in the case of Figure 4.4, so that the moment "**u**" will be just formed due to the positive or negative pitch μ, $\$ = [\mathbf{s}, \mu\mathbf{s}]^T$.
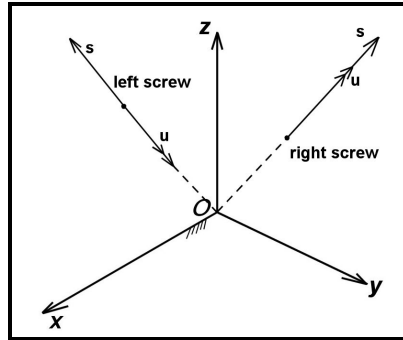
Figure 3.4. Right and left screws.

If there exists only a moment vector **u** with lack of main vector "**s**", the screw is called degenerated screw.

3.4. Intersections of Two Screws

Let's consider the two screws $\$_i$ and $\$_j$ that are intersected in space, (Figure 3.5). If the radius vector $\boldsymbol{\rho}$ (x,y,z) can be defined by using the components of related screw, the position of any rigid body can also be computed by defining two intersecting screws on the rigid body.
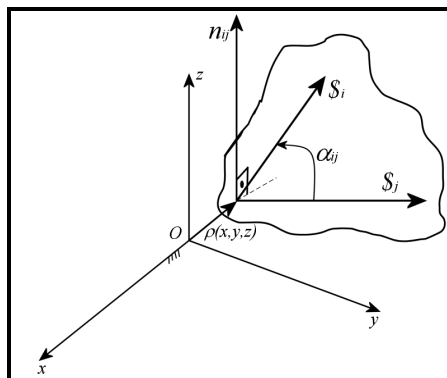
Figure 3.5. Intersections of two screws.

It is already known from the definition that the moment component of any screw can be defined by the formulation,

$$\mathbf{e}^{\circ} = \boldsymbol{\rho} \times \mathbf{e} \qquad (3.1)$$

If Equation (3.1) is opened with respect to the individual components, the equation of the screw axis or the line in space can be found as,

$$iP + jQ + kR = i\begin{vmatrix} n & m \\ z & y \end{vmatrix} + j\begin{vmatrix} l & n \\ x & z \end{vmatrix} + k\begin{vmatrix} m & l \\ y & x \end{vmatrix} \qquad (3.2)$$

Investigating the Equation (3.2), it will be revealed that $P = \begin{vmatrix} n & m \\ z & y \end{vmatrix} = ny - mz$,

$Q = \begin{vmatrix} l & n \\ x & z \end{vmatrix} = lz - nx$, and $R = \begin{vmatrix} m & l \\ y & x \end{vmatrix} = mx - ly$. Using the same analogy equations of the

two intersecting screw axis in space can be written as,

$$\begin{aligned} P_i &= n_i y - m_i z, \ Q_i = l_i z - n_i x, \ R_i = m_i x - l_i y \\ P_j &= n_j y - m_j z, \ Q_j = l_j z - n_j x, \ R_j = m_j x - l_j y \end{aligned} \qquad (3.3)$$

In order to find the three coordinates of the radius vector $\boldsymbol{\rho}$ (x,y,z), sufficient equation groups from Equation (3.3) can be used, such as (P_1, Q_1, R_2), (P_1, Q_2, R_1), and (P_2, Q_1, R_1). After solving the mentioned equation groups the three coordinates of the radius vector $\boldsymbol{\rho}$ (x,y,z) can be introduced as,

$$\begin{pmatrix} x = (q_i m_j + r_i n_j + l_i p_j) l_{ij}^{-1} \\ y = (m_i p_j - m_j p_i) l_{ij}^{-1} \\ z = (n_i p_j + n_j p_i) l_{ij}^{-1} \end{pmatrix}, \begin{pmatrix} x = (l_i q_j - l_j q_i) m_{ij}^{-1} \\ y = (p_i l_j + m_i q_j + n_j r_i) m_{ij}^{-1} \\ z = (n_i q_j - n_j q_i) m_{ij}^{-1} \end{pmatrix}, \begin{pmatrix} x = (l_i r_j - l_j r_i) n_{ij}^{-1} \\ y = (m_i r_j - m_j r_i) n_{ij}^{-1} \\ z = (l_j p_i + q_i m_j + n_i r_j) n_{ij}^{-1} \end{pmatrix} \qquad (3.4)$$

where in Equation (3.4), $l_{ij} = m_i n_j - m_j n_i$, $m_{ij} = n_i l_j - n_j l_i$, and $n_{ij} = l_i m_j - l_j m_i$ are the projections of normal vector $\mathbf{e_i} \times \mathbf{e_j} = \mathbf{n_{ij}}$ onto axes of system coordinates.

3.5. Transformation Unit Screw Equations

In order to create the mathematical models of kinematic pairs and design new mechanisms from various subspaces, theory of screw calculations should be clearly investigated. It is known that the axis of any screw can be described as a dual vector, which can be introduced as a complex number,

$$\$ = \mathbf{e} + \omega \mathbf{e}^{\circ} \qquad (3.5)$$

where in Equation (3.5), $\mathbf{e}$ is the unit vector of the screw axis, $\mathbf{e}^{\circ}$ is the moment of $\mathbf{e}$ with respect to the origin of the fixed coordinate system and ω is the Clifford's operator ($\omega^2 = 0$). Actually screw calculations can be described as the vector algebra of the dual vectors. Each screw can be characterized in space by three dual coordinates $\$(\tilde{L}, \tilde{M}, \tilde{N})$. Each of the dual coordinates can be represented as three dual components similar to the Equation (3.1) as,

$$\tilde{L} = l + \omega P, \qquad \tilde{M} = m + \omega Q, \qquad \tilde{N} = n + \omega R \qquad (3.6)$$

The six components $\$(l, m, n, P, Q, R)$ of the dual coordinates of Equation (3.6) are called Plücker coordinates in the theory of screw calculations of unit screws, where l, m, and n are the components of unit vector $\mathbf{e}$ while P, Q, and R are the components of moment $\mathbf{e}^{\circ}$.

Let's consider three unit screws in space $\$_i, \$_j$, and $\$_k$, Figure 3.6. In order to form the algorithm to find the dual coordinates of the third screw $\$_k(\tilde{L}_k, \tilde{M}_k, \tilde{N}_k)$ with respect to the known dual coordinates of unit screws $\$_i(\tilde{L}_i, \tilde{M}_i, \tilde{N}_i)$ and , unit screw $\$_j$ is directed along the short distance between $\$_i$ and $\$_k$. It is clear from Figure (3.4) that, two unit screw pairs $\$_i, \$_j$ and $\$_j, \$_k$ are orthogonal unit screws ($\alpha_{ij} = \alpha_{jk} = 90^{\circ}$, $a_{ij} = a_{jk} = 0$) and the position and orientation of unit screw $\$_k$ with respect to $\$_i$ can be described by two independent parameters a_{ik} and α_{ik}.
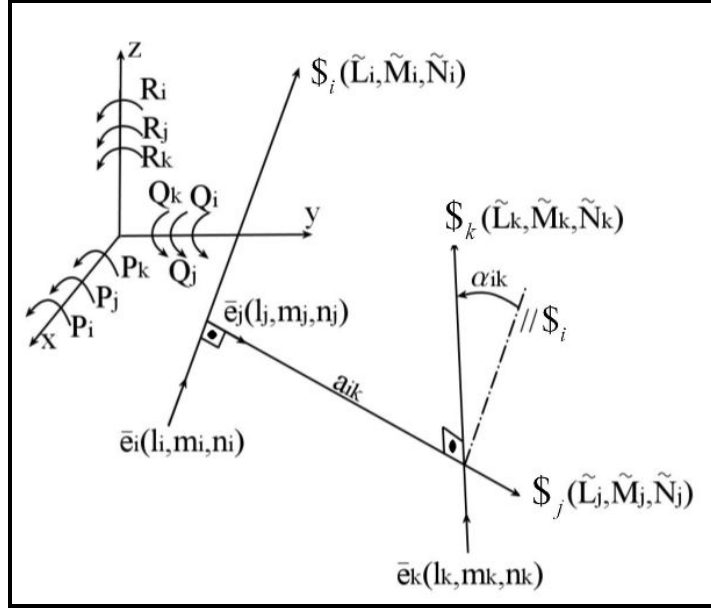
Figure 3.6. Three recurrent screws in space.

The orientation of any rigid body with respect to the reference frame can be represented by recurrent unit vector equations by using following formulation,

$$\mathbf{e}_k = \mathbf{B}\,\mathbf{e} \qquad (3.7)$$

where in Equation (3.7), $\mathbf{e}_k = [l_k, m_k, n_k]^T$, $\mathbf{e} = [l_i, l_{ij}, m_i, m_{ij}, n_i, n_{ij}]^T$, $l_{ij} = \begin{vmatrix} n_i & m_i \\ n_j & m_j \end{vmatrix}$,

$m_{ij} = \begin{vmatrix} l_i & n_i \\ l_j & n_j \end{vmatrix}$, $n_{ij} = \begin{vmatrix} m_i & l_i \\ m_j & l_j \end{vmatrix}$ and, $\mathbf{B} = \begin{bmatrix} C\alpha_{ik} & S\alpha_{ik} & 0 & 0 & 0 & 0 \\ 0 & 0 & C\alpha_{ik} & S\alpha_{ik} & 0 & 0 \\ 0 & 0 & 0 & 0 & C\alpha_{ik} & S\alpha_{ik} \end{bmatrix}$.

If the transferring principle of Kotel'nikov-Shtudi[1] is applied in the Equation (3.7), the dual coordinates of unit screw $\$_k(\tilde{L}_k, \tilde{M}_k, \tilde{N}_k)$ with respect to the known dual coordinates of unit screws $\$_i(\tilde{L}_i, \tilde{M}_i, \tilde{N}_i)$ and $\$_j(\tilde{L}_j, \tilde{M}_j, \tilde{N}_j)$ can be computed by using,

$$\$_k = \tilde{\mathbf{B}}\,\mathbf{E} \qquad (3.8)$$

---

[1] All formulas of vector algebra can be used in screw algebra formulations if and only if the values should be interpreted in dual forms

where in Equation (3.8), $\$_k = [\tilde{L}_k, \tilde{M}_k, \tilde{N}_k]^T$, $\quad \mathbf{E} = [\tilde{L}_i, \tilde{L}_{ij}, \tilde{M}_i, \tilde{M}_{ij}, \tilde{N}_i, \tilde{N}_{ij}]^T$,

$$\tilde{L}_{ij} = \begin{vmatrix} \tilde{N}_i & \tilde{M}_i \\ \tilde{N}_j & \tilde{M}_j \end{vmatrix}, \quad \tilde{M}_{ij} = \begin{vmatrix} \tilde{L}_i & \tilde{N}_i \\ \tilde{L}_j & \tilde{N}_j \end{vmatrix}, \quad \tilde{N}_{ij} = \begin{vmatrix} \tilde{M}_i & \tilde{L}_i \\ \tilde{M}_j & \tilde{L}_j \end{vmatrix}, \quad \mathbf{B} = \begin{bmatrix} CA_{ik} & SA_{ik} & 0 & 0 & 0 & 0 \\ 0 & 0 & CA_{ik} & SA_{ik} & 0 & 0 \\ 0 & 0 & 0 & 0 & CA_{ik} & SA_{ik} \end{bmatrix}$$

$$\tilde{L}_k = l_k + \omega P_k, \qquad \tilde{M}_k = m_k + \omega Q_k, \qquad \tilde{N}_k = n_k + \omega R_k$$
$$\text{and } \tilde{L}_i = l_i + \omega P_i, \qquad \tilde{M}_i = m_i + \omega Q_i, \qquad \tilde{N}_i = n_i + \omega R_i \quad .$$
$$\tilde{L}_j = l_j + \omega P_j, \qquad \tilde{M}_j = m_j + \omega Q_j, \qquad \tilde{N}_j = n_j + \omega R_j$$

To proceed further, it should be noted that, the angles between the unit screws $\$_i, \$_j$, and $\$_k$ can be indicated in dual angle form as,

$$A_{ij} = \alpha_{ij} + \omega a_{ij}, \quad A_{jk} = \alpha_{jk} + \omega a_{jk}, \quad A_{ik} = \alpha_{ik} + \omega a_{ik} \tag{3.9}$$

where in Equation (3.9) α_{ij}, α_{jk}, α_{ik}, a_{ij}, a_{jk} and a_{ik} are the angles between the screw axes and the short distances between corresponding screw axes in space respectively. If the trigonometric operations are to be carried out in the dual angles, following formulas should be used,

$$Sin(A) = Sin(\alpha) + \omega a \, Cos(\alpha), \quad Cos(A) = Cos(\alpha) + \omega a \, Sin(\alpha) \tag{3.10}$$

Using the rules of screw algebra, Equation (3.10) and after some arrangements in the elements of Equation (3.8), the transformation unit screw equations with real Plücker coordinates can be introduced as follows,

$$\$_k = \tilde{\mathbf{B}} \mathbf{E}$$

$$\$_k = [l_k, m_k, n_k, P_k, Q_k, R_k]^T, \quad \mathbf{E} = [l_i, l_{ij}, m_i, m_{ij}, n_i, n_{ij}, P_i, P_{ij}, Q_i, Q_{ij}, R_i R_{ij}]^T$$

$$P_{ij} = \begin{vmatrix} n_i & Q_i \\ n_j & Q_j \end{vmatrix} - \begin{vmatrix} m_i & R_i \\ m_j & R_j \end{vmatrix}, \quad Q_{ij} = \begin{vmatrix} l_i & R_i \\ l_j & R_j \end{vmatrix} - \begin{vmatrix} n_i & P_i \\ n_j & P_j \end{vmatrix}, \quad R_{ij} = \begin{vmatrix} m_i & P_i \\ m_j & P_j \end{vmatrix} - \begin{vmatrix} l_i & Q_i \\ l_j & Q_j \end{vmatrix}$$

$$\tilde{\mathbf{B}} = \begin{bmatrix} C\alpha_{ik} & S\alpha_{ik} & 0 & 0 & 0 & 0 & 0 & 0 & 0 & 0 & 0 & 0 \\ 0 & 0 & C\alpha_{ik} & S\alpha_{ik} & 0 & 0 & 0 & 0 & 0 & 0 & 0 & 0 \\ 0 & 0 & 0 & 0 & C\alpha_{ik} & S\alpha_{ik} & 0 & 0 & 0 & 0 & 0 & 0 \\ -a_{ik}S\alpha_{ik} & a_{ik}C\alpha_{ik} & 0 & 0 & 0 & 0 & C\alpha_{ik} & S\alpha_{ik} & 0 & 0 & 0 & 0 \\ 0 & 0 & -a_{ik}S\alpha_{ik} & a_{ik}C\alpha_{ik} & 0 & 0 & 0 & 0 & C\alpha_{ik} & S\alpha_{ik} & 0 & 0 \\ 0 & 0 & 0 & 0 & -a_{ik}S\alpha_{ik} & a_{ik}C\alpha_{ik} & 0 & 0 & 0 & 0 & C\alpha_{ik} & S\alpha_{ik} \end{bmatrix}$$

As it is shown above each unit screw is determined by six Plücker coordinates, and only four of them are independent as $\mathbf{e} \cdot \mathbf{e} = 1$ and $\mathbf{e} \cdot \mathbf{e}^\circ = 0$. So that the rigid body in space can be defined by using six independent parameters as $l_k, m_k, P_k, Q_k, a_{ik}, \alpha_{ik}$ or other combinations.

3.6. Transformation Unit Screw Equations by Using Denavit Hartenberg Notations

The transformation unit screw equations with real plucker coordinates can be modified in notation wise by using Denavit-Hartenberg parameters. As seen in Figure 3.7, joint parameters (θ, S) and link parameters (α, a) are indicated disdinctly in classical Denavit-Hartenberg notations.
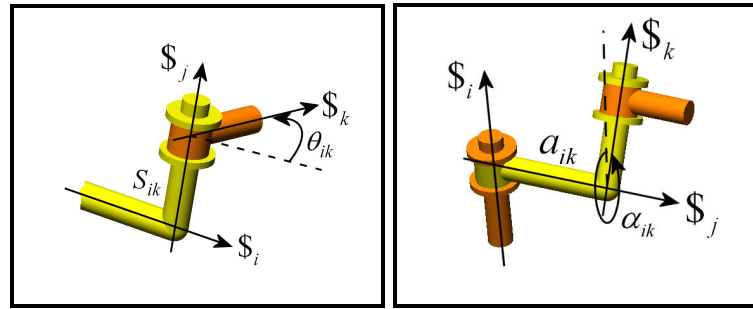
Figure 3.7. Joint and link parameters.

As it is already stated, Equation (3.8) can be used to find the third screw $(\$_k)$, if the components of first and second screws $(\$_i, \$_j)$ are known along with the short distance and the angle between the first and the third screws. However the matrix $\tilde{\mathbf{B}}$ should be modified, if the joint parameters are to be used as,

$$\alpha_{ik} \rightarrow \theta_{ik}, \ a_{ik} \rightarrow S_{ik}$$

$$\tilde{\mathbf{B}} = \begin{bmatrix} C\theta_{ik} & S\theta_{ik} & 0 & 0 & 0 & 0 & 0 & 0 & 0 & 0 & 0 & 0 \\ 0 & 0 & C\theta_{ik} & S\theta_{ik} & 0 & 0 & 0 & 0 & 0 & 0 & 0 & 0 \\ 0 & 0 & 0 & 0 & C\theta_{ik} & S\theta_{ik} & 0 & 0 & 0 & 0 & 0 & 0 \\ -S_{ik}S\theta_{ik} & S_{ik}C\theta_{ik} & 0 & 0 & 0 & 0 & C\theta_{ik} & S\theta_{ik} & 0 & 0 & 0 & 0 \\ 0 & 0 & -S_{ik}S\theta_{ik} & S_{ik}C\theta_{ik} & 0 & 0 & 0 & 0 & C\theta_{ik} & S\theta_{ik} & 0 & 0 \\ 0 & 0 & 0 & 0 & -S_{ik}S\theta_{ik} & S_{ik}C\theta_{ik} & 0 & 0 & 0 & 0 & C\theta_{ik} & S\theta_{ik} \end{bmatrix}$$

CHAPTER 4

RIGID BODY MOTIONS IN SPACE AND SUBSPACES BY USING METHOD OF INTERSECTIONS

This chapter concentrates on the development of rigid body geometries by using method of intersections, where simple geometric shapes representing revolute (R) and prismatic (P) joint motions are intersected by means of desired space or subspace requirements to create specific rigid body geometries in predefined octahedral fixed frame. Using the methodical approach, space and subspace motions can be clearly visualized by the help of resulting geometrical entities that have physical constraints with respect to the fixed working volume.

4.1. Rigid Body Motions

A rigid body with no general constraints ($d = 0$) has six independent motions in Euclidean space ($\lambda = 6$), three revolutions around and three translations along x, y and z axes (Figure 4.1) of the Cartesian frame. These motions can be represented as $RRRPPP$, where R and P stand for revolute rotational and prismatic motions (translations) respectively. It is very important to note that, any rigid body whether in space or subspaces cannot have more than three independent rotations or translations; due to the fact that, there exist only three independent directions in Cartesian frame.
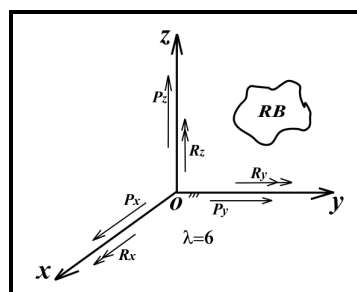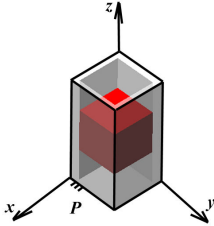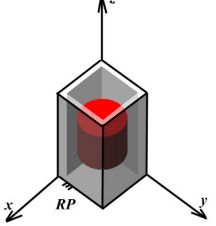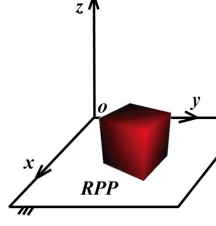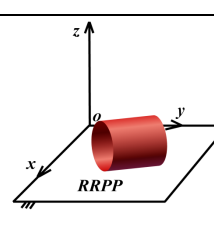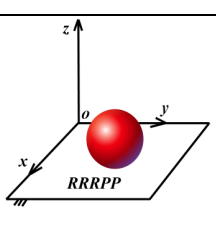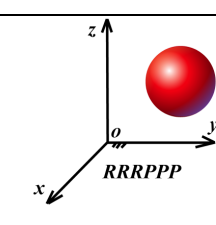
Figure 4.1. Rigid body motions in Cartesian space $\lambda = 6$.

Making use of this rule, achievable independent motions of the rigid bodies in various subspaces can easily be tabulated. As it is seen in Table 4.1, one example for a specific motion related with each of the subspaces is given for different rigid body geometries and fixed frames.

Table 4.1. Possible independent motion configurations of rigid bodies in subspaces.

λ	1	2	3
Motions	R, P	RR, RP, PP	RRR, RRP RPP, PPP
Examples	*Cube in Slot*	*Cylinder in Slot*	*Cube on Plane*
λ	4	5	6
Motions	$RRRP, RRPP$ $RPPP$	$RRRPP$ $RRPPP$	$RRRPPP$
Examples	*Cylinder on Plane*	*Sphere on Plane*	*Sphere in Space*

In the cases of examples, cube in a slot is simply a prismatic joint that have only one translational motion (P) along the z axis. If the cube is swapped with a cylindrical rigid body, it gains additional capability to rotate (R) around the z axis keeping its translational motion, so that its subspace is increased by one. On the cube on plane case, without loosing area of contact, the rigid body can rotate around the z axis and translate along the x, y axes ($RPP, \lambda = 3$). If the area of contact is swapped with line of contact by using cylinder instead of a cube, the rigid body gains another rotation around x or y axis preserving its other motions ($RRPP, \lambda = 4$). Similarly, if the cylinder is replaced by a sphere, its line of contact is transformed into a point of contact which adds another

rotational capability around x or y axis ($RRRPP, \lambda = 5$). Note that, if there is no contact constraint, $RRRPPP$ motion in $\lambda = 6$ is reached.

Although representing rigid body motions this way clarifies the subspace concept, it is difficult to find examples for all motion configurations that preserve one common analogy. As a result, One contribution of this thesis study to the literature is an easy approach that simplifies the visualization of rigid body motions in space or subspaces by introducing unique methodology called method of intersections.

4.2. Method of Intersections

Briefly, the idea behind the methodology is based on the construction of the octahedral fixed frame, which will be called "**_moi frame_**" hereafter, and the intersections of the simple geometric shapes that carry the behaviors of the prismatic or revolute motions (Figure 4.2).
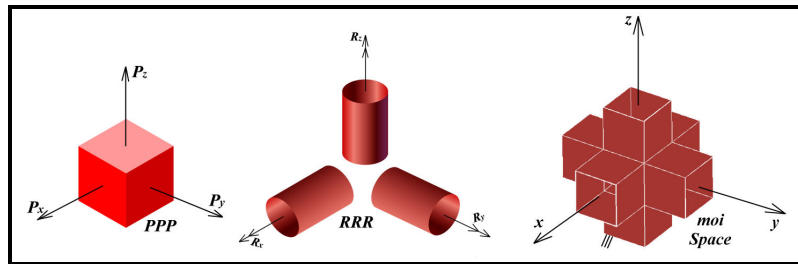
Figure 4.2. Simple geometric rigid bodies with unique motion behaviors and moi space.

It can be easily seen from the figure that the selected cube element is just capable of exiting three translational motions along x, y and z axes unless any other constraints prevent it to do so. The other three unique cylinders represent three distinct rotational motions around the Cartesian coordinate axes and the moi frame is composed of three slots with square cross sections that are orthogonally combined. Assuming the length of the side of the cube, the height and the diameter of the cylinders and the side of the inner square cross section of the moi frame slots are equal, the following procedure can be performed to visualize the rigid body motions in a specific subspace.

- Select the desired space or subspace number λ_i $(i = 1, 2, ..., 6)$.

- Select the motion configuration of the determined subspace from Table 4.1.

- Intersect the geometrical representations of individual motions resulting in a unique geometrical shape.
- If there exist missing translational motions, remove a slot from moi frame that is representing missing translational motion axis to create constrained moi frame (Note that, if there are not any translational motions in the selected motion configuration, the constrained moi frame will just transformed into a hollow cube).
- Put the resultant geometrical shape into moi or constrained moi frame to identify the rigid body motion in determined space or subspace.

The idea can appear confusing; however, examples will clarify the concept.

Example 1: Consider that subspace $\lambda = 5$ is selected with the motion configuration $R_x R_y PPP$. After the intersection of the related simple geometrical shapes, the resultant rigid body is placed into the moi frame (Figure 4.3). Due to the fact that the rigid body has a square cross section on xy plane, its rotation around z axis is constrained as desired. On the other hand circular cross sections on xz and yz planes makes the rotations around x and y axes possible. Also note that all of the translations can be fulfilled thanks to the unconstrained moi frame.
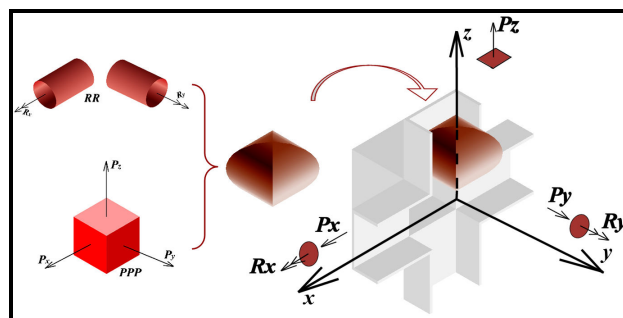
Figure 4.3. Visualization of rigid body motions $R_x R_y PPP$ in $\lambda = 5$.

Example 2: Consider that subspace $\lambda = 5$ is selected again, but with different motion configuration $RRRP_x P_y$. As translation along the z axis is not included, z slot of the moi space is removed. After the intersection of the related simple geometrical shapes, the resultant rigid body is placed into the constrained moi frame (Figure 4.4). Due to the

fact that the rigid body has circular cross sections on all planes, its rotations around x, y and z axes are possible. However, removed z slot of the moi frame constrains the z translation of the rigid body, while other translations are achievable.
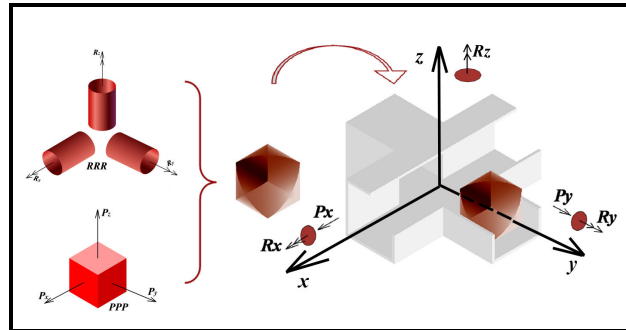
Figure 4.4. Visualization of rigid body motions $RRRP_xP_y$ in $\lambda = 5$.

Despite of being a useful tool for visualization of rigid body motions in space or subspaces, the methodology explained in this chapter can also be used for designing new mechanisms. In the light of *example 1*, two dyads are required to represent two cylinders, where they should be assembled together and articulated in the Cartesian frames to end up with a $\lambda = 5$ mechanism. The dyads are selected as $P - R - R$ chains as they are sufficient for cylinder creation and orthogonal assembly, where prismatic joints are translated along x and y axes. Finally $\lambda = 5$ mechanism with mobility $M = 1$ is created by using the idea behind the method of intersections (Figure 4.5).
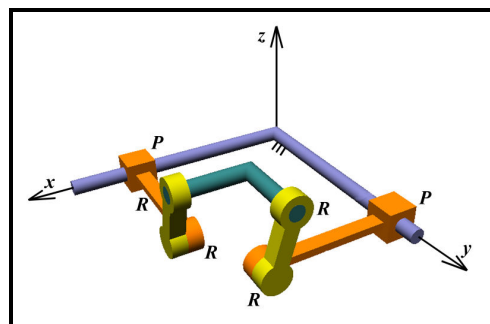
Figure 4.5. $\lambda = 5$, $M = 1$ mechanism created by using method of intersections

Note that by fixing another link instead of the one in the figure, different motions of the desired end-effector point in $\lambda = 5$ can be achieved.

CHAPTER 5

STRUCTURAL SYNTHESIS OF ROBOT MANIPULATORS BY USING SCREW THEORY

This chapter deals with one of the main areas of the fundamental mechanism and machine science as the structural synthesis of robot manipulators by using screw theory. The investigation will start by focusing on the smallest elements of the robot manipulators, kinematic pairs. Throughout the chapter physical representations and kinematic representations of both lower and higher kinematic pairs with recurrent screws (screws that have directions intersected one another in series) will be given. Using transformation unit screw concept, the mathematical models of selected kinematic pairs will be defined and the procedure to find mathematical models of remaing pairs will be introduced. Also at the end of the chapter a new universal mobility formulation for both kinematic pairs and robot manipulators will be presented in terms of screw theory.

5.1. Kinematic Pairs and Mathematical Models

In order to form a kinematic pair, exactly two rigid bodies must be attached to each other by specified geometry. If the contact geometry between two attached rigid bodies is a surface, lower kinematic pairs are formed. Otherwise, if the contact geometry between two attached rigid bodies is a line or a point contact, higher kinematic pairs are formed. During this study they will be referred as *Type I, Type II,* and *Type III* kinematic pairs respectively with respect to their contact geometries for the ease of use. In fact, kinematic pairs can be constructed not only in different structures as described previously but also in various mobilities. However, their mobilities can not be higher than five; due to the fact that, the unconstrained space has six independent motions, and kinematic pairs need at least one constraint in order to be defined properly. The most common kinematic pairs in all types and mobilities are shown in Table 5.1 with their physical and kinematic representations by using recurrent screws.

Table 5.1. Kinematic pairs with their physical and kinematic representations.

Type	Mobility	Kinematic Pair	Physical Representation & Kinematic Representation	\$	s
1	**1**	Revolute (R)		3	0
		Prismatic (P)		3	0

(cont. on next page)

Table 5.1. (cont.)

Type	Mobility	Kinematic Pair	Physical Representation & Kinematic Representation	$	s
1	1	Helical (H)		3	0
1	2	Cylindrical (C)		3	1

(cont. on next page)

Table 5.1. (cont.)

Type	Mobility	Kinematic Pair	Physical Representation & Kinematic Representation	$	s
1	2	Spherical with Finger (S_f)		4	0
	3	Spherical (S)		5	0

Table 5.1. (cont.)

Type	Mobility	Kinematic Pair	Physical Representation & Kinematic Representation	\$	s
2	3	Spherical with Finger in Slot (S_{fs})		5	1
	4	Spherical in Slot (S_s)		6	1

(cont. on next page)

42

Table 5.1. (cont.)

Type	Mobility	Kinematic Pair	Physical Representation & Kinematic Representation	$	s
2	4	Spherical in Torus (S_t)		6	1
3	5	Spherical on Plane (S_p)		7	2

In order to define the mathematical models of the kinematic pairs by using transformation unit screw concept, the last output screw should be defined in terms of variable (•), constant (x), and dependent variables (   ). As seen in Table 5.2, although the screw structures resemble with each other, the parameter structure of all the joints

Table 5.2. Variable, constant and dependent parameters of kinematic pairs.

	a_{ik}	$a_{j\,k+1}$	$a_{k\,k+2}$	$a_{k+1\,k+3}$	$a_{k+2\,k+4}$	α_{ik}	$\alpha_{j\,k+1}$	$\alpha_{k\,k+2}$	$\alpha_{k+1\,k+3}$	$\alpha_{k+2\,k+4}$
R	x	-	-	-	-	•	-	-	-	-
P	•	-	-	-	-	x	-	-	-	-
H		-	-	-	-		-	-	-	-
C	•	-	-	-	-	•	-	-	-	-
S$_f$	0	0	-	-	-	•	•	-	-	-
S	0	0	0	-	-	•	•	•	-	-
S$_{fs}$	•	0	0	-	-	•	•	x	-	-
S$_s$	•	0	0	0	-	•	x	•	•	-
S$_t$	•	0	0	0	-	•	x	•	•	-
S$_p$	x	0	•	•	0	x	$\dfrac{\pi}{2}$	•	•	•

are different. Assuming that the first two screws ($\$_i, \$_j$) are known, the final output screw can be computed by using Equation (3.8). Now let's look at the mathematical models of the first five joints in Table 5.1 or Table 5.2. After the sequential operations are carried out the mathematical models of the revolute, prismatic, helical and cylindrical joints can be introduced as, $\$_k(l_k, m_k, n_k, P_k, Q_k, R_k)$ in Figure 5.1.

$$\$_k = \begin{pmatrix} \text{Cos}[\alpha_{ik}]\, l_i + \text{Sin}[\alpha_{ik}]\, l_{ij} \\ \text{Cos}[\alpha_{ik}]\, m_i + \text{Sin}[\alpha_{ik}]\, m_{ij} \\ \text{Cos}[\alpha_{ik}]\, n_i + \text{Sin}[\alpha_{ik}]\, n_{ij} \\ \text{Cos}[\alpha_{ik}]\, (a_{ik}\, l_{ij} + P_i) + \text{Sin}[\alpha_{ik}]\, (-a_{ik}\, l_i + P_{ij}) \\ \text{Cos}[\alpha_{ik}]\, (a_{ik}\, m_{ij} + Q_i) + \text{Sin}[\alpha_{ik}]\, (-a_{ik}\, m_i + Q_{ij}) \\ \text{Cos}[\alpha_{ik}]\, (a_{ik}\, n_{ij} + R_i) + \text{Sin}[\alpha_{ik}]\, (-a_{ik}\, n_i + R_{ij}) \end{pmatrix}$$

Figure 5.1. Mathematical models of R, P, H and C kinematic pairs

It is clear that the mathematical models are the same for all of the four joints in terms of formulation structure, however the behavior of the parameters a_{ik} and α_{ik} are different for each joint; for instance, both of the parameters a_{ik} and α_{ik} are independent variables in cylindrical joint while they are dependent to each other in the case of helical joint. If the same operations are applied to the screw structure of spherical with finger joint the resulting matrix of the final screw $\$_{k+1}(l_{k+1}, m_{k+1}, n_{k+1}, P_{k+1}, Q_{k+1}, R_{k+1})$ will be computed, Figure 5.2. By using the same analogy mathematical models of the other remaining kinematic

$$\$_{k+1} = \begin{pmatrix} \text{Cos}[\alpha_{jk1}]\, l_j + \text{Sin}[\alpha_{jk1}]\,(-m_j\,(\text{Cos}[\alpha_{ik}]\, n_i + \text{Sin}[\alpha_{ik}]\, n_{ij}) + (\text{Cos}[\alpha_{ik}]\, m_i + \text{Sin}[\alpha_{ik}]\, m_{ij})\, n_j) \\ \text{Cos}[\alpha_{jk1}]\, m_j + \text{Sin}[\alpha_{jk1}]\,(l_j\,(\text{Cos}[\alpha_{ik}]\, n_i + \text{Sin}[\alpha_{ik}]\, n_{ij}) - (\text{Cos}[\alpha_{ik}]\, l_i + \text{Sin}[\alpha_{ik}]\, l_{ij})\, n_j) \\ \text{Sin}[\alpha_{jk1}]\,(-l_j\,(\text{Cos}[\alpha_{ik}]\, m_i + \text{Sin}[\alpha_{ik}]\, m_{ij}) + (\text{Cos}[\alpha_{ik}]\, l_i + \text{Sin}[\alpha_{ik}]\, l_{ij})\, m_j) + \text{Cos}[\alpha_{jk1}]\, n_j \\ \text{Cos}[\alpha_{jk1}]\, P_j + \text{Sin}[\alpha_{jk1}]\,(\text{Cos}[\alpha_{ik}]\,(n_j\, Q_i - n_i\, Q_j - m_j\, R_i + m_i\, R_j) + \text{Sin}[\alpha_{ik}]\,(n_j\, Q_{ij} - n_{ij}\, Q_j - m_j\, R_{ij} + m_{ij}\, R_j)) \\ \text{Cos}[\alpha_{jk1}]\, Q_j + \text{Sin}[\alpha_{jk1}]\,(l_j\,(\text{Cos}[\alpha_{ik}]\, R_i + \text{Sin}[\alpha_{ik}]\, R_{ij}) - (\text{Cos}[\alpha_{ik}]\, l_i + \text{Sin}[\alpha_{ik}]\, l_{ij})\, R_j) \\ \text{Sin}[\alpha_{jk1}]\,(m_j\,(\text{Cos}[\alpha_{ik}]\, P_i + \text{Sin}[\alpha_{ik}]\, P_{ij}) - (\text{Cos}[\alpha_{ik}]\, m_i + \text{Sin}[\alpha_{ik}]\, m_{ij})\, P_j) + \text{Cos}[\alpha_{jk1}]\, R_j \end{pmatrix}$$

Figure 5.2. Mathematical models of S_f kinematic pair.

pairs can be computed. However it should be noted that, if the number of screws in the pair structure increases, the resulting components of the final screw will become more complex.

5.2 Mobility Equations

The reason behind the usage of recurrent screws in the study of kinematic pairs is the fact that, they can clarify the motion concept easily. From this point of view, a new mobility formulation for all types of kinematic pairs can be introduced as,

$$M_k = \$ + s - \Gamma \tag{5.1}$$

where, $\$$ represents the total number of screws, s is the number of screws with variable pitch, and Γ is the contact origin of the kinematic pair that can also be calculated by using the formulation,

$$\Gamma = T + 1 \tag{5.2}$$

Note that, in Equation (5.2), *T* stands for the type number of the kinematic pair. The concept will be clarified by the following examples.

Example 1: Let's start with the most common kinematic pair, the revolute joint. As seen in Table 5.1, the revolute pair can be represented by the total of three screws, where none of them has a variable pitch. Being a *Type I* kinematic pair, its mobility can be calculated by using Equations (5.1 & 5.2) as,

$$M_k = \$ + s - (T+1) = 3 + 0 - (1+1) = 1.$$

Example 2: Let's consider the cylindrical pair. Although it seems having the same screw structure with the revolute pair, cylindrical pair is represented by three screws, one of which has a variable pitch. So that the mobility of *Type I* kinematic pair will become,

$$M_k = \$ + s - (T+1) = 3 + 1 - (1+1) = 2.$$

Example 3: The idea is the same for the higher *Type II* and *Type III* kinematic pairs. Let's take spherical in slot joint that can be represented by six screws, where one of them has variable pitch. The mobility of *Type II* kinematic pair can be calculated as $M_k = \$ + s - (T+1) = 6 + 1 - (2+1) = 4$. In the case of *Type III* spherical on plane pair that is represented by seven screws, where two of them have variable pitches, the mobility will result in,

$$M_k = \$ + s - (T+1) = 7 + 2 - (3+1) = 5.$$

It is important to note that, any screw that carries two independent motions as rotation around and translation along its axis is said to be a screw with variable pitch.

Although the examples clarify the mobility criterion of the kinematic pairs, contact origin Γ of the kinematic pair should also be discussed. As it can be seen in Figure 5.3, the simple planar surface can be represented by two screws. The intersection of two planar surfaces that will result in a line can be represented by three screws and the intersection of three planar surfaces that will result in a point can be represented by four screws. In the light of these, the origin of the kinematic pair is equals to the number of screws needed to represent the creation of its associated contact geometry.

Figure 5.3. Screw representations of planar surface intersections.

Having learned the idea behind the mobility of kinematic pairs by the help of recurrent screws, the subject can be extended beyond by applying the same analogy to the mechanisms and robot manipulators. From this perspective, Equation (5.1) can be enhanced into a new general mobility equation for mechanisms and manipulators as,

$$M = \$ + s - 2l - \sum_{i=1}^{l} (N_i - 2) - \sum_{j=2}^{3} (j-1)T_j - \sum_{k=1}^{L} \lambda_k \qquad (5.3)$$

where, l is the total number of links including ground link, N_i is the number of elements on i^{th} link, T_j is the number of pairs with j^{th} type, L is the number of independent loops and finally λ_k is the space or subspace number of kth independent loop. Applying the new mobility equation, to the robot manipulators in Figure 5.4, examples 4 and 5 will clarify the idea.

Figure 5.4. Parallel platform manipulators with higher kinematic pairs.

Example 4: Checking the number of screws needed to represent each individual pair of the Euclidean platform manipulator in Figure 5.6a from Table 5.1 and summing them up, $ can be calculated as, $\$ = 6(S_t).6 + 12(R).3 = 72$. As there are six spherical in torus kinematic pairs, s will be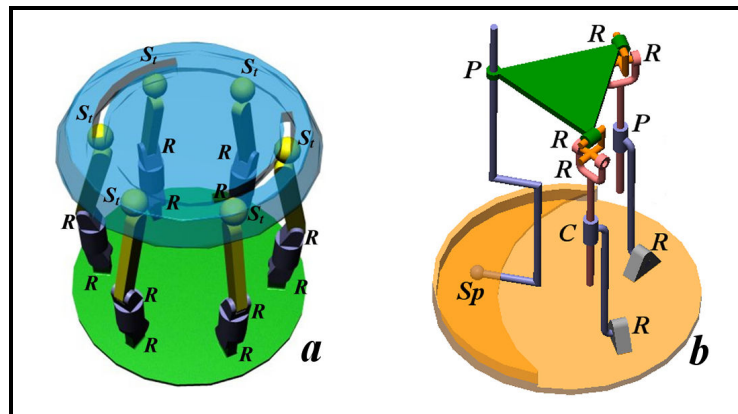 equal to six ($s=6$). There exist fourteen links ($l=14$) in total, where twelve of them are two element and two of them are six element links ($\sum_{i=1}^{l}(N_i - 2) = 8$). Due to the fact that spherical in torus joints are the only higher kinematic pairs in manipulator, $\sum_{j=2}^{3}(j-1)T_j$ will result in 6. As the manipulator is working on space $\lambda=6$, and it has five identical independent loops, $\sum_{k=1}^{5}\lambda_k = 5.\lambda$ will result in 30. Finally, using the defined parameters, the mobility of the Euclidean parallel manipulator can be calculated as,

$$M = 72 + 6 - 2.14 - 8 - 6 - 30 = 6.$$

Example 5: Similarly using the same procedure with the previous example for the parallel platform manipulator in Figure 5.6b, the variables of the Equation (5.3) can be calculated as, $\$ = 6(R).3 + 2(P).3 + 1(C).3 + 1(S_p).7 = 34$, $s = 1(S_p).2 + 1(C).1 = 3$, $l=9$, $\sum_{i=1}^{l}(N_i - 2) = 2$, $\sum_{j=2}^{3}(j-1)T_j = 2$, $L=2$, $\sum_{k=1}^{2}\lambda_k = 2.6 = 12$. The mobility of the parallel platform manipulator will be,

$$M = 34 + 3 - 18 - 2 - 2 - 12 = 3.$$

As verified by the examples, the proposed recurrent screw technique and the mobility equations are valid for both individual kinematic pairs and robot manipulators.

CHAPTER 6

KINEMATIC SYNTHESIS OF MECHANISMS BY USING QUATERNION AND DUAL QUATERNION ALGEBRA

This chapter focuses on the function generation synthesis of spherical four bar mechanism for six independent construction parameters $\varphi_0, \psi_0, \alpha_1, \alpha_2, \alpha_3,$ and α_4 by giving six or more design points with respect to the methods that are used in the synthesis procedure. Quaternion algebra will be used to derive the objective function of spherical four bar mechanism by following some rotational sequences. Three different methods as interpolation approximation, least squares approximation and Chebyshev approximation will be used during synthesis procedure. During the consecutive trials in Chebyshev approximation, a new approach will be proposed to renew the design points that is plotting the graph of the objective functions derivative and taking the roots of it as new design points with the two boundary points. Discussions about the procedure and comparisons between the used methods will be introduced. Also this chapter tries to use dual quaternions in the process of kinematic synthesis to compute the objective function of mechanisms that are desired to be synthesized. Before introducing the algebra, a mixed method of quaternion and vector algebra will be used to show the limitations of quaternions and to verify the results of the dual quaternion algebra in the synthesis procedure. One DoF mechanism from subspace five and RP serial robot manipulator will be used for the calculations. A novel approach will be proposed in the synthesis of subspace five mechanism by integrating both function generation and body guidance operation in one synthesis problem. RP serial manipulator will be synthesized for path generation synthesis.

6.1. Objective Function (Spherical Four Bar)

The main problem in the synthesis of any mechanism is the fact that, the objective function of the mechanism that will be synthesized should be found and simplified by using appropriate algebraic method. Due to common intersection point of

all the joint axes in a spherical mechanism, quaternion algebra can be used as a great tool for this purpose. Note that, any quaternion operator $q(\ )q^{-1}$ will rotate any vector around any axis by the desired amount of angle provided that they are passing from a common point (Figure 6.1).

$$r' = q(r)q^{-1}$$
$$q = Cos(\frac{\theta}{2}) + \hat{m}Sin(\frac{\theta}{2})$$
$$q^{-1} = Cos(\frac{\theta}{2}) - \hat{m}Sin(\frac{\theta}{2})$$

Figure 6.1. Rotation of a vector by using quaternion operator.

Consider that two unit vectors of the input and output joint axes in spherical four bar mechanism is selected as $\hat{r}_1$ and $\hat{r}_4$, and the coordinate system is placed so that $\hat{r}_1 = \mathbf{i}$ (Figure 6.2).

Figure 6.2. Spherical Four Bar Mechanism.

Starting from $\hat{r}_1$, $\hat{r}_4$ can be reached by using two distinct routes. The first one includes the construction parameters α_1, α_2 and α_3 where $\hat{r}_1$ is rotated around the normal of

AOB plane $\mathbf{N_1}$ by the angle α_1 to reach $\hat{\mathbf{r}}_2$, than $\hat{\mathbf{r}}_2$ is rotated around the normal of *BOC* plane $\mathbf{N_2}$ by the angle α_2 to reach $\hat{\mathbf{r}}_3$, and finally $\hat{\mathbf{r}}_3$ is rotated around the normal of *COD* plane $\mathbf{N_3}$ by the angle α_3 to reach $\hat{\mathbf{r}}_4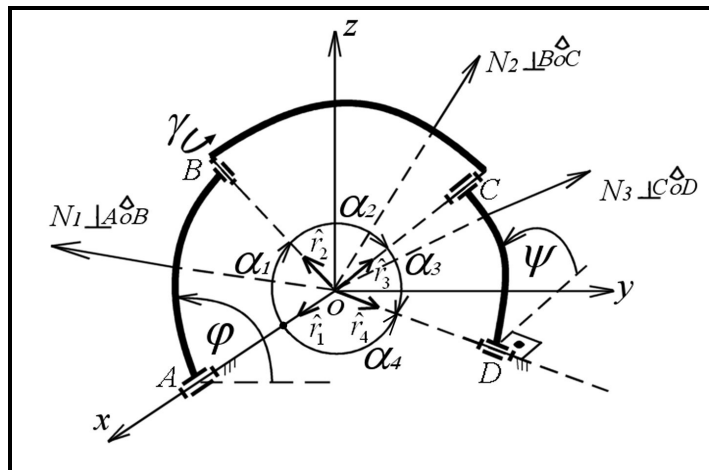$ (Equation 6.1). The second one includes the construction parameter α_4 where $\hat{\mathbf{r}}_1$ is rotated around z axis by the angle α_4 to reach $\hat{\mathbf{r}}_4$ (Equation 6.2).

$$\hat{\mathbf{r}}_4 = q_3 q_2 q_1 (\hat{\mathbf{r}}_1) q_1^{-1} q_2^{-1} q_3^{-1}$$

$$q_1 = Cos(\frac{\alpha_1}{2}) + \hat{\mathbf{n}}_1 Sin(\frac{\alpha_1}{2}), \ q_2 = Cos(\frac{\alpha_2}{2}) + \hat{\mathbf{n}}_2 Sin(\frac{\alpha_2}{2}), \ q_3 = Cos(\frac{\alpha_3}{2}) + \hat{\mathbf{n}}_3 Sin(\frac{\alpha_3}{2}) \tag{6.1}$$

$$\hat{\mathbf{r}}_4 = q_4 (\hat{\mathbf{r}}_1) q_4^{-1}, \quad q_4 = Cos(\frac{\alpha_4}{2}) + \mathbf{k} Sin(\frac{\alpha_4}{2}) \tag{6.2}$$

From this point, to make the calculations possible, $\hat{\mathbf{n}}_1, \hat{\mathbf{n}}_2$ and $\hat{\mathbf{n}}_3$ should be defined clearly.

$\hat{\mathbf{n}}_1$ can be reached by rotating the unit vector of z axis "$\mathbf{k}$" around x axis by the input angle φ (Equation 6.3), $\hat{\mathbf{n}}_2$ can be reached by rotating $\hat{\mathbf{n}}_1$ around $\hat{\mathbf{r}}_2$ axis by the angle γ (Equation 6.4), and $\hat{\mathbf{n}}_3$ can be reached by rotating the negative unit vector of z axis "$-\mathbf{k}$" around $\hat{\mathbf{r}}_4$ axis by the output angle ψ (Equation 6.5).

$$\hat{\mathbf{n}}_1 = q_5 (\mathbf{k}) q_5^{-1}, \quad q_5 = Cos(\frac{\varphi}{2}) + \mathbf{i} Sin(\frac{\varphi}{2}) \tag{6.3}$$

$$\hat{\mathbf{n}}_2 = q_6 (\hat{\mathbf{n}}_1) q_6^{-1}, \quad q_6 = Cos(\frac{\gamma}{2}) + \hat{\mathbf{r}}_2 Sin(\frac{\gamma}{2}), \quad \hat{\mathbf{r}}_2 = q_1 (\hat{\mathbf{r}}_1) q_1^{-1} \tag{6.4}$$

$$\hat{\mathbf{n}}_3 = q_7 (-\mathbf{k}) q_7^{-1}, \quad q_7 = Cos(\frac{\psi}{2}) + \hat{\mathbf{r}}_4 Sin(\frac{\psi}{2}), \quad \hat{\mathbf{r}}_4 = q_4 (\hat{\mathbf{r}}_1) q_4^{-1} \tag{6.5}$$

Defining $\hat{\mathbf{n}}_1, \hat{\mathbf{n}}_2$ and $\hat{\mathbf{n}}_3$, Equations (6.1 & 6.2) can be recalled. Both of the equations result in a quaternion with null scalar part and three vector components $\mathbf{i}, \mathbf{j}$ and $\mathbf{k}$. If the vector components of two resulting quaternions are equalized, three equations, including construction parameters ($\alpha_1, \alpha_2, \alpha_3, \alpha_4$), input parameter ($\varphi$), and output parameter (ψ), will be reached. However, these equations also include γ, in the form of $Cos(\gamma)$ and $Sin(\gamma)$ as variable parameters. Owing to the fact that γ is neither

construction nor input-output parameter, it is not needed during the function generation synthesis problem and it should be eliminated. In the light of this, using algebraic operations and manipulations, three equations are reduced into one equation that is free of γ. After the simplification of this equation, the objective function of spherical four bar mechanism is attained as,

$$C\alpha_2 - C\alpha_1 C\alpha_3 C\alpha_4 + C\alpha_1 C\psi S\alpha_3 S\alpha_4 - S\alpha_1 C\alpha_4 C\psi C\varphi S\alpha_3 - S\alpha_1 C\alpha_3 C\varphi S\alpha_4$$
$$-S\alpha_1 S\alpha_3 S\psi S\varphi = 0 \tag{6.6}$$

where, S and C stand for sine and cosine of the angles respectively. On the other hand, when Equation (6.6) is inspected, it can be seen that there exist only four design parameters ($\alpha_1, \alpha_2, \alpha_3, \alpha_4$). Hence, the pole positions of the input link φ_0 and the output link ψ_0 is selected to fulfill the place of the remaining two parameters. When φ and ψ are replaced with ($\varphi_0 + \varphi_i$) and ($\psi_0 + \psi_i$) respectively in Equation (6.6), the new objective function of the six independent parameters function generation synthesis of spherical four bar mechanism in open form will become,

$$C\alpha_2 - C\alpha_1 C\alpha_3 C\alpha_4 + C\alpha_1 S\alpha_3 S\alpha_4 C\psi_0 C\psi_i - C\alpha_1 S\alpha_3 S\alpha_4 S\psi_0 S\psi_i - C\alpha_3 S\alpha_1 S\alpha_4 C\varphi_0 C\varphi_i$$
$$+C\alpha_3 S\alpha_1 S\alpha_4 S\varphi_0 S\varphi_i - C\alpha_4 S\alpha_1 S\alpha_3 C\psi_0 C\varphi_0 C\psi_i C\varphi_i + S\alpha_1 S\alpha_3 S\psi_0 S\varphi_0 C\psi_i C\varphi_i$$
$$-S\alpha_1 S\alpha_3 C\psi_0 C\varphi_0 S\psi_i S\varphi_i + C\alpha_4 S\alpha_1 S\alpha_3 S\psi_0 S\varphi_0 S\psi_i S\varphi_i + C\alpha_4 S\alpha_1 S\alpha_3 C\varphi_0 S\psi_0 C\varphi_i S\psi_i \tag{6.7}$$
$$-S\alpha_1 S\alpha_3 C\psi_0 S\varphi_0 C\varphi_i S\psi_i + C\alpha_4 S\alpha_1 S\alpha_3 C\psi_0 S\varphi_0 C\psi_i S\varphi_i - S\alpha_1 S\alpha_3 C\varphi_0 S\psi_0 C\psi_i S\varphi_i = 0$$

Note that the new objective function (set of equations $i = 1, 2, .., 6$) includes six independent parameters ($\varphi_0, \psi_0, \alpha_1, \alpha_2, \alpha_3, \alpha_4$) to design.

6.2. Interpolation Approximation

Before proceeding further, dividing both sides by $S\alpha_1 S\alpha_3 S\psi_0 S\varphi_0$ Equation (6.7) can be rewritten in a polynomial form as,

$$\sum_{j=0}^{11} P_j f_j^i - F_i = 0, \ (i = 1, 2, .., 6) \tag{6.8}$$

where, the constant parameters are,

$$P_0 = (C\alpha_2 - C\alpha_1 C\alpha_3 C\alpha_4)/(S\alpha_1 S\alpha_3 S\psi_0 S\varphi_0), \quad P_1 = -C\alpha_4, \quad P_2 = -Cot\psi_0,$$
$$P_3 = -Cot\alpha_1 S\alpha_4 / S\varphi_0, \quad P_4 = Cot\alpha_3 S\alpha_4 / S\psi_0, \quad P_5 = -Cot\varphi_0, \quad P_6 = P_2 P_3,$$
$$P_7 = P_4 P_5, \quad P_8 = P_1 P_2 P_5, \quad P_9 = P_1 P_2, \quad P_{10} = -P_2 P_5, \quad P_{11} = P_1 P_5$$

and the continuous independent functions are,

$$f_0^i = 1, \quad f_1^i = S\psi_i S\varphi_i, \quad f_2^i = S\psi_i C\varphi_i, \quad f_3^i = S\psi_i, \quad f_4^i = S\varphi_i, \quad f_5^i = C\psi_i S\varphi_i, \quad f_6^i = C\psi_i,$$
$$f_7^i = C\varphi_i, \quad f_8^i = C\psi_i C\varphi_i, \quad f_9^i = f_5^i, \quad f_{10}^i = f_1^i, \quad f_{11}^i = f_2^i, \quad F_i = f_8^i, \quad (i = 1, 2, .., 6)$$

It is apparent that, in Equation (6.8), there exist six unknowns $\{P_j\}_0^5$, and six

nonlinear terms $\{P_j\}_6^{11}$. If the nonlinear terms are rewritten in terms of nonlinear

operators $\{\lambda_k\}_1^6$, a new set of equations will be reached as,

$$P_2 P_3 - \lambda_1 = 0, \quad P_4 P_5 - \lambda_2 = 0$$
$$P_1 P_2 P_5 - \lambda_3 = 0, \quad P_1 P_2 - \lambda_4 = 0 \qquad\qquad (6.9)$$
$$-P_2 P_5 - \lambda_5 = 0, \quad P_1 P_5 - \lambda_6 = 0$$

where, $P_6 = \lambda_1, P_7 = \lambda_2, P_8 = \lambda_3, P_9 = \lambda_4, P_{10} = \lambda_5, P_{11} = \lambda_6$. If the terms with nonlinear

operators are gathered to the same side of the equation, Equation (6.8) becomes,

$$\sum_{j=0}^{5} P_j f_j^i = f_8^i - \lambda_1 f_6^i - \lambda_2 f_7^i - \lambda_3 f_8^i - \lambda_4 f_5^i - \lambda_5 f_1^i - \lambda_6 f_2^i, \quad (i = 1, 2, .., 6) \quad (6.10)$$

Now, all the terms on the left side of Equation (6.10) is linear, so that the unknown

parameters $\{P_j\}_0^5$ can be assumed as linearly proportional with the nonlinear operators

as,

$$P_j = l_j + m_j \lambda_1 + n_j \lambda_2 + p_j \lambda_3 + q_j \lambda_4 + r_j \lambda_5 + s_j \lambda_6, \quad (j = 0, 1, .., 5) \qquad (6.11)$$

If Equation (6.11) is inserted into Equation (6.10), and the parameters with the same

nonlinear operators are equalized, 42 equations with 42 unknowns

$(l_j, m_j, n_j, p_j, q_j, r_j, s_j \quad j = 0, 1, .., 5)$ will be reached. These equations can be written in

matrix form as below,

$$
\begin{bmatrix}
[A]_{6x6} & . & . & . & . & . & . \\
. & [A]_{6x6} & . & . & . & . & . \\
. & . & [A]_{6x6} & . & . & . & . \\
. & . & . & [A]_{6x6} & . & . & . \\
. & . & . & . & [A]_{6x6} & . & . \\
. & . & . & . & . & [A]_{6x6} & . \\
. & . & . & . & . & . & [A]_{6x6}
\end{bmatrix}
\begin{bmatrix} L \\ M \\ N \\ P \\ Q \\ R \\ S \end{bmatrix}
=
\begin{bmatrix} T \\ U \\ V \\ W \\ Y \\ Z \\ G \end{bmatrix}
\qquad (6.12)
$$

where,

$$
A = \begin{bmatrix}
\{f_j^1\}_0^5 \\
\{f_j^2\}_0^5 \\
\{f_j^3\}_0^5 \\
\{f_j^4\}_0^5 \\
\{f_j^5\}_0^5 \\
\{f_j^6\}_0^5
\end{bmatrix},
$$

$$
\begin{array}{ll}
L = [\{l_k\}_0^5]^T & T = [\{f_8^i\}_1^6]^T \\
M = [\{m_k\}_0^5]^T & U = [\{-f_6^i\}_1^6]^T \\
N = [\{n_k\}_0^5]^T & V = [\{-f_7^i\}_1^6]^T \\
P = [\{p_k\}_0^5]^T, & W = [\{-f_8^i\}_1^6]^T \\
Q = [\{q_k\}_0^5]^T & Y = [\{-f_5^i\}_1^6]^T \\
R = [\{r_k\}_0^5]^T & Z = [\{-f_1^i\}_1^6]^T \\
S = [\{s_k\}_0^5]^T & G = [\{-f_2^i\}_1^6]^T
\end{array}
$$

Solution of Equation (6.12) will give the unknowns $(l_j, m_j, n_j, p_j, q_j, r_j, s_j \; j = 0,1,..,5)$. After substituting them into Equations (6.9 & 6.11), six nonlinear equations with six unknown nonlinear operators $\{\lambda_k\}_1^6$ are attained. Solving these equations numerically for nonlinear operators and inserting one of the real solutions into the Equation (6.11), $\{P_j\}_0^5$ can be calculated and the six construction parameters will become,

$$
\psi_0 = Cot^{-1}(-P_2), \quad \varphi_0 = Cot^{-1}(-P_5), \quad \alpha_4 = Cos^{-1}(-P_1), \quad \alpha_1 = Cot^{-1}(-P_3 S\varphi_0 / S\alpha_4)
$$
$$
\alpha_3 = Cot^{-1}(P_4 S\psi_0 / S\alpha_4), \quad \alpha_2 = Cos^{-1}(S\alpha_1 S\alpha_3 S\psi_0 S\varphi_0 + C\alpha_1 C\alpha_3 C\alpha_4)
$$
$$
(6.13)
$$

6.2.1. Numerical Example

In the case of numerical example, the input of the mechanism is decided to be selected from an interval of $2\pi/3 < \varphi < 4\pi/3$, the output function is selected as $\psi = \varphi^{0.8}$, and the six design points in prescribed interval are given with respect to the Chebyshev spacing. The given design points and the calculated construction parameters

are tabulated in Table 6.1. Also the designed spherical four bar mechanism and the plot of its objective function in the design interval can be seen in Figure 6.3.

Table 6.1. Given design points and calculated construction parameters for NE 6.2.1.

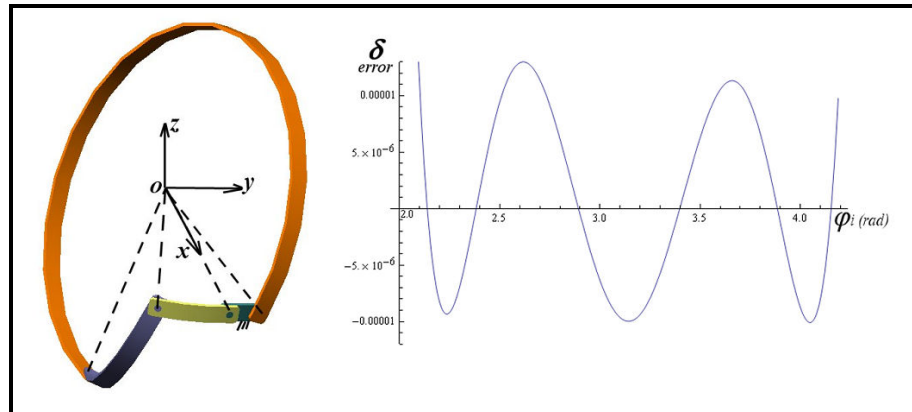| i	1	2	3	4	5	6
$\varphi_i(rad)$	2.13008	2.40111	2.87056	3.41263	3.88207	4.15311
$\psi_i(rad)$	1.83112	2.01525	2.32473	2.66975	2.95972	3.12391
Construction Parameters	$\varphi_0(rad)$	$\psi_0(rad)$	$\alpha_1(rad)$	$\alpha_2(rad)$	$\alpha_3(rad)$	$\alpha_4(rad)$
	1.23867	-0.52161 (5.76158)	0.38103	1.32361	-1.49412 (4.78907)	0.17546

Figure 6.3. Designed spherical four bar mechanism and its objective function.

Note that the objective function takes its zero values only at the six precision points that are equal to the six design points as expected. Although the errors in intervals between the precision points seem to be uniform, there are small deviations on the extremum values.

6.3. Least Square Approximation

In the previous section, the fitting error was $\delta = F(\varphi_i, \overline{c}) - F(\varphi_i)$, where $\overline{c}$ stands for the construction parameters, $F(\varphi_i)$ is the actual function, and $F(\varphi_i, \overline{c})$ is the predicted function from the given design points. As a result, the fitting error vanishes at

the six design points. However, in that specific example, number of design points that are given just equal to the number of unknown parameters. Now consider the case when the design points are over determined; that is, number of design points n are greater than the number of construction parameters m.

The problem can be solved by using least square approximation method to find the best fitting function with respect to the given design point set. The least square approximation method suggests that, the best fitting function is reached when the sum of squared fitting errors (η) is a minimum.

$$\eta = \sum_{i=1}^{n} \delta^2 = \sum_{i=1}^{n} (F(\varphi_i, \overline{c}) - F(\varphi_i))^2 \qquad (6.14)$$

The minimum η is reached if and only if when the partial derivations of Equation (6.14) with respect to the construction parameters are zero.

$$\frac{\partial \eta}{\partial P_j} = 0, \ (j = 0, 1, ..., l) \qquad (6.15)$$

Using Equation (6.15), $l+1$ equations ($l = m-1$) are generated for the same amount of construction parameters and should be solved with respect to the given design conditions.

For the synthesis problem of this study, Equation (6.14) can be rewritten as,

$$\eta = \sum_{i=1}^{n} (\sum_{j=0}^{11} (P_j f_j^i) - F_i)^2 \qquad (6.16)$$

If Equation (6.11) is inserted into Equations (6.15 & 6.16), and the parameters with the same nonlinear operators are equalized, 42 equations with 42 unknowns can be written in matrix form,

$$
\begin{bmatrix}
[B]_{6x6} & \cdot & \cdot & \cdot & \cdot & \cdot & \cdot \\
\cdot & [B]_{6x6} & \cdot & \cdot & \cdot & \cdot & \cdot \\
\cdot & \cdot & [B]_{6x6} & \cdot & \cdot & \cdot & \cdot \\
\cdot & \cdot & \cdot & [B]_{6x6} & \cdot & \cdot & \cdot \\
\cdot & \cdot & \cdot & \cdot & [B]_{6x6} & \cdot & \cdot \\
\cdot & \cdot & \cdot & \cdot & \cdot & [B]_{6x6} & \cdot \\
\cdot & \cdot & \cdot & \cdot & \cdot & \cdot & [B]_{6x6}
\end{bmatrix}
\begin{bmatrix} L \\ M \\ N \\ P \\ Q \\ R \\ S \end{bmatrix}
=
\begin{bmatrix} T^* \\ U^* \\ V^* \\ W^* \\ Y^* \\ Z^* \\ G^* \end{bmatrix}
\quad (6.17)
$$

where,

$$
B = \begin{bmatrix}
[f_0^i f_0^i] & [f_0^i f_1^i] & [f_0^i f_2^i] & [f_0^i f_3^i] & [f_0^i f_4^i] & [f_0^i f_5^i] \\
[f_1^i f_0^i] & [f_1^i f_1^i] & [f_1^i f_2^i] & [f_1^i f_3^i] & [f_1^i f_4^i] & [f_1^i f_5^i] \\
[f_2^i f_0^i] & [f_2^i f_1^i] & [f_2^i f_2^i] & [f_2^i f_3^i] & [f_2^i f_4^i] & [f_2^i f_5^i] \\
[f_3^i f_0^i] & [f_3^i f_1^i] & [f_3^i f_2^i] & [f_3^i f_3^i] & [f_3^i f_4^i] & [f_3^i f_5^i] \\
[f_4^i f_0^i] & [f_4^i f_1^i] & [f_4^i f_2^i] & [f_4^i f_3^i] & [f_4^i f_4^i] & [f_4^i f_5^i] \\
[f_5^i f_0^i] & [f_5^i f_1^i] & [f_5^i f_2^i] & [f_5^i f_3^i] & [f_5^i f_4^i] & [f_5^i f_5^i]
\end{bmatrix},
$$

$$
\begin{aligned}
T^* &= [[f_8^i f_0^i][f_8^i f_1^i][f_8^i f_2^i][f_8^i f_3^i][f_8^i f_4^i][f_8^i f_5^i]]^T \\
U^* &= [-[f_6^i f_0^i]-[f_6^i f_1^i]-[f_6^i f_2^i]-[f_6^i f_3^i]-[f_6^i f_4^i]-[f_6^i f_5^i]]^T \\
V^* &= [-[f_7^i f_0^i]-[f_7^i f_1^i]-[f_7^i f_2^i]-[f_7^i f_3^i]-[f_7^i f_4^i]-[f_7^i f_5^i]]^T \\
W^* &= [-[f_8^i f_0^i]-[f_8^i f_1^i]-[f_8^i f_2^i]-[f_8^i f_3^i]-[f_8^i f_4^i]-[f_8^i f_5^i]]^T \\
Y^* &= [-[f_5^i f_0^i]-[f_5^i f_1^i]-[f_5^i f_2^i]-[f_5^i f_3^i]-[f_5^i f_4^i]-[f_5^i f_5^i]]^T \\
Z^* &= [-[f_1^i f_0^i]-[f_1^i f_1^i]-[f_1^i f_2^i]-[f_1^i f_3^i]-[f_1^i f_4^i]-[f_1^i f_5^i]]^T \\
G^* &= [-[f_2^i f_0^i]-[f_2^i f_1^i]-[f_2^i f_2^i]-[f_2^i f_3^i]-[f_2^i f_4^i]-[f_2^i f_5^i]]^T
\end{aligned}
$$

and, $[f_j^i f_k^i] = \sum\limits_{i=1}^{n} f_j^i f_k^i$.

From this point, following the same analogy, the solution of Equation (6.17) will give the unknowns $(l_j, m_j, n_j, p_j, q_j, r_j, s_j \ j = 0,1,..,5)$. Inserting these parameters into Equations (6.9 & 6.11) and solving the equations numerically for nonlinear operators $\{\lambda_k\}_1^6$, Equations (6.11 & 6.13) can be used to find construction parameters $(\varphi_0, \psi_0, \alpha_1, \alpha_2, \alpha_3, \alpha_4)$.

6.3.1. Numerical Example

Using the same interval ($2\pi/3 < \varphi < 4\pi/3$), and the output function ($\psi = \varphi^{0.8}$), fourteen design points in prescribed interval is given again with respect to the Chebyshev spacing. The given design points and the calculated construction parameters are tabulated in Table 6.2. Also the plot of the designed mechanisms objective function and the sum of squared fitting errors η with the mean of η in the design interval can be seen in Figure 6.4.

Table 6.2. Given design points and calculated construction parameters for NE 6.3.1.

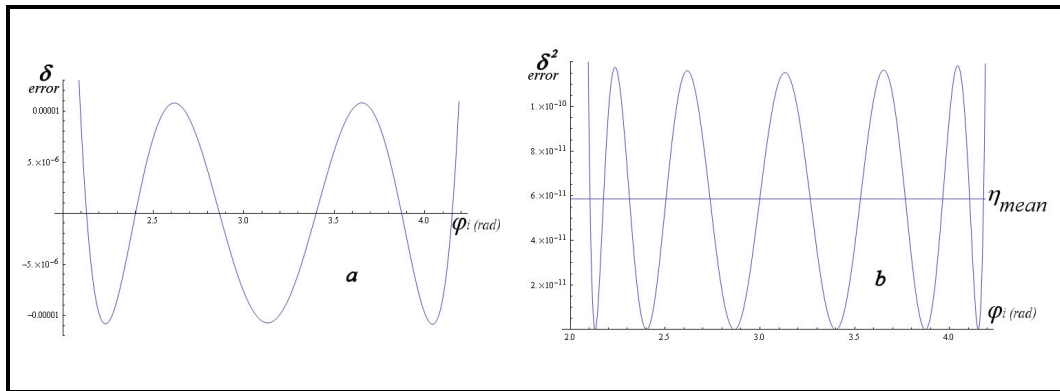| i	1	2	3	4	5	6	7
$\varphi_i(rad)$	2.10098	2.15316	2.25491	2.40111	2.58445	2.79573	3.02434
$\psi_i(rad)$	1.81108	1.84698	1.91647	2.01525	2.13744	2.27612	2.42385
i	8	9	10	11	12	13	14
$\varphi_i(rad)$	3.25884	3.48746	3.69874	3.88207	4.02828	4.13002	4.18221
$\psi_i(rad)$	2.57306	2.71649	2.84736	2.95972	3.04857	3.11001	3.14141
Construction Parameters	$\varphi_0(rad)$	$\psi_0(rad)$	$\alpha_1(rad)$	$\alpha_2(rad)$	$\alpha_3(rad)$	$\alpha_4(rad)$	
	1.24252	-0.51943 (5.76376)	0.38098	1.32458	-1.49467 (4.78852)	0.17518	

Figure 6.4. a) Objective function of the designed spherical four bar mechanism
b) Sum of squared fitting errors η with η_{mean}

It is important to note that, although 14 design points are given, the fitting error vanishes only at six precision points. Also, when compared with the previous method, the values of the construction parameters ($\varphi_0, \psi_0, \alpha_1, \alpha_2, \alpha_3, \alpha_4$) are close but different. This small difference on the other hand affects the extremum values of the fitting errors; that is, the max or min errors in intervals between the precision points are more uniform than the previous results.

6.4. Chebyshev Approximation

Although the square approximation gives the reasonable results for the fitting error extremums in the design interval, the errors are not equal. Knowing that the best fitting error function, in this study the objective function, will be reached when it oscillates between an error bound of $\pm\Gamma$ with maximum absolute error Γ in each

sections in the design interval (Equation 6.18), Chebyshev approximation method is decided to be used to in the synthesis problem.

$$\left| F(\varphi_i, \overline{c}) - F(\varphi_i) \right| = \Gamma, \quad (i = 1, 2, ..., n) \tag{6.18}$$

Consider that the objective function is in the form of,

$$\sum_{j=0}^{l} P_j f_j + \sum_{j=l+1}^{l+k} P_j f_j - F = \delta \tag{6.19}$$

where, k is the number of nonlinear parameters. The function in Equation (6.19) consecutively changes sign $(l+2)$ times, so that it has $(l+2)$ extremums in the design interval, where two of them are the boundary precision points. Due to the fact that max/min error value $\pm\Gamma$ is also being searched to bind the objective function at the given design points in the design interval, Γ should be defined as a design parameter in synthesis equation that is again assumed to be linearly proportional with the nonlinear operators as,

$$\Gamma = l_6 + m_6\lambda_1 + n_6\lambda_2 + p_6\lambda_3 + q_6\lambda_4 + r_6\lambda_5 + s_6\lambda_6 \tag{6.20}$$

As a result, total number of parameters to be calculated with needed design points will increase by one, and Equation (6.18) can be rewritten to form $n = l + 2$ equations.

$$\sum_{j=0}^{11} P_j f_j^i - F_i = (-1)^{i+1}\Gamma, \quad (i = 1, 2, ..., 7) \tag{6.21}$$

If Equation (6.11) is inserted into Equation (6.21), and the parameters with the same nonlinear operators are equalized, 49 equations with 49 unknowns can be written in matrix form as,

$$
\begin{bmatrix}
[C]_{7x7} & . & . & . & . & . & . \\
. & [C]_{7x7} & . & . & . & . & . \\
. & . & [C]_{7x7} & . & . & . & . \\
. & . & . & [C]_{7x7} & . & . & . \\
. & . & . & . & [C]_{7x7} & . & . \\
. & . & . & . & . & [C]_{7x7} & . \\
. & . & . & . & . & . & [C]_{7x7}
\end{bmatrix}
\begin{bmatrix}
L^* \\ M^* \\ N^* \\ P^* \\ Q^* \\ R^* \\ S^*
\end{bmatrix}
=
\begin{bmatrix}
T^{**} \\ U^{**} \\ V^{**} \\ W^{**} \\ Y^{**} \\ Z^{**} \\ G^{**}
\end{bmatrix}
\quad (6.22)
$$

where,

$$
C=\begin{bmatrix}
\{f_j^1\}_0^5 & -1 \\
\{f_j^2\}_0^5 & 1 \\
\{f_j^3\}_0^5 & -1 \\
\{f_j^4\}_0^5 & 1 \\
\{f_j^5\}_0^5 & -1 \\
\{f_j^6\}_0^5 & 1 \\
\{f_j^7\}_0^5 & -1
\end{bmatrix},
$$

$$
\begin{aligned}
L^* &= [\{l_k\}_0^6]^T & T^{**} &= [\{f_8^i\}_1^7]^T \\
M^* &= [\{m_k\}_0^6]^T & U^{**} &= [\{-f_6^i\}_1^7]^T \\
N^* &= [\{n_k\}_0^6]^T & V^{**} &= [\{-f_7^i\}_1^7]^T \\
P^* &= [\{p_k\}_0^6]^T & W^{**} &= [\{-f_8^i\}_1^7]^T \\
Q^* &= [\{q_k\}_0^6]^T & Y^{**} &= [\{-f_5^i\}_1^7]^T \\
R^* &= [\{r_k\}_0^6]^T & Z^{**} &= [\{-f_1^i\}_1^7]^T \\
S^* &= [\{s_k\}_0^6]^T & G^{**} &= [\{-f_2^i\}_1^7]^T
\end{aligned}
$$

Using again the same analogy, the solution of Equation (6.22) will give the unknowns $(l_j, m_j, n_j, p_j, q_j, r_j, s_j \ \ j=0,1,..,6)$. Inserting the unknowns into Equation (6.9), and solving numerically for nonlinear operators $\{\lambda_k\}_1^6$, Equations (6.11, 6.13 & 6.20) can be used to find construction parameters $(\varphi_0, \psi_0, \alpha_1, \alpha_2, \alpha_3, \alpha_4)$ and fitting error limit Γ. After the parameters are calculated, the derivative of Equation (6.21) with respect to φ_i is taken and its function is drawn in the design interval to find $(n-2)$ roots of the derivative equation. As the roots are the extremums of the generated objective function with the synthesized parameters, they will become new φ_i values with the previous boundary precision points. Newer construction parameters and fitting error limit Γ will be recalculated by using Equations (6.22, 6.9, 6.11, 6.20 & 6.13) in this order. This consecutive process should be continued until Equation (6.18) is satisfied.

6.4.1. Numerical Example

Picking the same interval $(2\pi/3 < \varphi < 4\pi/3)$, and the output function $(\psi = \varphi^{0.8})$, seven design points in prescribed interval is given with respect to the

Chebyshev spacing. The given design points and the calculated construction parameters are tabulated in Table 6.3 for each consecutive trials until the construction parameters are not changing in five decimals and the Equation (6.18) is satisfied. Also the plot of the designed mechanisms objective function and its derivative in the design interval can be seen in Figure 6.5 for trial 1 and trial 2 as the change between them is more visible.

When the results are compared with both of the previous methods, the values of the construction parameters ($\varphi_0, \psi_0, \alpha_1, \alpha_2, \alpha_3, \alpha_4$) are too close again. However, by using Chebyshev approximation, at the end of the forth trial the fitting errors are equalized for each of the extremum values. Note that, unlike the first method, design points in Chebyshev approximation are the points, where the fitting error reaches its extremum values in the design interval. Also the fitting error still vanishes at the six precision points.

Table 6.3. Given design points and calculated construction parameters for NE 6.4.1.

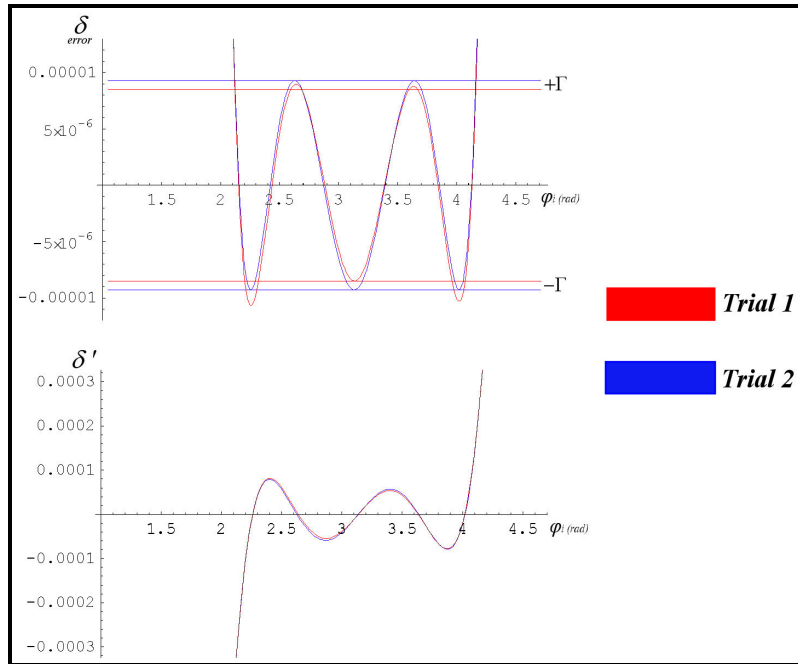| Trial 1	1	2	3	4	5	6	7
$\varphi_i (rad)$	2.12065	2.32286	2.68723	3.14159	3.59595	3.96032	4.16253
$\psi_i (rad)$	1.82463	1.96254	2.20518	2.49873	2.78389	3.00735	3.12958
Construction Parameters	$\varphi_0 (rad)$	$\psi_0 (rad)$	$\alpha_1 (rad)$	$\alpha_2 (rad)$	$\alpha_3 (rad)$	$\alpha_4 (rad)$	Γ
	1.24133	-0.52034 (5.76285)	0.37989	1.32471	-1.49455 (4.78864)	0.17462	8.48283 10^{-6}
Trial 2	1	2	3	4	5	6	7
$\varphi_i (rad)$	2.12065	2.25868	2.63882	3.13495	3.63403	4.02038	4.16253
$\psi_i (rad)$	1.82463	1.91904	2.17335	2.49451	2.80745	3.04379	3.12958
Construction Parameters	$\varphi_0 (rad)$	$\psi_0 (rad)$	$\alpha_1 (rad)$	$\alpha_2 (rad)$	$\alpha_3 (rad)$	$\alpha_4 (rad)$	Γ
	1.24225	-0.51978 (5.76341)	0.38008	1.32487	-1.49468 (4.78851)	0.17467	9.26939 10^{-6}
Trial 3	1	2	3	4	5	6	7
$\varphi_i (rad)$	2.12065	2.25770	2.62865	3.13255	3.64097	4.02100	4.16253
$\psi_i (rad)$	1.82463	1.91838	2.16664	2.49298	2.81174	3.04416	3.12958
Construction Parameters	$\varphi_0 (rad)$	$\psi_0 (rad)$	$\alpha_1 (rad)$	$\alpha_2 (rad)$	$\alpha_3 (rad)$	$\alpha_4 (rad)$	Γ
	1.24227	-0.51977 (5.76342)	0.38008	1.32488	-1.49468 (4.78851)	0.17467	9.27502 10^{-6}
Trial 4	1	2	3	4	5	6	7
$\varphi_i (rad)$	2.12065	2.25775	2.62866	3.13247	3.64093	4.02096	4.16253
$\psi_i (rad)$	1.82463	1.91841	2.16665	2.49293	2.81171	3.04414	3.12958
Construction Parameters	$\varphi_0 (rad)$	$\psi_0 (rad)$	$\alpha_1 (rad)$	$\alpha_2 (rad)$	$\alpha_3 (rad)$	$\alpha_4 (rad)$	Γ
	1.24227	-0.51977 (5.76342)	0.38008	1.32488	-1.49468 (4.78851)	0.17467	9.27502 10^{-6}

Figure 6.5. Objective function of the designed spherical four bar mechanism and its derivative in trial 1 and trial 2

6.5. Discussion (Spherical Four Bar)

Although the synthesis methods shown up to this point are applied only to spherical four bar mechanism, they are also valid for more common planar four bar function generators (similarly the joint axes are intersecting at infinity) as well as other mechanisms. On the other hand, it should be noted that the maximum number of independent parameters that can be synthesized in planar four bar function generators are limited to five (φ_0, ψ_0, a, b, c) due to the ability of scaling (Figure 6.6).
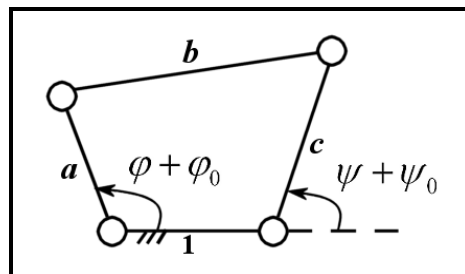

Figure 6.6. Parameters of planar four bar mechanism function generator.

On the calculation side, the reason behind the usage of the quaternion algebra in order to find the objective function of the mechanism is the simplicity of the tool for the rotations and the spherical four bar mechanism is just composed of rotational sequences. Moreover, the non-linear equations that are used to find the non-linear operators $\{\lambda_k\}_1^6$ in each example are solved numerically by using Mathematica software. Also, as an alternative method used by many authors in literature, the non-linear equation sets can be reduced into one equation with only one variable of non-linear operator in some order and again solved numerically in the end, if the order is high to solve analytically. After the results are acquired, the synthesized mechanisms are controlled in the simulation environment with respect to the calculated independent parameters. Note that as a different constraint additional conditions as rotability, branch and circuit defect elimination can also be controlled after the synthesis problem in other studies.

It is important that, the strategy followed up to this point by using introduced methodologies is error based. The aim is not only to reduce the error but also to bind the error into some limits $\pm\Gamma$ so that the maximum absolute error in each interval between the precision points will be the same and oscillates back and forth in that interval. The Chebyshev approximation gave the best results in that manner with respect to the given examples. Also, throughout the chapter the notion *"design points"* are used for the points that are given by the designer and the *"precision points"* are used for the points where the objective function of the synthesized mechanism takes zero values.

It should also be noted that, during the consecutive trials in Chebyshev approximation, a new approach is taken to renew the precision points φ_i. As it is not an easy task to find the precision points from the equations generated by the derivation of Equation (6.21) with respect to φ_i, and equating them to zero, function of the derived equation is drawn in the design interval to compute $(n-2)$ roots. Afterwards, these roots are used as new φ_i values with the previous boundary design points for the next trial. At the end of each method, a numerical example is given providing that the design intervals and the output function remains the same. Although values of the construction parameters $\varphi_0, \psi_0, \alpha_1, \alpha_2, \alpha_3$, and α_4 of the three designed spherical four bar mechanisms are near, the generated objective functions and their fitting errors differ (Figure 6.7).
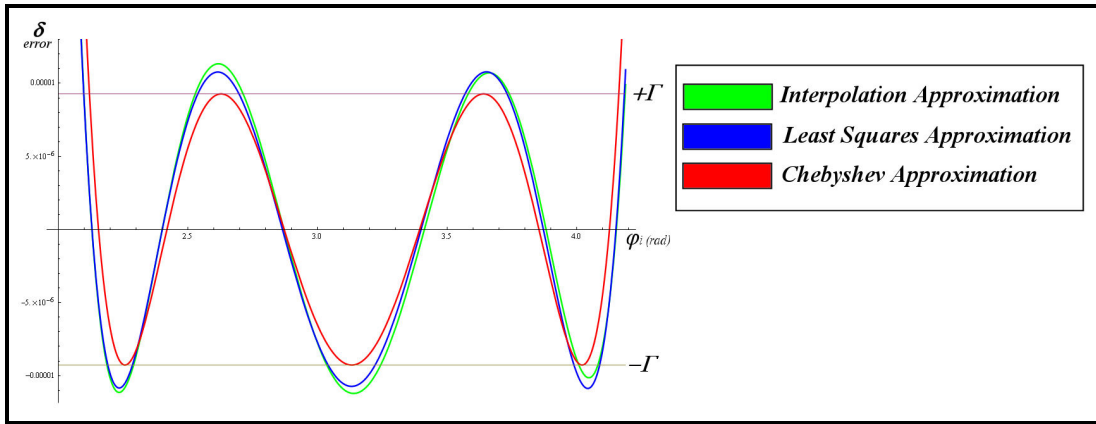
Figure 6.7. Objective functions of the designed spherical four bar mechanisms for three different methods

As it can be seen in Figure 6.7, interpolation approximation generates the highest fitting error, and also the error values at the extremums are not equal. On the other hand, least squares approximation decreased the highest fitting error value when compared with the interpolation approximation. However, the fitting error extremums are still not bounded in the same error values. Finally by using Chebyshev approximation, after the fourth trial, not only the maximum fitting error values are decreased with respect to the previous methods, but also the objective function starts to oscillate between an error bound of $\pm\Gamma$ with maximum absolute error Γ.

6.6. Dual Quaternions in Rigid Body Rotations and Translations

As mentioned earlier the dual quaternions have eight components, where four of them represent real part and the remaining represent the dual part. Although quaternions can only be used for the rotational sequences of the rigid bodies, the addition of this dual part gives the dual quaternions the ability to represent translational motions as well as the rotational motions.

Any dual quaternion operator $Q(\ )Q^{-1}$ can rotate or translate any given vector by the desired amount provided that dual quaternion multiplication is used for the product (Table 2.1). However, it should also be noted that unlike the usual representation, the inverse of the unit dual quaternion Q^{-1} should be taken as the third type conjugate of the dual quaternion (Equation 2.33).

64

To translate a rigid body by a specified amount $\delta_1 = (x_1, y_1, z_1)$ (Figure 6.8), following equation should be used,

$$r_2 = Q(r_1)Q^{-1} \qquad (6.23)$$

where r_1 is the first position of the rigid body $\delta = (x, y, z)$ in the dual quaternion form as $r_1 = 1 + x\varepsilon i + y\varepsilon j + z\varepsilon k$, r_2 is the final position of the rigid body in dual quaternion form and Q will be $Q = 1 + \dfrac{x_1}{2}\varepsilon i + \dfrac{y_1}{2}\varepsilon j + \dfrac{z_1}{2}\varepsilon k$.

Figure 6.8. Translation of rigid body.

To rotate a rigid body by a specified angle α around any axis $\hat{m}$ (Figure 6.9), the same equation can be used (Equation 6.23) However Q should be modified to $Q = Cos(\dfrac{\alpha}{2}) + \hat{m}Sin(\dfrac{\alpha}{2})$.
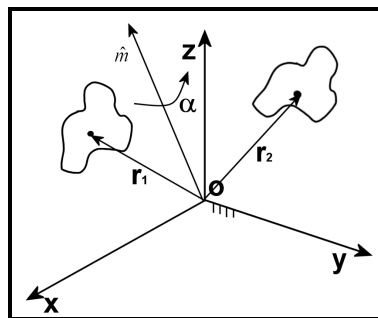

Figure 6.9. Rotation of rigid body.

Also note that for mixed rigid body simultaneous translation and rotation motions, dual quaternion operations can be applied sequentially to the initial position vector.

6.7. Objective Functions

As the previous sections clearly states, the main problem in the synthesis of any mechanism is building its objective function in simplest form by using appropriate algebraic method. Although quaternion algebra was introduced before as an easy and fast tool, it can not be used solely in all mechanisms due to its rotational nature with spherical geometry requirement. On the other hand, using together with the classical vector algebra, quaternions can be applied to other non-spherical mechanisms as well.

In the light of this idea, let's consider subspace $\lambda=5$, M=1 mechanism, where its input is aligned with x_1 axis and the output is aligned with x_2 axis (Figure 6.10).
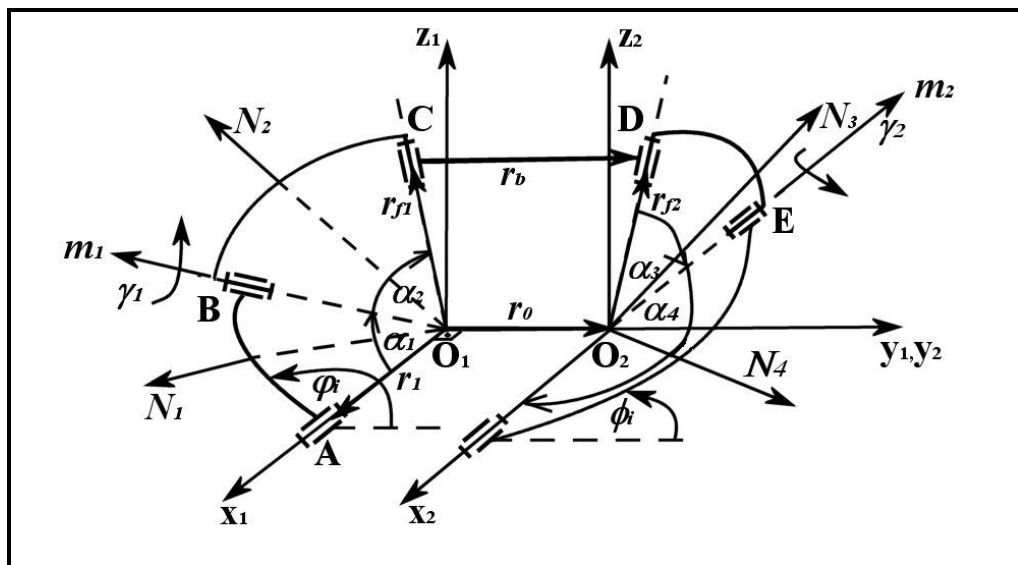

Figure 6.10. Subspace $\lambda=5$, M=1 mechanism.

As it can easily be seen in Figure 6.10, link $|CD|$ will move in the surfaces of two spheres, if the mechanism is actuated. These two spheres are taken to be unit spheres that are just touching each other ($\mathbf{r_0} = 2\mathbf{j}$) for the simplicity of the problem, where the task is to find five unknown construction parameters $\alpha_1, \alpha_2, \alpha_3, \alpha_4$ and $|\mathbf{r_b}|$ by giving

some function $\Phi_i = f(\varphi_i)$ and orientation of link $|CD|$ ($\hat{\mathbf{r}}_{bi}$) in five design points (i=1,2,…,5). The objective function of the task will be generated by using the procedure below.

- The mechanism will be divided into two serial RR spherical manipulators centered in O_1, O_2 and touching one end of the link $|CD|$ with their end effectors (Figure 6.11).

- $\mathbf{r}_{f1}$ and $\mathbf{r}_{f2}$ vectors will be found by applying quaternion algebra in two different but equally oriented coordinate systems.

- Vector loop equation $\mathbf{r}_{f1} + \mathbf{r}_b = \mathbf{r}_0 + \mathbf{r}_{f2}$ will be constructed in any of the coordinate systems to end up with three equations in component wise ($\mathbf{i}, \mathbf{j}, \mathbf{k}$).

- By using these three equations, an objective function will be developed by removing unwanted parameters γ_1 and γ_2.
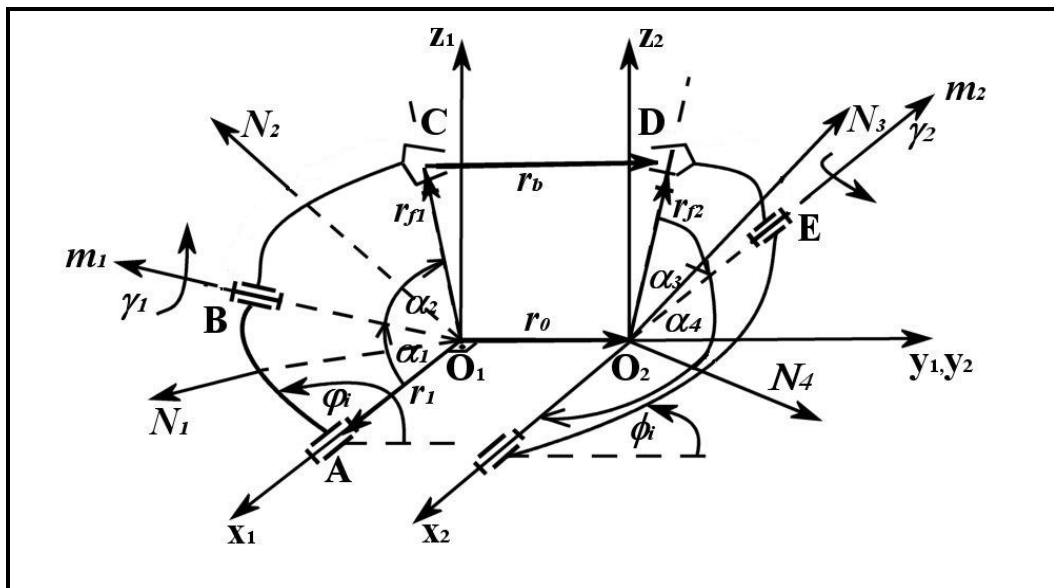

Figure 6.11. Two serial RR spherical manipulators.

Let's start to apply the quaternion algebra to the first half of the mechanism. To reach $\mathbf{r}_{f1}$, $\mathbf{r}_1$ is rotated around the normal of AO_1B plane $\mathbf{N}_1$ by the angle α_1 than the resulting vector is rotated around the normal of BO_1C plane $\mathbf{N}_2$ by the angle α_2.

$$\mathbf{r_{f1}} = q_2 q_1 (\mathbf{r_1}) q_1^{-1} q_2^{-1}$$

$$q_1 = Cos(\frac{\alpha_1}{2}) + \hat{\mathbf{n}}_1 Sin(\frac{\alpha_1}{2}), \ q_2 = Cos(\frac{\alpha_2}{2}) + \hat{\mathbf{n}}_2 Sin(\frac{\alpha_2}{2})$$

(6.24)

Similarly in the second half of the mechanism, To reach $\mathbf{r_{f2}}$, $\mathbf{r_2}$ is rotated around the normal of EO_2F plane $\mathbf{N}_4$ by the angle α_4 than the resulting vector is rotated around the normal of DO_2E plane $\mathbf{N}_3$ by the angle α_3.

$$\mathbf{r_{f2}} = q_4 q_3 (\mathbf{r_2}) q_3^{-1} q_4^{-1}$$

$$q_3 = Cos(\frac{\alpha_4}{2}) + \hat{\mathbf{n}}_4 Sin(\frac{\alpha_4}{2}), \ q_4 = Cos(\frac{\alpha_3}{2}) + \hat{\mathbf{n}}_3 Sin(\frac{\alpha_3}{2})$$

(6.25)

In order to solve Equations (6.24 & 6.25), $\hat{\mathbf{n}}_1, \hat{\mathbf{n}}_2, \hat{\mathbf{n}}_3$ and $\hat{\mathbf{n}}_4$ should clearly be defined. $\hat{\mathbf{n}}_1$ can be reached by rotating the unit vector of z_1 axis $\mathbf{k}$ around x_1 axis by the input angle φ (Equation 6.26), $\hat{\mathbf{n}}_2$ can be reached by rotating $\hat{\mathbf{n}}_1$ around $\hat{\mathbf{m}}_1$ axis by the angle γ_1 (Equation 6.27), $\hat{\mathbf{n}}_4$ can be reached by rotating the negative unit vector of z_2 axis $-\mathbf{k}$ around x_2 axis by the output angle ϕ (Equation 6.28) and $\hat{\mathbf{n}}_3$ can be reached by rotating $\hat{\mathbf{n}}_4$ around $\hat{\mathbf{m}}_2$ axis by the angle γ_2 (Equation 6.29).

$$\hat{\mathbf{n}}_1 = q_5 (\mathbf{k}) q_5^{-1}, \ \ q_5 = Cos(\frac{\varphi}{2}) + \mathbf{i} Sin(\frac{\varphi}{2})$$

(6.26)

$$\hat{\mathbf{n}}_2 = q_6 (\hat{\mathbf{n}}_1) q_6^{-1}, \ \ q_6 = Cos(\frac{\gamma_1}{2}) + \hat{\mathbf{m}}_1 Sin(\frac{\gamma_1}{2}), \ \ \hat{\mathbf{m}}_1 = q_1 (\hat{\mathbf{r}}_1) q_1^{-1}$$

(6.27)

$$\hat{\mathbf{n}}_4 = q_7 (-\mathbf{k}) q_7^{-1}, \ \ q_7 = Cos(\frac{\psi}{2}) + \mathbf{i} Sin(\frac{\psi}{2})$$

(6.28)

$$\hat{\mathbf{n}}_2 = q_8 (\hat{\mathbf{n}}_4) q_8^{-1}, \ \ q_8 = Cos(\frac{\gamma_2}{2}) + \hat{\mathbf{m}}_2 Sin(\frac{\gamma_2}{2}), \ \ \hat{\mathbf{m}}_2 = q_3 (\hat{\mathbf{r}}_2) q_3^{-1}$$

(6.29)

After defining normal vectors, Equations (6.24 & 6.25) can be recalled. Both of the equations result in a quaternion with a null scalar part and three vector components $\mathbf{i}, \mathbf{j}$ and $\mathbf{k}$; so that, as the third step suggested vector loop equation $\mathbf{r_{f1}} + \mathbf{r_b} = \mathbf{r_0} + \mathbf{r_{f2}}$ that includes all of the construction parameters $\alpha_1, \alpha_2, \alpha_3, \alpha_4$ and $|\mathbf{r_b}|$ is constructed.

However, these set of three equations also include γ_1 and γ_2. Due to the fact that γ_1 and γ_2 are neither construction nor input-output parameters, they are not needed during the synthesis problem and should be eliminated. As a result, using algebraic operations and manipulations, three equations should be reduced into one equation, objective function, that is free of γ_1 and γ_2. After the computation of objective function is fulfilled, construction parameters $\alpha_1, \alpha_2, \alpha_3, \alpha_4$ and $|\mathbf{r_b}|$ can be found by using desired synthesis procedure.

In order to verify the results between the mixed algebra and the dual quaternion algebra, let's start with a relatively easier task as the synthesis of RP serial manipulator. As seen in Figure 6.12 the rotation axis of the first revolute joint and the translation axis of the second prismatic joint are intersecting at a common point, which is selected as the origin of the global coordinate system. The task includes the path generation synthesis of the RP manipulator by giving the position of the end effector $(|\boldsymbol{\delta}_i|, \varphi_i, \psi_i)$ and the rotation angle of the first input actuator (θ_i) in desired design points, where their numbers should be equal to the number of construction parameters of the manipulator. Note that in the current task α_1, α_2, and a are taken as the construction parameters so that the number of design points should be three ($i = 1, 2, 3$).
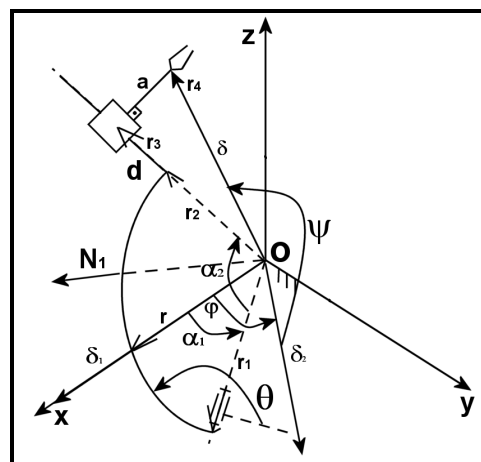

Figure 6.12. Serial RP manipulator.

Now let's start with the objective function generation by using quaternion algebra in accordance with the vector algebra. To reach the position of the end effector,

two distinct ways can be used. The first route includes the construction parameters α_1, α_2, a and actuator inputs θ, d while the second one includes the given parameters $|\delta|, \varphi$ and, ψ. To end up with the gripper position vector $\mathbf{r_4}$ from the first route, the unit vector $\mathbf{r}$ should be rotated around z axis by α_1 degrees; the resultant vector $\mathbf{r_1}$ should be rotated around the normal $\mathbf{N_1}$ by the angle α_2; the resultant vector $\mathbf{r_2}$ should be translated along its axis by d amount and finally $\mathbf{r_3}$ should be translated along the gripper axis by a amount. The calculations of the given procedure can be carried out by using the mixed method as below,

$$\mathbf{r_1} = q_1(\mathbf{r})q_1^{-1}, \ \mathbf{r} = \mathbf{i}, \ q_1 = Cos(\frac{\alpha_1}{2}) + \mathbf{k} \, Sin(\frac{\alpha_1}{2})$$

$$\mathbf{n_1} = q_2(\mathbf{k})q_2^{-1}, \ q_2 = Cos(\frac{\theta_1}{2}) + \mathbf{r_1} \, Sin(\frac{\theta_1}{2})$$

$$\mathbf{r_2} = q_3(\mathbf{r_1})q_3^{-1}, \ q_3 = Cos(\frac{\alpha_2}{2}) + \mathbf{n_1} \, Sin(\frac{\alpha_2}{2}) \qquad (6.30)$$

$$\mathbf{r_3} = \mathbf{r_2} + d \, \mathbf{r_2}$$

$$\mathbf{r'} = q_4(\mathbf{r_2})q_4^{-1}, \ q_4 = Cos(\frac{\pi}{4}) + \mathbf{n_1} \, Sin(\frac{\pi}{4}), \ \mathbf{r_4} = \mathbf{r_3} + a \, \mathbf{r'}$$

where $\mathbf{r'}$ is the direction of the gripper axis and $\mathbf{n_1}$ is the unit vector of the normal $\mathbf{N_1}$. To end up with the gripper position vector $\boldsymbol{\delta}$ from the second route, the vector $\boldsymbol{\delta_1}$ should be rotated around negative y axis by the angle ψ amount and finally the resultant vector $\boldsymbol{\delta_2}$ should be rotated around z axis by the angle φ. The calculations of the given procedure can be carried out by using the mixed method as below,

$$\boldsymbol{\delta_1} = \delta \mathbf{i}, \ \boldsymbol{\delta_2} = q_5(\boldsymbol{\delta_1})q_5^{-1}, \ q_5 = Cos(\frac{\psi}{2}) - j \, Sin(\frac{\psi}{2})$$

$$\boldsymbol{\delta} = q_6(\boldsymbol{\delta_2})q_6^{-1}, \ q_6 = Cos(\frac{\varphi}{2}) + k \, Sin(\frac{\varphi}{2}) \qquad (6.31)$$

By using the results from Equations (6.30 & 6.31), $\mathbf{r_4} = \boldsymbol{\delta}$, three equations in component wise $(\mathbf{i, j, k})$ is constructed. The last step of the objective function generation includes the removal of the unwanted variable parameters from the equation sets to get single equation, objective function, with desired parameters. It should be also

noted that for path generation synthesis the second actuator variable d should be eliminated from the equations. After the elimination procedure the generated objective function can be introduced as,

$$Ca_2\delta_i S\psi_i + Ca_1\delta_i S\psi_i S\theta_i - \frac{S\alpha_1}{S\alpha_2} aS\theta_i - \delta C\psi_i S\varphi_i S\theta_i = 0$$

$$P_0 f_0 + P_1 f_1 + P_2 f_2 - F_i = 0, \ (i = 1, 2, 3)$$

(6.32)

As the current study also focuses on the dual quaternion algebra, the same operations in two distinct routes should be expressed in dual quaternion form. Equations of the first route can be expressed as,

$$\mathbf{r_1} = Q_1(\mathbf{r})Q_1^{-1}, \ \mathbf{r} = 1 + \varepsilon \mathbf{i}, \ Q_1 = Cos(\frac{\alpha_1}{2}) + \mathbf{k} \, Sin(\frac{\alpha_1}{2})$$

$$\mathbf{n_1} = Q_2(1 + \varepsilon \mathbf{k})Q_2^{-1}, \ Q_2 = Cos(\frac{\theta_1}{2}) + \mathbf{r_1} \, Sin(\frac{\theta_1}{2})$$

$$\mathbf{r_2} = Q_3(\mathbf{r_1})Q_3^{-1}, \ Q_3 = Cos(\frac{\alpha_2}{2}) + \mathbf{n_1} \, Sin(\frac{\alpha_2}{2})$$

$$\mathbf{r_3} = Q_4(\mathbf{r_2})Q_4^{-1}, \ Q_4 = 1 + \frac{d\,\mathbf{r}_{2x}}{2}\varepsilon \mathbf{i} + \frac{d\,\mathbf{r}_{2y}}{2}\varepsilon \mathbf{j} + \frac{d\,\mathbf{r}_{2z}}{2}\varepsilon \mathbf{k}$$

(6.33)

$$\mathbf{r'} = Q_5(\mathbf{r_2})Q_5^{-1}, \ Q_5 = Cos(\frac{\pi}{4}) + \mathbf{n_1} \, Sin(\frac{\pi}{4})$$

$$\mathbf{r_4} = Q_6(\mathbf{r'})Q_6^{-1}, \ Q_6 = 1 + \frac{d\,\mathbf{r'}_x}{2}\varepsilon \mathbf{i} + \frac{d\,\mathbf{r'}_y}{2}\varepsilon \mathbf{j} + \frac{d\,\mathbf{r'}_z}{2}\varepsilon \mathbf{k}$$

Equations of the second route can be expressed as,

$$\boldsymbol{\delta}_1 = 1 + \delta \varepsilon \mathbf{i}, \ \boldsymbol{\delta}_2 = Q_7(\boldsymbol{\delta}_1)Q_7^{-1}, \ Q_7 = Cos(\frac{\psi}{2}) - j \, Sin(\frac{\psi}{2})$$

$$\boldsymbol{\delta} = Q_8(\boldsymbol{\delta}_2)Q_8^{-1}, \ Q_8 = Cos(\frac{\varphi}{2}) + k \, Sin(\frac{\varphi}{2})$$

(6.34)

Following the same procedure with the previous method, the same objective function is generated (Equation 6.32). So it is verified that, in the procedures in need of translational motions dual quaternion algebra is solely sufficient.

6.7.1. Numerical Example

After the generation of the objective function of the RP serial manipulator, numerical example can be given to calculate the desired construction parameters α_1, α_2, and a. Using interpolation approximation, three design points are needed to compute the unknown construction parameters. The given parameters and the calculated construction parameters can be seen in Table 6.4.

Table 6.4. Given parameters with calculated construction parameters

θ_i (rad)	δ_i	ψ_i (rad)	φ_i (rad)	α_1 (rad)	α_2 (rad)	a
$\dfrac{\pi}{12}$	3	$\dfrac{\pi}{6}$	$\dfrac{\pi}{9}$			
$\dfrac{\pi}{9}$	6	$\dfrac{\pi}{3}$	$\dfrac{\pi}{3}$	0.951014	0.862584	0.477219
$\dfrac{\pi}{6}$	9	$\dfrac{\pi}{3}$	$\dfrac{\pi}{6}$			

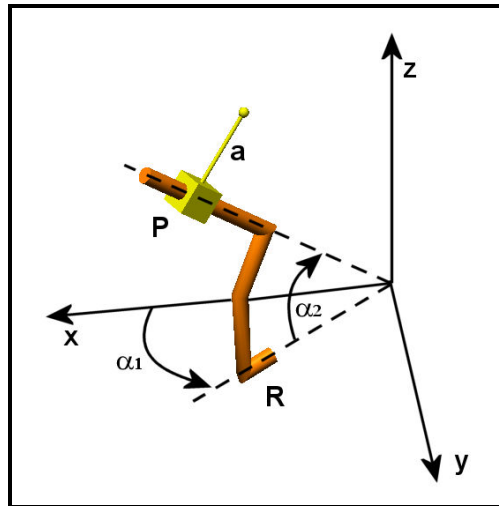The synthesized manipulator can be seen in Figure 6.13.

Figure 6.13. Synthesized serial RP manipulator.

CHAPTER 7

BIOKINEMATIC ANALYSIS OF HUMAN BODY

This chapter of the thesis deals with the type synthesis of the human body by investigating the various important elements of it in terms of their kinematic structure and DoF. Throughout the chapter, each individual joint will be illustrated with their possible achievable motions, and kinematic representations of the joints will be given in terms of their mechanism counterparts. Various examples are introduced with respect to the motion mimicry by using different types of mechanisms and manipulators that includes both new designs and existing designs from the literature. As stated before, further studies can be focused on the combination of related individual mechanism architectures to form one hybrid manipulator to fully mimic human body complexes.

7.1. Human Eyes

Eyes can be categorized as one of the most important organs in human body (Figure 7.1), due to their ability to provide vision.
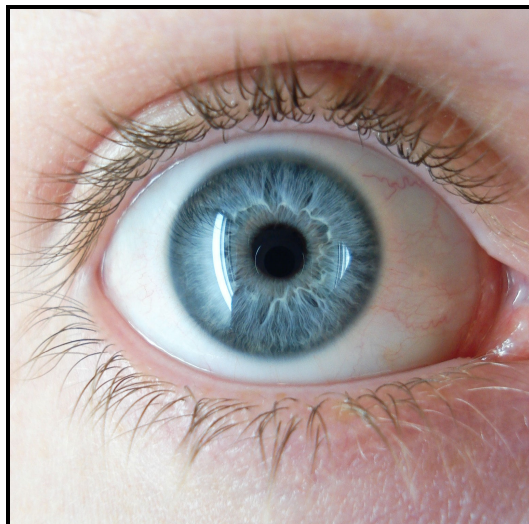

Figure 7.1. Human eye.
(Source: Wikipedia, 2010)

Most of the time, the motion of the eye is thought to be solely voluntary. On the other hand, in order to precisely process images, the brain should compensate for the head motions during body movements by turning the eyes rapidly by involuntary motions. Due to this fact, mobility of the eyes has great importance. Controlled by six muscles, (Figure 7.2), the eye actually has six DoF, which are three rotations and three translations that provide compensation during the motion of the body. However this study will focus on only the three main rotations around the horizontal, vertical and optical axes, due to the fact that translations along the coordinate axes are infinitesimal motions due to the head movements.
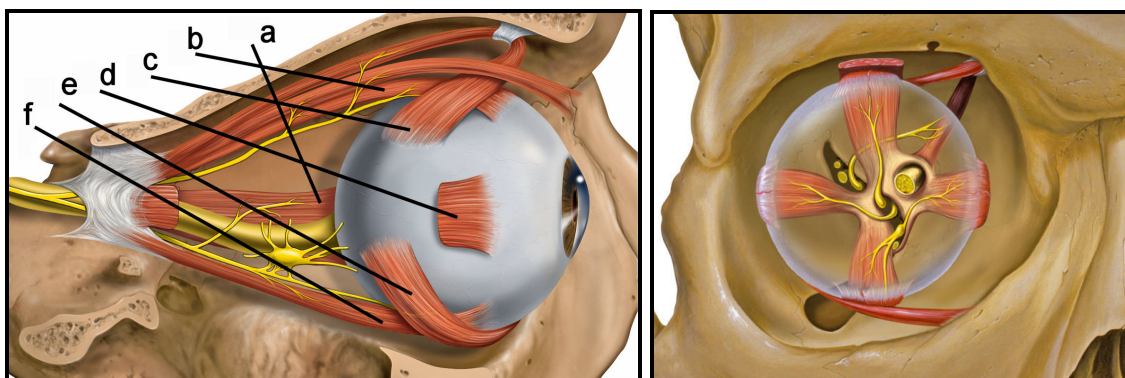

Figure 7.2. Eye muscles: a) Medial rectus, b) Superior rectus, c) Superior oblique, d) Lateral rectus, e) Inferior oblique, f) Inferior rectus. (Source: Wikipedia, 2010)

As it can clearly be seen in Figure 7.3, each pair of the six muscles of the eye is responsible for one individual rotational motion around one of the coordinate axes. Lateral and medial rectus muscles are capable of actuating the eye orientation in the vertical eye axis, inferior and superior rectus eye muscles are capable of actuating the eye orientation in the horizontal eye axis and finally inferior and superior oblique muscles are capable of actuating the eye orientation in the optical eye axis. In conclusion, the total DoF of the single eye can be described as three by omitting the three infinitesimal translational motions. As these three motions are only independent rotations around the axes, appropriate three DoF spherical manipulators can mimic the eye movements. To form a spherical manipulator, first the designer should calculate the number of joints needed to form the manipulator with respect to the given constraints
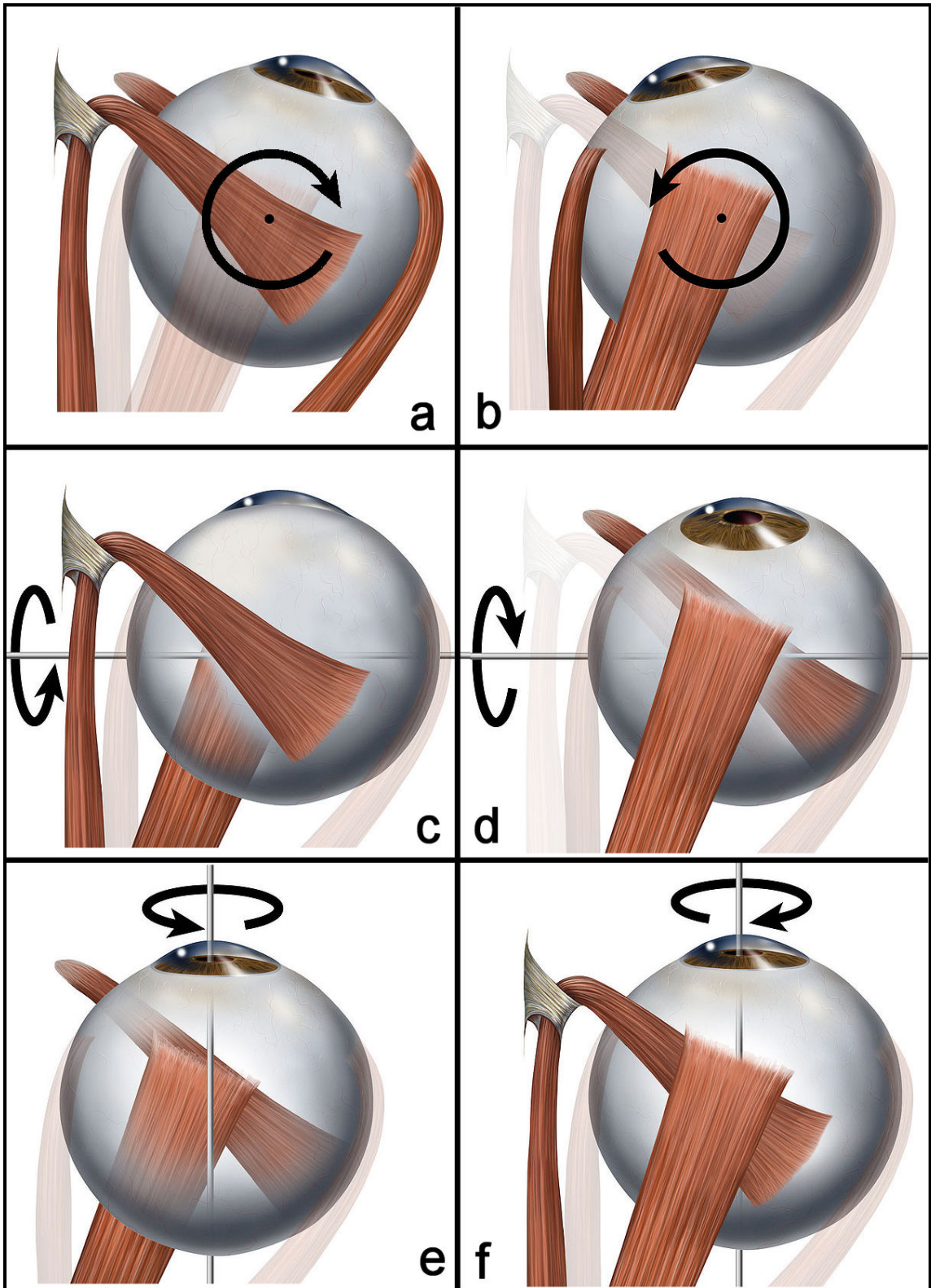
Figure 7.3. Eye movements from the superior view: a) Lateral rectus, b) Medial rectus, c) Inferior rectus, d) Superior rectus, e) Inferior oblique, f) Superior oblique. (Source: Wikipedia, 2010)

and later each of the individual joints should be intersected at a common point. Examples will clarify the idea for both serial and parallel manipulators.

Example 1: Let's construct three DoF serial spherical manipulator that can mimic all of the rotational motions of the human eye. Due to its serial nature, it is clear that the manipulator should have three one degree of freedom motors and the axis of the motors should be intersected at a common point, where the origin of the eye coordinate system is situated (Figure 7.4).
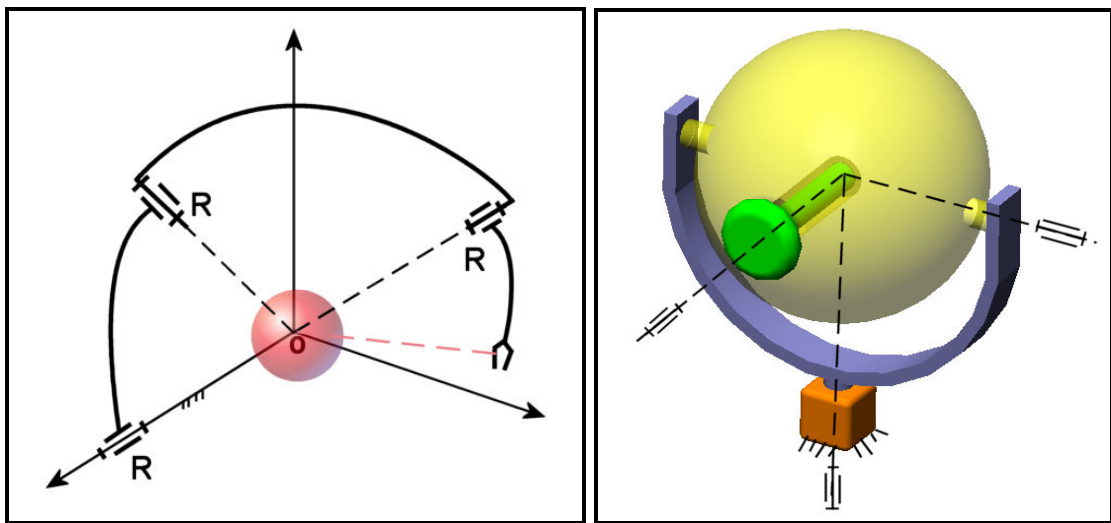
Figure 7.4. Three DoF serial spherical manipulator.

Example 2: Let's construct three DoF parallel spherical platform manipulator that has one triangular platform. Due to its triangular platform the manipulator shall have three legs and therefore will have two independent loops. Knowing that the loops of a spherical manipulator will be in subspace λ=3, the number of one degree of freedom joints needed to form the manipulator can be calculated from the Alizade mobility formula, $M = \sum f_i - \sum \lambda, \sum f_i = M + \sum \lambda, \sum f_i = 3 + (3+3) = 9$. Calculated nine joints can be distributed evenly all the legs. Note that similar to the serial spherical manipulator, all the axis of the joints should be intersected at a common point where the origin of the eye coordinate system is located (Figure 7.5).
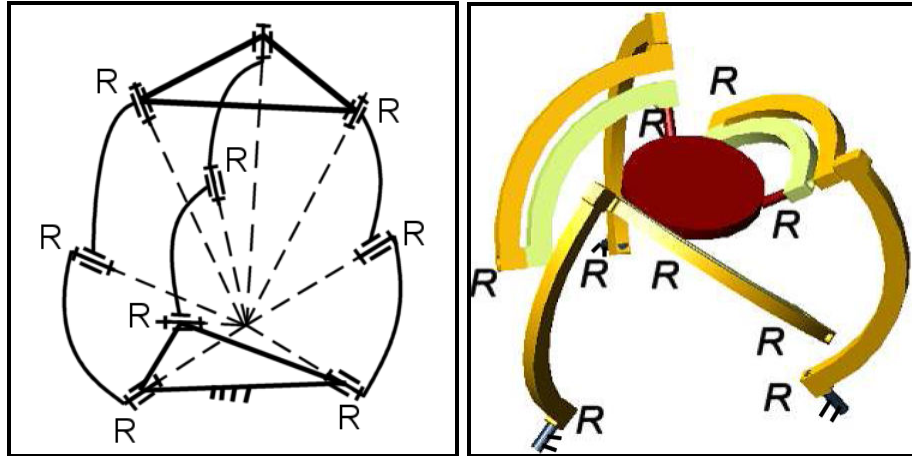
Figure 7.5. Three DoF parallel spherical platform manipulator.

The two examples given above are the mechanisms that can mimic the motion of one eye. On the other hand, human visual system is composed of two eyes, where each move in coordination with another. Although the visual complexity can be simulated by using two individual mechanisms, it will be more convenient to design a mechanism that can fulfill all of the coordinated motions of the ocular system.

Before starting to design targeted mechanism, the coordinated motions of the two eyes should be clearly investigated and the constraints should be given correctly. Due to the fact that, the rotations around the optical axes are infinitesimal and can be achieved by other means such as camera rotation or software adjustments, they will be excluded in the designed mechanism. As it can be seen in figure 7.6, with the
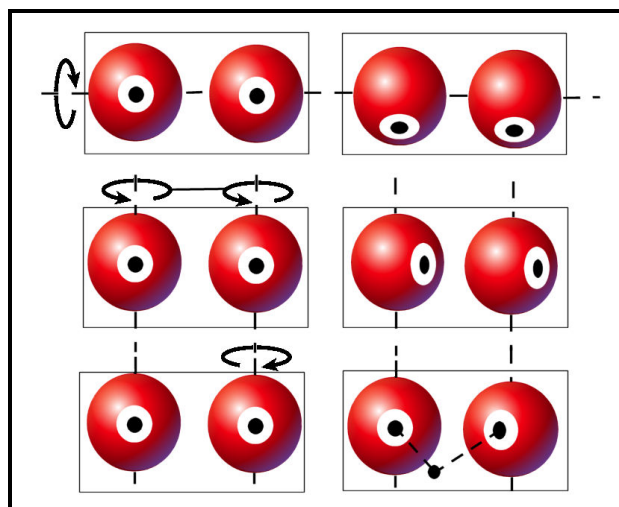

Figure 7.6. Motions of the eye complex.

elimination of optical axes rotations, the ocular system has three DoF. One simultaneous rotational motion around the horizontal eye axis, one simultaneous rotational motion around the vertical eye axes and another independent rotational motion of one eye around its vertical axis to achieve focusing into one point. When compared with the two individual mechanism structure, it is clear that using combined three degrees of mechanism has several advantages such as reduced number of motors, easier control scheme, precision and robustness.

In the light of given constraints in terms of desired motions, the designed novel mechanism can be constructed as in figure 7.7. The focusing movement is carried out by the prismatic joint that is circled in red inside the figure. Other vertical and horizontal rotational motions can be given either by using revolute and prismatic joints that are attached to the ground and circled in blue or by using remaining two prismatic joints.
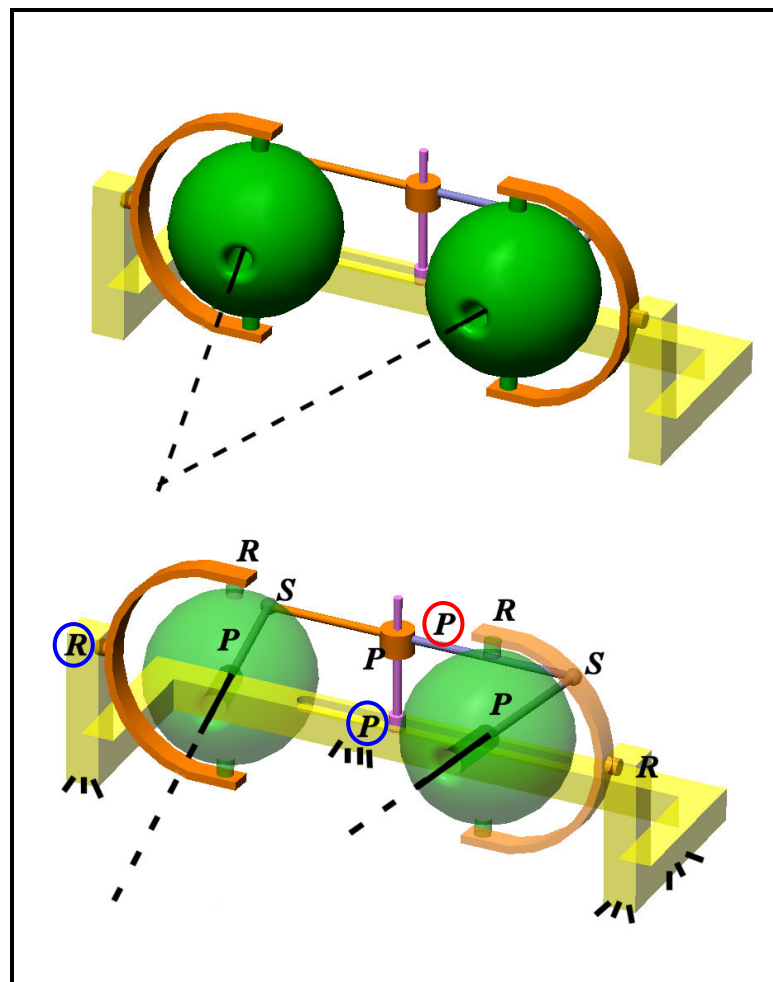

Figure 7.7. Novel three DoF manipulator for the eye complex.

In fact, clear investigation will reveal that, the mechanism that is introduced in figure 7.7 is a spatial parallel manipulator with triangular platform that has two independent loops in $\lambda=6$ (figure 7.8). When the prismatic joint that is responsible for the independent focusing motion is locked, the manipulator will become two degrees of
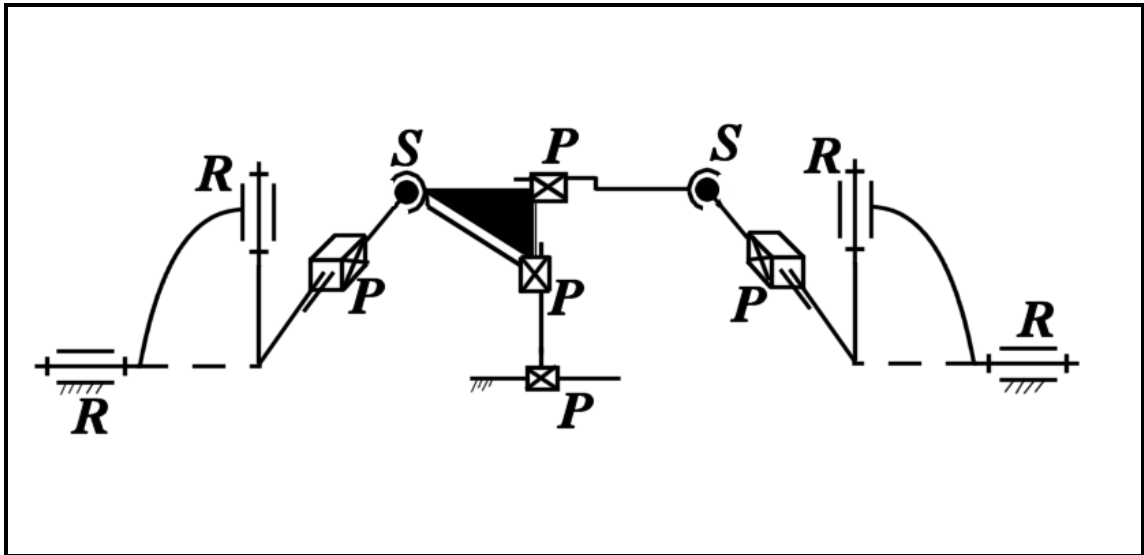

Figure 7.8. Novel three DoF spatial parallel manipulator.

freedom manipulator with normal leg configuration 6-2-6 in $\lambda=6$. However, when the prismatic joint is activated the total mobility of the kinematic pairs of the third leg will become seven (6-2-7). This activation gives the third leg an extra mobility in $\lambda=6$ that will not affect the platform of the manipulator. As a result, when the focusing movement occurs only the third leg will be affected while the overall behavior of the manipulator is protected.

The case seems simple but important. Usually, in structural synthesis and design of the parallel manipulators, the total degree of freedom of the pairs in each leg is not selected to be greater than the space or the subspace number of the manipulators operating environment. The reason of this precaution is the fact that this redundancy will give extra mobility to the related leg. This extra mobility can only be used to move the leg instead of the platform and cause the leg to become instable if not properly controlled. However, in this example this extra mobility that is controlled by the linear actuator, is desired and proved to be usable while achieving focusing motion of the eye complex.

7.2. Human Arm

Being the complex that has the largest workspace in human body, human arm has many sections including multiple bones, such as clavicle, scapula, humerus, radius and ulna (Figure 7.9). The bones of the human arm complex start from the shoulder and end in the wrist. The longest bone of the arm humerus creates the upper portion, while two parallel bones radius and ulna create the lower portion of the human arm. The nearly spherical head of the humerus stays in the cavity of scapula, where it creates the shoulder or glenohumeral joint. The connection between the other end of the humerus and the two parallel relatively small bones radius and ulna creates the elbow joint.
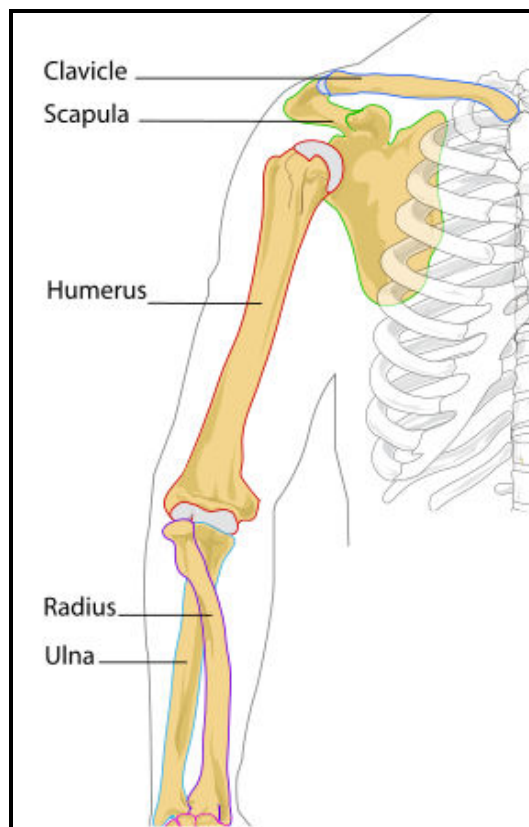

Figure 7.9. Structure of the human arm.
(Source: Wikipedia, 2010)

Although the clavicle is not a totally member of the arm, its motions contribute to the motion of the scapula to increase the overall workspace, so it should be mentioned in the biokinematic analysis of the human arm.

7.2.1. The Clavicle

The clavicle forms the front portion of the shoulder girdle. It can be described as a long bone that is curved somewhat like the italic letter *f*, and placed horizontally at the upper and front part of the thorax, immediately above the first rib (Figure 7.10).
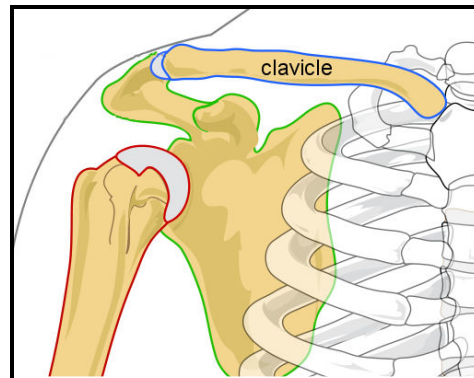

Figure 7.10. The clavicle.
(Source: Wikipedia, 2010)

Actually the clavicle serves as a rigid support with scapula to the shoulder and helps to align the shoulder with the rest of the chest. It is connected to the thorax with a ball and socket type joint, as a result it has three rotational motions (Figure 7.11).
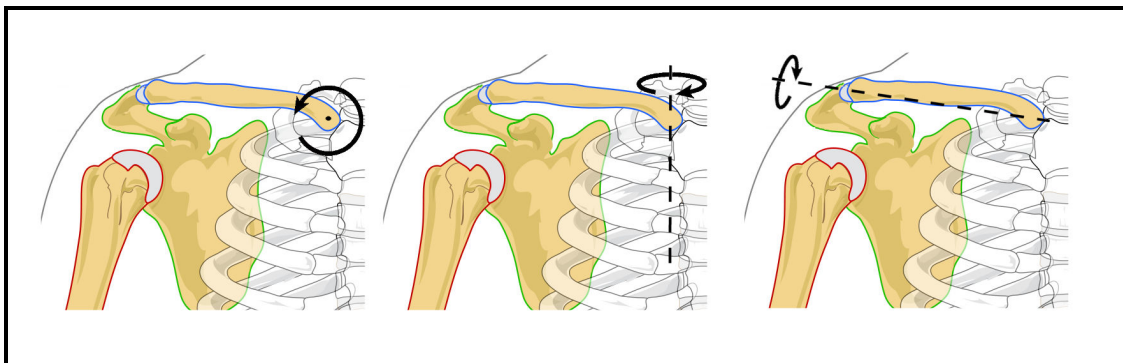

Figure 7.11. Clavicle rotations.
(Source: Wikipedia, 2010)

The first rotational degree of freedom controls the elevation and the depression of the shoulder girdle, the second one controls the protraction and retraction of the shoulder girdle and the last one controls the backward and forward rotation of the shoulder

girdle. Owing to the fact that the whole three DoF consists of just independent orientations, single spherical joint can illustrate the motions. On the other hand, as the workspace of the clavicle is not so wide, three DoF spatial orientation parallel manipulator that has similar workspace can be used to illustrate the clavicle mobility (Figure 7.12).

Example 3: Let's construct three DoF spatial orientation parallel manipulator that have moving platform with a pyramid shape. Due to its rectangular platform the manipulator should have four legs and therefore will have three independent loops. Knowing that the loops of a spatial manipulator will be in space $\lambda=6$, the number of one degree of freedom joints needed to form the manipulator can be calculated from the Alizade mobility formula, $M = \sum f_i - \sum \lambda, \ \sum f_i = M + \sum \lambda, \ \sum f_i = 3 + (6x3) = 21$. Calculated twenty one joints will be distributed to the four legs as (6,6,6,3). After applying the exchangeability of kinematic pairs the orientation platform can be constructed (Figure 7.12).
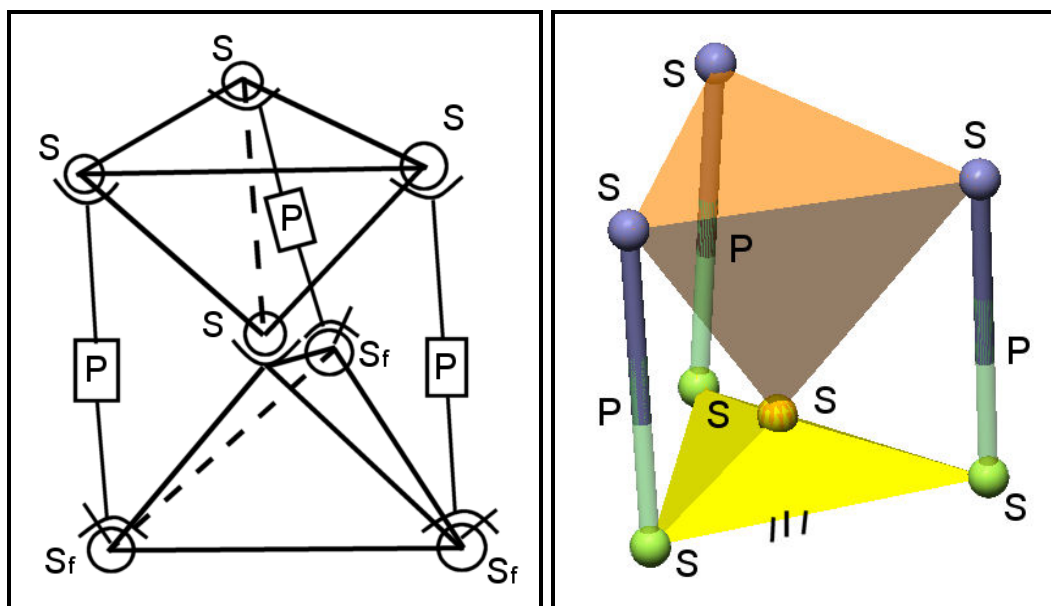

Figure 7.12. Three DoF orientation manipulator.

It should be noted that, in the right portion of the Figure (7.12), two DoF spherical with finger joints are replaced by spherical joints to make the operation of the manipulator easier by giving three passive rotations around each leg.

7.2.2. The Humerus

As mentioned before, humerus is the largest bone of the arm that creates the upper portion of the complex. Connecting to the cavity of the scapula by a ball and socket type joint with its nearly spherical head, humerus creates the shoulder or glenohumeral joint (Figure 7.13). Due to the fact that, the workspace of the humerus is affected by the workspace of the scapula, scapula motions should be introduced
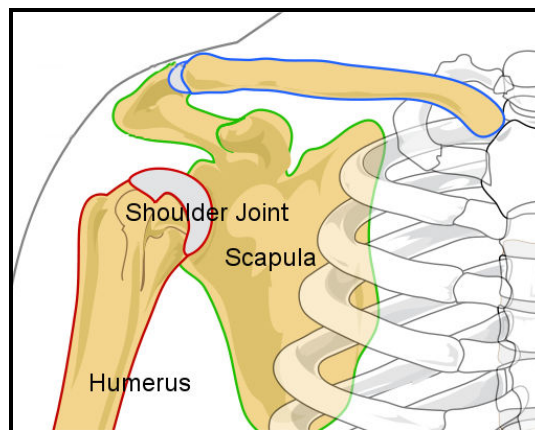

Figure 7.13. Humerus and the shoulder joint.
(Source: Wikipedia, 2010)

before advancing into humerus. In fact scapula has also a limited workspace similar to its neighbor bone. Scapula movements (Figure 7.14) are created by another ball and socket type joint in the connection between itself and the clavicle. Related with the
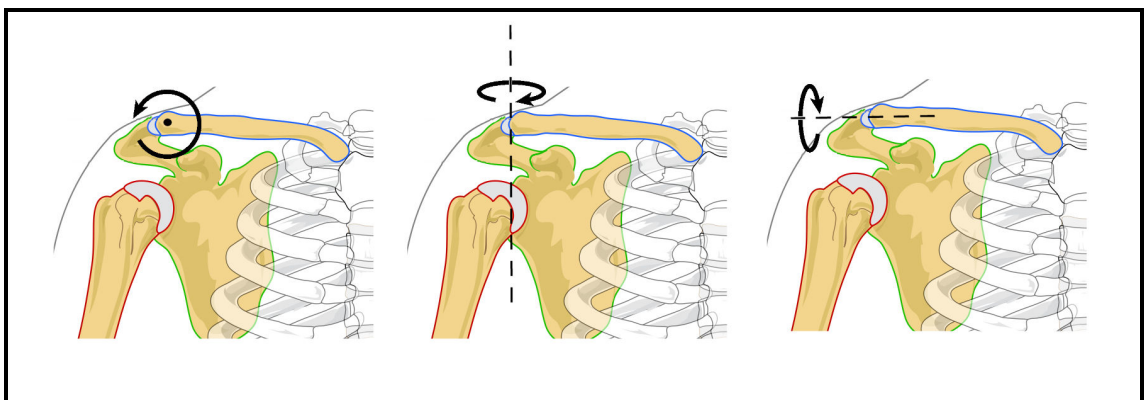

Figure 7.14. Scapula rotations.
(Source: Wikipedia, 2010)

nature of the spherical joint, scapula has three DoF orientation capability around its axes.

Having learned the structure and the capabilities of the scapula, humerus can be introduced. Despite the fact that humerus and scapula connection (shoulder joint) is also a ball and socket type joint, it provides a larger workspace for the humerus when compared with the scapula motion. As seen in Figure (7.15) humerus has also three DoF orientation capability around its axes by the help of spherical shoulder joint.
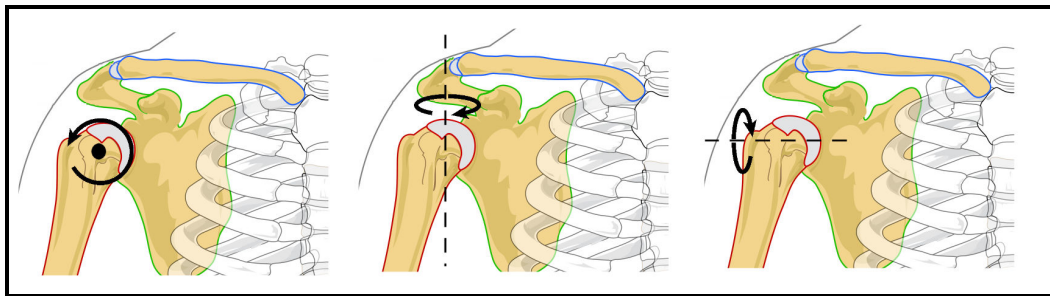

Figure 7.15. Humerus rotations.
(Source: Wikipedia, 2010)

In order to create a mechanism that can mimic the scapula and humerus motions, some simplifications should be made. It is clear that by the addition of the workspaces of the scapula and clavicle, the humerus can move in a very large workspace. To fullfill such large workspace capability by introducing two individual mechanisms for both scapula and humerus in addition to the clavicle will be more complex and hard to control. As a result, the joints of clavicle-scapula and scapula-humerus can be simulated as one spherical mechanism since the distance between them is small. In the light of this, a three DoF serial manipulator with larger workspace can be used to mimic the upper arm motion. However, it should be noted that as the motions should be just three independent rotations, the axis of the motors should again be intersected at a common point where the origin of the shoulder joint coordinate system is located.

Example 4: Let's construct three DoF serial spherical manipulator. Due to its serial nature the manipulator should have three, one degree of freedom motors (Figure 7.16).
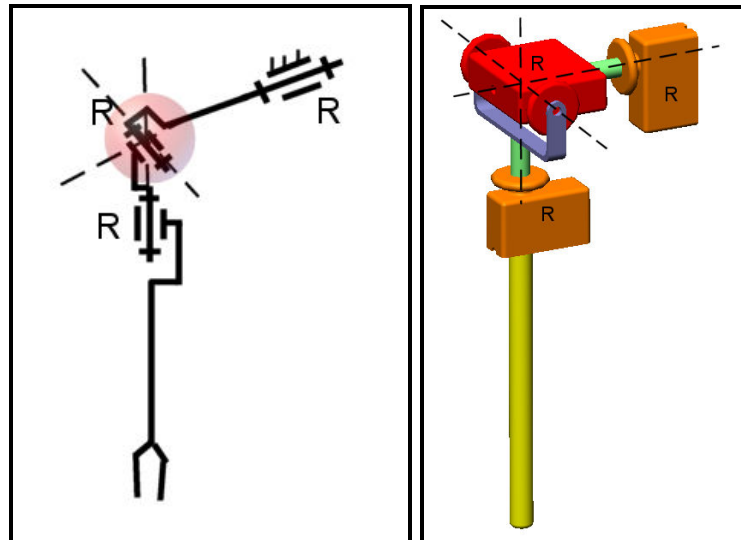
Figure 7.16. Three DoF serial spherical manipulator.

7.2.3. The Radius and the Ulna

The main function of the radius is to act as the main supporting bone of the forelimb. It articulates both with the humerus to form the elbow joint, and with the carpal bones to form the main joint of the wrist. The twist motion of the wrist is generated by the radius that can rotate over the ulna. When compared in structure, it is shorter than the ulna, which serves as a point for muscle attachment. The motions of the bone couples include one degree of freedom motion in the elbow that is used to bend the forearm up and down, and one degree of freedom motion in the wrist that gives the wrist and the hand its axial rotation, (Figure 7.17).
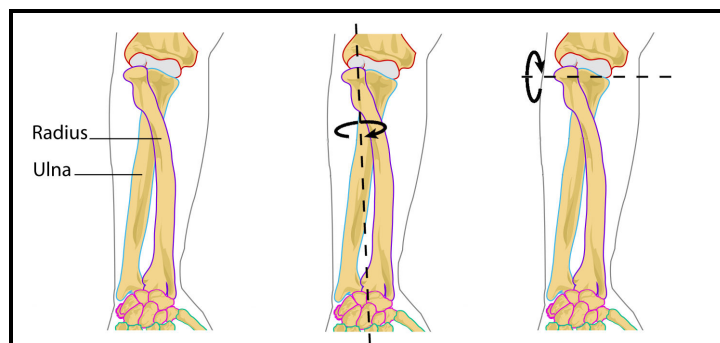

Figure 7.17. Motions of the radius and ulna.
(Source: Wikipedia, 2010)

Due to the simplicity of the structure and its motions, the kinematic representation of the lower arm system can be developed as a simple mechanism (Figure 7.18).
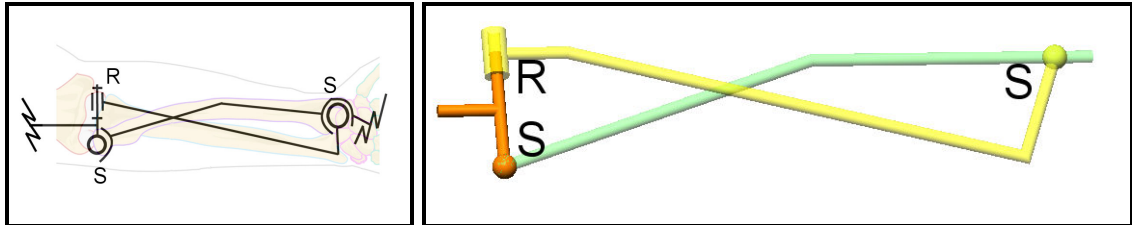

Figure 7.18. Two DoF mechanism.

7.3. Kinematic Analysis of Human Arm Complex by Using Theory of Transformation Unit Screws

Up to this point, the chapter of biokinematic analysis of human body has dealt with the type and structural synthesis problem. The procedure of the process can be simply summarized in few steps as,

- Investigate or define the mobility and motion relationship of the desired joint or the complex of the human body.
- Decide the type of the mechanism that can be used to mimic the targeted joint (Serial manipulator, parallel manipulator, cam systems etc.).
- Propose an existing mechanism from the literature or design a novel mechanism that can fulfill the desired task with respect to the type decision and given constraints.

Now let's deal with mathematical tools and carry out the kinematic analysis of human arm complex by using theory of transformation unit screws that is introduced in the previous chapters. For this task, human arm will be taken as five DoF serial manipulator from shoulder to wrist point that includes three DoF shoulder rotations, one DoF elbow rotation of forearm bending, and one DoF axial rotation of the wrist (Figure 7.19).
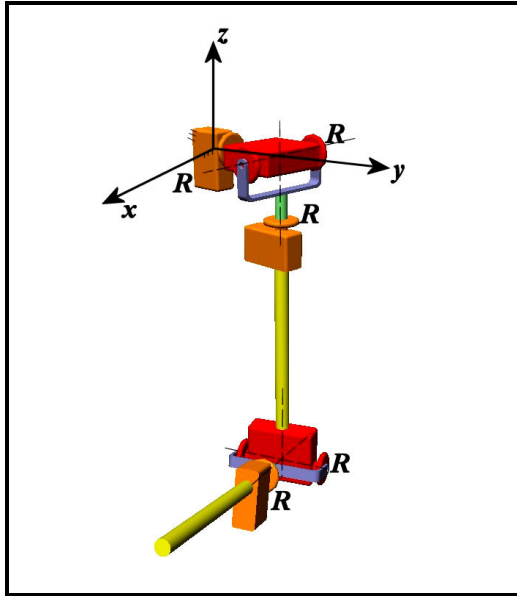
Figure 7.19. Five DoF serial manipulator of human arm complex.

7.3.1. Direct Kinematic Analysis

Before proceeding into the direct analysis problem, let's construct the kinematical representation of five DoF serial manipulator and represent the variable parameters as well as constant ones (Figure 7.20).
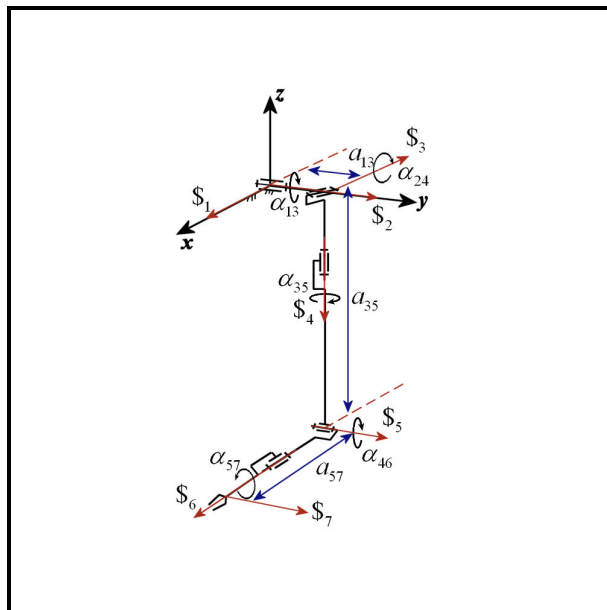

Figure 7.20. Kinematic representation of serial arm complex manipulator.

In the problem of direct kinematics, the aim is to find the position and orientation of the end effector by using known values of variable and constant parameters. In the case presented in this subsection, these parameters for the five DoF serial manipulator are shown in Table 7.1. As the first and second unit screws lie on the x and y axes, their values are already known, $\$_1(1,0,0,0,0,0), \$_2(0,1,0,0,0,0)$.

Table 7.1. Variable and constant parameters of serial arm complex manipulator.

Variable Parameters	Constant Parameters
$\alpha_{13},\ \alpha_{24},\ \alpha_{35},\ \alpha_{46},\ \alpha_{57}$	$a_{13},\ a_{24}=0,\ a_{35},\ a_{46}=0,\ a_{57}$

To achieve the orientation and the position of the end effector, it is needed to find the last two screws $\$_6(l_6,\ m_6,\ n_6,\ P_6,\ Q_6,\ R_6)$ and $\$_7(l_7,\ m_7,\ n_7,\ P_7,\ Q_7,\ R_7)$. As mentioned in the previous chapters, any k^{th} screw $\$_k$ can be found by using i^{th} screw $\$_i$ and j^{th} screw $\$_j$ by using the transformation unit screw equations, Equation (3.8). In order to find the last two screws $\$_6(l_6,\ m_6,\ n_6,\ P_6,\ Q_6,\ R_6)$ and $\$_7(l_7,\ m_7,\ n_7,\ P_7,\ Q_7,\ R_7)$, previous screws $\{\$_i\}_3^5$ should be found sequentially by applying Equation (3.8) as,

$\$_3$ (C$_{13}$, 0, -S$_{13}$, -S$_{13}$a$_{13}$, 0, -C$_{13}$ a$_{13}$);
$\$_4$ (S$_{13}$ S$_{24}$, C$_{24}$, C$_{13}$ S$_{24}$, C$_{13}$ S$_{24}$ a$_{13}$, 0, S$_{13}$ S$_{24}$ a$_{13}$);
$\$_5$ (C$_{13}$ C$_{35}$ - C$_{24}$ S$_{13}$ S$_{35}$, S$_{24}$ S$_{35}$, C$_{35}$ S$_{13}$ - C$_{13}$ C$_{24}$ S$_{35}$, -(C$_{35}$ S$_{13}$ + C$_{13}$ C$_{24}$ S$_{35}$) a$_{13}$ - (C$_{24}$ C$_{35}$ S$_{13}$ + C$_{13}$ S$_{35}$) a$_{35}$, C$_{35}$ S$_{24}$ a$_{35}$, (-C$_{13}$ C$_{35}$ + C$_{24}$ S$_{13}$ S$_{35}$) a$_{13}$ + (-C$_{13}$ C$_{24}$ C$_{35}$ + S$_{13}$ S$_{35}$) a$_{35}$);
$\$_6$ (C$_{46}$ S$_{13}$ S$_{24}$ + (C$_{24}$ C$_{35}$ S$_{13}$ + C$_{13}$ S$_{35}$) S$_{46}$, C$_{24}$ C$_{46}$ - C$_{35}$ S$_{24}$ S$_{46}$, -S$_{13}$ S$_{35}$ S$_{46}$ + C$_{13}$ (C$_{46}$ S$_{24}$ + C$_{24}$ C$_{35}$ S$_{46}$), C$_{13}$ C$_{46}$ S$_{24}$ a$_{13}$ + C$_{13}$ C$_{35}$ S$_{46}$ (C$_{24}$ a$_{13}$ + a$_{35}$) - S$_{13}$ S$_{35}$ S$_{46}$ (a$_{13}$ + C$_{24}$ a$_{35}$), S$_{13}$ S$_{24}$ (-C$_{13}$ C$_{24}$ C$_{35}$ + S$_{13}$ S$_{35}$) S$_{46}$ a$_{35}$, -C$_{46}$ S$_{13}$ S$_{24}$ a$_{13}$ - (C$_{24}$ C$_{35}$ S$_{13}$ + C$_{13}$ S$_{35}$) S$_{46}$ (a$_{13}$ + C$_{24}$ a$_{35}$));
$\$_7$ (C$_{13}$ (C$_{35}$ C$_{57}$ - C$_{46}$ S$_{35}$ S$_{57}$) - S$_{13}$ (-S$_{24}$ S$_{46}$ S$_{57}$ + C$_{24}$ (C$_{57}$ S$_{35}$ + C$_{35}$ C$_{46}$ S$_{57}$)), C$_{57}$ S$_{24}$ S$_{35}$ + (C$_{35}$ C$_{46}$ S$_{24}$ + C$_{24}$ S$_{46}$) S$_{57}$, -C$_{57}$ (C$_{35}$ S$_{13}$ + C$_{13}$ C$_{24}$ S$_{35}$) + (C$_{46}$ S$_{13}$ S$_{35}$ + C$_{13}$ (-C$_{24}$ C$_{35}$ C$_{46}$ + S$_{24}$ S$_{46}$)) S$_{57}$, -C$_{57}$ ((C$_{35}$ S$_{13}$ + C$_{13}$ C$_{24}$ S$_{35}$) a$_{13}$ + (C$_{24}$ C$_{35}$ S$_{13}$ + C$_{13}$ S$_{35}$) a$_{35}$) + $\dfrac{1}{32}$ S$_{57}$ (32 (C$_{46}$

S$_{13}$ S$_{35}$ + C$_{13}$ (-C$_{24}$ C$_{35}$ C$_{46}$ + S$_{24}$ S$_{46}$)) a$_{13}$ + (32 C$_{24}$ C$_{46}$ S$_{13}$ S$_{35}$ + (S3$_{13}$ (5 S$_{24}$ + S3$_{24}$) + S$_{13}$ (-7 S$_{24}$ + 5 S3$_{24}$)) S2$_{35}$ S$_{46}$ − 8 C$_{13}$ (4 C$_{35}$ C$_{46}$ + (-1+C2$_{13}$ C2$_{35}$) S2$_{24}$ S$_{46}$)) a$_{35}$) - C$_{57}$ (C$_{46}$ (C$_{24}$

C$_{35}$ S$_{13}$ + C$_{13}$ S$_{35}$) - S$_{13}$ S$_{24}$ S$_{46}$) a$_{57}$ + (-C$_{13}$ C$_{35}$ + C$_{24}$ S$_{13}$ S$_{35}$) S$_{57}$ a$_{57}$, C$_{35}$ C$_{57}$ S$_{24}$ a$_{35}$ − $\dfrac{1}{4}$ S$_{13}$

(C$_{13}$ (-2 C$_{35}$ C$_{46}$ S2$_{24}$ + 4 S$_{24}$2 S$_{35}$2 S$_{46}$) + S$_{13}$ S$_{24}$ (4 C$_{46}$ S$_{35}$ + S2$_{24}$ S2$_{35}$ S$_{46}$)) S$_{57}$ a$_{35}$ + C$_{57}$ (C$_{35}$ C$_{46}$ S$_{24}$ + C$_{24}$ S$_{46}$) a$_{57}$ - S$_{24}$ S$_{35}$ S$_{57}$ a$_{57}$, (C$_{13}$ (-C$_{35}$ C$_{57}$ + C$_{46}$ S$_{35}$ S$_{57}$) + S$_{13}$ (-S$_{24}$ S$_{46}$ S$_{57}$ +

C$_{24}$ (C$_{57}$ S$_{35}$ + C$_{35}$ C$_{46}$ S$_{57}$))) a$_{13}$ + $\dfrac{1}{2}$ (2 C$_{13}$ C$_{24}$ (-C$_{35}$ C$_{57}$ + C$_{46}$ S$_{35}$ S$_{57}$) + S$_{13}$ (2 C$_{57}$ S$_{35}$ + (2

C$_{24}$2 C$_{35}$ C$_{46}$ - S2$_{24}$ S$_{46}$) S$_{57}$)) a$_{35}$ + (S$_{13}$ (C$_{46}$ C$_{57}$ S$_{35}$ + C$_{35}$ S$_{57}$) + C$_{13}$ (C$_{57}$ S$_{24}$ S$_{46}$ + C$_{24}$ (-C$_{35}$ C$_{46}$ C$_{57}$ + S$_{35}$ S$_{57}$))) a$_{57}$)

(7.1)

After the numerical values of the last two screws $\$_6(l_6, m_6, n_6, P_6, Q_6, R_6)$ and $\$_7(l_7, m_7, n_7, P_7, Q_7, R_7)$ are computed, Equation. (7.1), the orientation of the end effector can be found from the two unit vectors $\mathbf{e}_6(l_6, m_6, n_6)$ and $\mathbf{e}_7(l_7, m_7, n_7)$. Also the position of the end effector x, y and z can be calculated from the intersections of the last two screws by using Equation (3.4).

7.3.2. Inverse Kinematic Analysis

In the problem of inverse kinematics, the aim is to find the values of the variable parameters by using known values of constant parameters, orientation and position of the end effector. In the case of targeted serial manipulator, in order to give the orientation of the end effector, any three given components of the unit vectors of the last two screws is sufficient. However it should be noted that at least one component should be given from each unit screw $\mathbf{e}_6$ and $\mathbf{e}_7$. The other remaining three components can be calculated by using three equations as,

$$\mathbf{e}_6 \cdot \mathbf{e}_6 = 1, \quad \mathbf{e}_7 \cdot \mathbf{e}_7 = 1, \quad \mathbf{e}_6 \cdot \mathbf{e}_7 = Cos\alpha_{67} = Cos\frac{\pi}{2} \qquad (7.2)$$

After using Equation (7.2), the unit vector parts of the last two screws will be revealed. To continue the inverse task, other remaining moment vector parts of the last two screws $\mathbf{e}_6°(P_6, Q_6, R_6)$ and $\mathbf{e}_7°(P_7, Q_7, R_7)$ should be calculated. Using the given values of the position of the end effector x, y and z, Equation (3.4), and the relations below,

$$\mathbf{e}_6 \cdot \mathbf{e}_6° = 0, \quad \mathbf{e}_7 \cdot \mathbf{e}_7° = 0, \quad \$_6 \otimes \$_7 = \mathbf{e}_6 \cdot \mathbf{e}_7° + \mathbf{e}_7 \cdot \mathbf{e}_6° = -a_{67}Sin\alpha_{67} = 0 \qquad (7.3)$$

$\mathbf{e}_6°(P_6, Q_6, R_6)$ and $\mathbf{e}_7°(P_7, Q_7, R_7)$ will be calculated, (Note that $\otimes$ sign in Equation (7.3) refers to the mutual moment operation). After the numerical values of the last two screws $\$_6(l_6, m_6, n_6, P_6, Q_6, R_6)$ and $\$_7(l_7, m_7, n_7, P_7, Q_7, R_7)$ are computed, all possible combinations of variable parameters $\alpha_{13}, \alpha_{24}, \alpha_{35}, \alpha_{46}, \alpha_{57}$ can be calculated by using components of $\$_6$ and $\$_7$ that are computed from the direct task in Equation (7.1).

7.4. Human Hand

Hands (Figure 7.21) are another important part of the human body due to their ability to physically manipulating the environment by coarse and fine motions such as grasping a large obstacle or a tiny object. In the light of this importance, the sections of the hand should be clearly investigated with respect to their structure and motion capabilities.
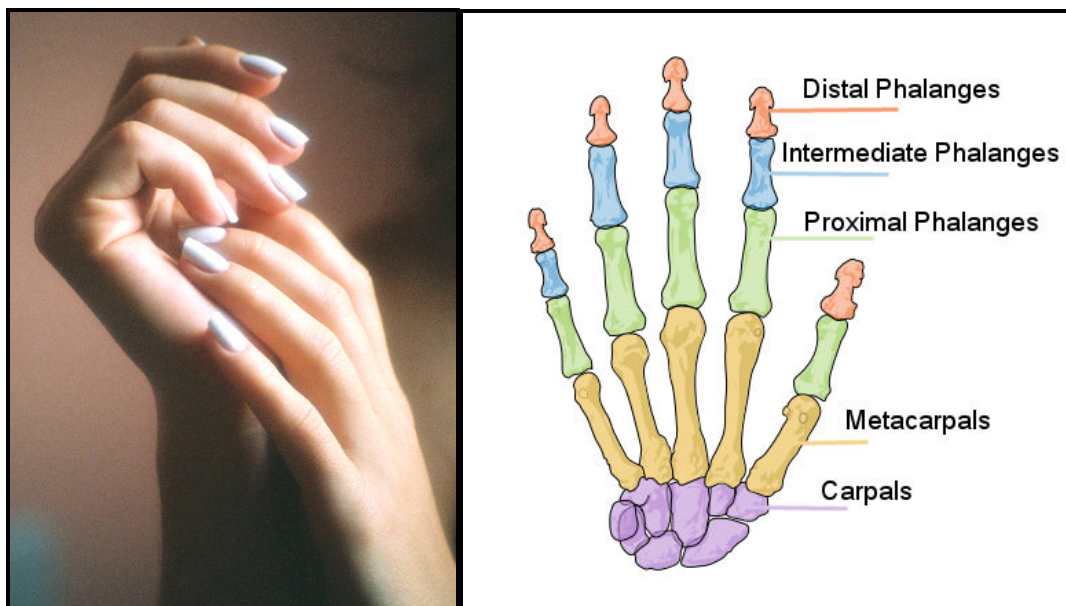

Figure 7.21. Human hand and the bones.
(Source: Wikipedia, 2010)

Actually the human hand can be split into two parts as the wrist and the fingers. The whole structure consists of many bones as distal phalanges, intermediate phalanges, proximal phalanges, metacarpals and carpals (Figure 7.21). Although the structure of the hand seems complicated, the motions can be easily identified.

7.4.1. The Wrist

The human wrist composed of carpals that are the composed of eight small bones. The carpals of the hand can be categorized into two groups as midcarpals and radiocarpals. Three bones that are just located after the radius of the lower arm create

the wrist joint by the connection with the radius and the midcarpals (Figure 7.22). It should be noted that the midcarpals are formed by the remaining five bones of the carpals that are located just after the radiocarpals.
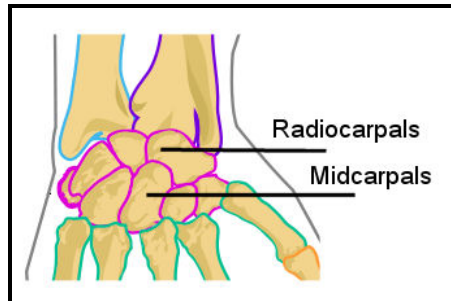

Figure 7.22. Human wrist.
(Source: Wikipedia, 2010)

Despide the complexity of the carpal region, the wrist joint has just two DoF that are all composed of rotational motions around the axes passing through mostly the midcarpals. These rotations are responsible for not only extension and flexion but also the ulnar and radial deviation motions. Ulnar and radial deviation motions occur around the vertical axis of the largest carpal bone capitate that is located in the middle of the midcarpals, extension occurs mostly around the midcarpal joints lateral axis and the flexion occurs mostly around the radiocarpal joints lateral axis (Figure 7.23).
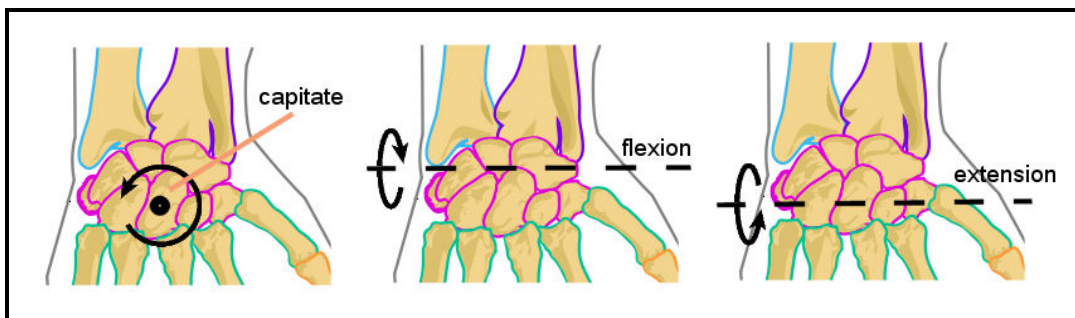

Figure 7.23. Human wrist motions.
(Source: Wikipedia, 2010)

Wrist motions are composed of two independent simple orientation motions. Due to this simplicity, the kinematic representation of the wrist system can easily be reduced to an ordinary two DoF cardan or universal joint (Figure 7.24). Due to the small

distance between the actual axes, in this configuration extension and flexion of the human wrist are assumed to occur around the same axis.
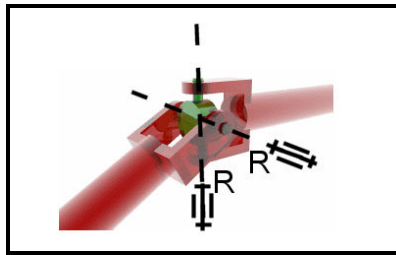

Figure 7.24. Cardan joint.
(Source: Wikipedia, 2010)

7.4.2. The Fingers

As the fingertips have a large density of nerve endings, the fingers are great for the tactile feedbacks in the human body. Thus, the fingers of the human body have greater positioning capability when compared with the other sections of human skeletal system.
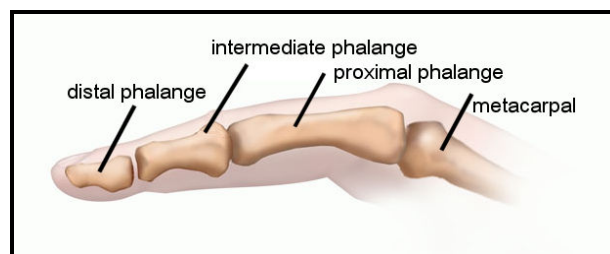

Figure 7.25. Bones of the finger.
(Source: RelayHealth, 2010)

The finger structure is composed of four different bones as distal phalanges, intermediate phalanges, proximal phalanges and metacarpals (Figure 7.25). The joints between the first, second and the third phalange are called interphalangeal joints, while the joint between the third phalange and the metacarpal is called metacarpophalangeal joint. The interphalangeal joints have one rotational degree of freedom that is the flexion motion. On the other hand metacarpophalangeal joint has two rotational DoF

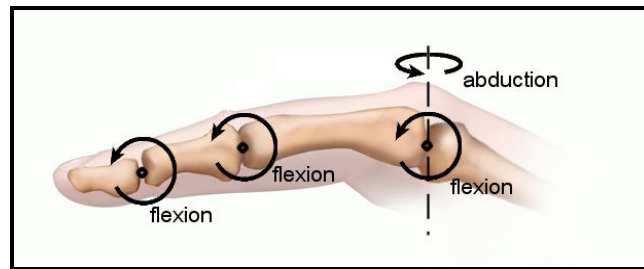that are both the flexion – extension and the abduction – adduction couple motions, (Figure 7.26).

Figure 7.26. Motions of the finger bones.
(Source: RelayHealth, 2010)

The visualization of the motions reveals that the great positioning capability of the human finger is caused by simple rotational flexion and abduction motions. Also it is clear that all of the three flexion motions occur in the same vertical plane, where the finger lies. The forth abduction motion just changes the orientation of mentioned vertical plane around the vertical axis. Following example will clarify the motion concept of the human finger.

Example 5: Let's construct four DoF serial manipulator, where the first three joints will make three DoF planar motion and the forth joint will change the orientation of the plane around the vertical axis. Being a serial manipulator, it should have four, one-DoF motors and due to the planar motion requirement, the axes of the first three joints should be parallel to each other and the fourth joint axis should be perpendicular to the other joint axes to achieve the desired motion configuration (Figure 7.27).
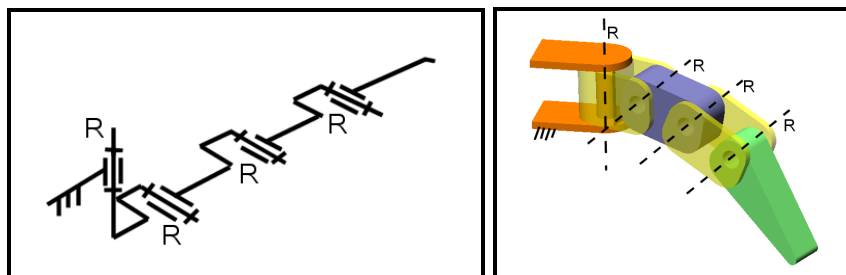

Figure 7.27. Four DoF serial mechanism.

7.5. Human Leg

Closer investigation of the human leg reveals that, it has roughly similar kinematic structure with the human arm with the exception of workspace limitations. Similar to the human arm, human leg can be divided into two parts as upper portion and lower portion. The upper portion of the leg starts with the longest and the largest bone of the human skeletal system that is called femur. The lower portion of the leg continues with the two bones that are called tibia and fibula. Carrying the overall weight of the human body, tibia is the strongest bone of the skeletal system. There are two important joint formations in the system. The connection of the femurs nearly spherical head with the hip bone results in the formation of the hip joint, while the connection of femurs lower extremity with the tibia forms the knee joint. The knee joint is protected and covered by a thick circular and triangular bone patella (knee cap or kneepan),
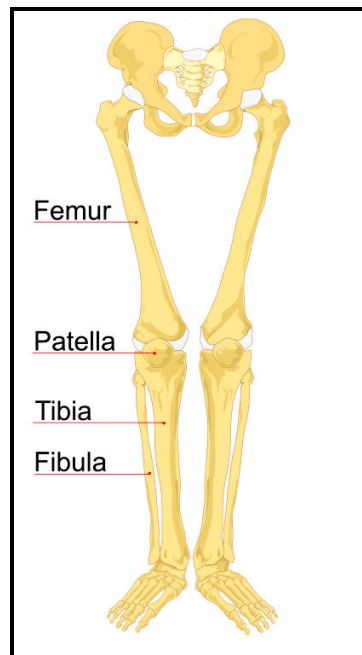

Figure 7.28. Human leg.
(Source: Wikipedia, 2010)

which articulates with the femur (Figure 7.28). As the human legs are specifically adapted to the bipedal locomotion by the help of the location of human body gravity center and stay under the heavy load of the human body, all of the mentioned bones have special strength values, structures and mobilities.

7.5.1. The Femur

As mentioned earlier, the femur is the longest and the second strongest bone of the human skeletal system. Its shape is smilar to a cylindrical shaft that is curved forward with respect to the normal body pose. The femur can be divided into three main sections as the upper extremity including the head, neck and trochanters; the body and the lower extremity (Figure 7.28).
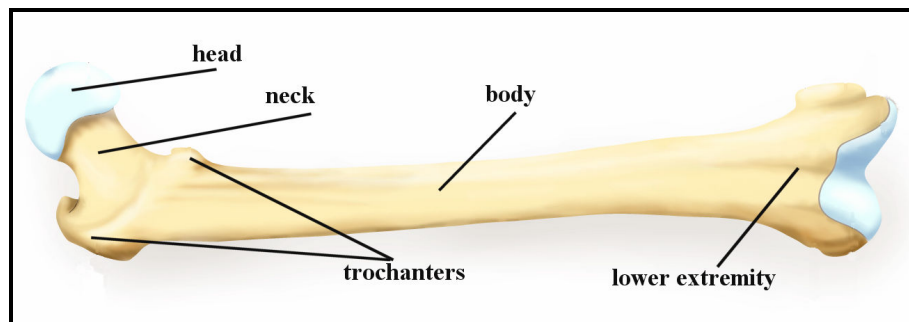
Figure 7.28. Femur of the leg.
(Source: Wikipedia, 2010)

When connected with the hip bone, the head of the femur creates the hip joint that has the similar characteristics of the ball and socket type kinematic pair. Due to its spherical nature hip joint has three independent rotational motions (Figure 7.29).
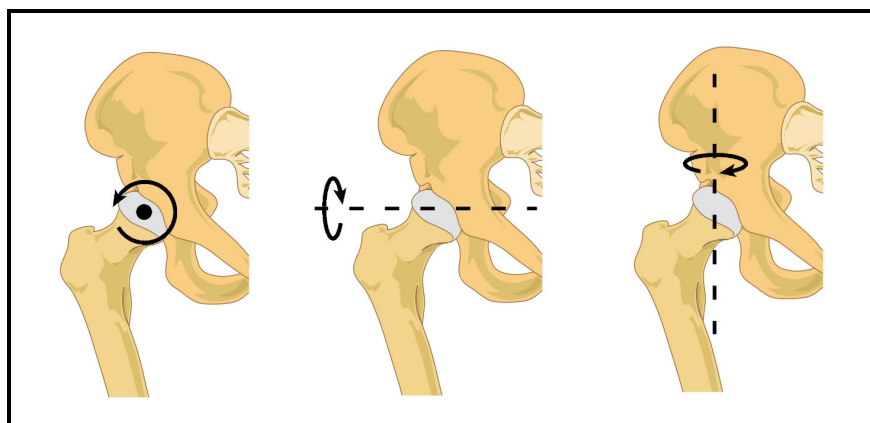
Figure 7.29. Femur of the leg.
(Source: Wikipedia, 2010)

It should be noted that, similarly with the humerus of the arm, the femur motions can easily be modeled by using three DoF serial manipulator (Figure 7.16).

7.5.2. The Tibia and the Fibula

The tibia is the largest of the two bones located at the lower portion of the human leg. Due to the fact that it carries the whole body weight, it is the strongest bone of the human skeletal system. The tibia has a prismoid shaft in section that is extended
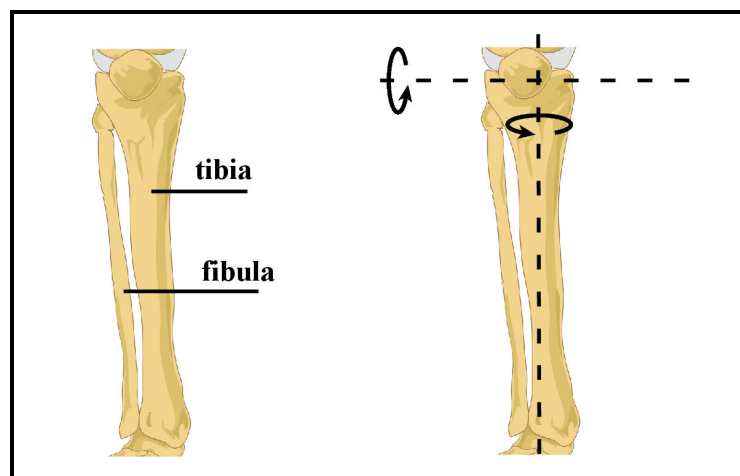

Figure 7.30. Tibia, fibula and the knee motion.
(Source: Wikipedia, 2010)

above and connected with the femur inside the knee joint. Compared with the tibia, fibula is a thinner bone (Figure 7.30). As its upper extremity is connected to the tibia below the knee, fibula is excluded from the knee joint. On the other hand, both bones help the formation of the ankle joint in each of their lower extremities.

Although the knee joint permits not only the flexion and extension but also medial and lateral rotation to the lower portion of the leg, the latter pair of motions are small (Figure 7.30). It is clear from the definitions that, both independent motions are related with the orientation of the knee joint. Owing to the fact that the kinematic representation of the system again resembles with the human elbow structure, two DoF cardan or universal joint can be used to model the knee joint motions (Figure 7.24).

7.6. Human Foot

In a general description, human foot can be introduced as the lowest complex of the human body that bears the overall weight and responsible for the locomotion of the body. Although the definition seems to point out a simple area of skeletal system, its mechanical structure comes with great complexity including twenty six bones, thirty three joints and more than a hundred muscles, tendons and ligaments that actuate the joints of the foot to reach the desired mobility, (Figure 7.31).
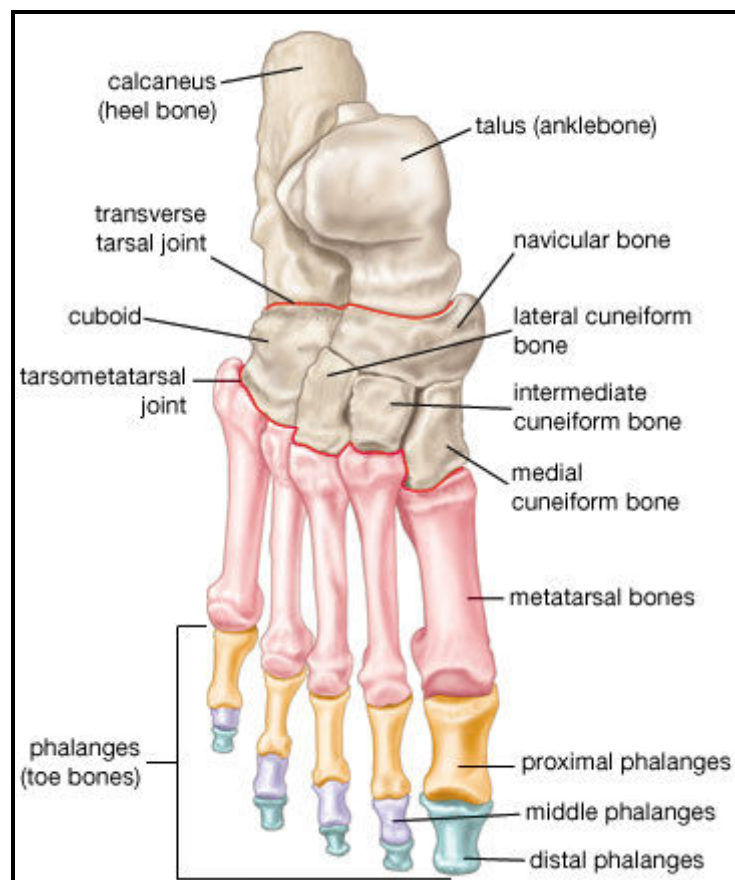

Figure 7.31. Human foot bones.
(Source: Encyclopedia Britannica, 2010)

If closely investigated, it will be revealed that this complex structure gives the foot its capability of overcoming extreme conditions such as excessive bending, instantaneous shock absorption and continuous mechanical stresses during various situations like running, jumping, standing etc. (Figure 7.32).

Figure 7.32. Human foot in extreme conditions.
(Source: Wikipedia, 2010)

In order to clearly define the mobility constraints, the foot can be divided into three subsections as the posterior of the foot or the hindfoot, the midfoot and the forefoot.

7.6.1. Hindfoot

The hindfoot behaves like a bridge between the ankle bone talus and the midfoot. The connection of the talus with two lower portion leg bones tibia and fibula creates a hinge like joint that has one degree of freedom. This mobility creates the dorsiflexion and the plantarflexion of the foot (Figure 7.33).
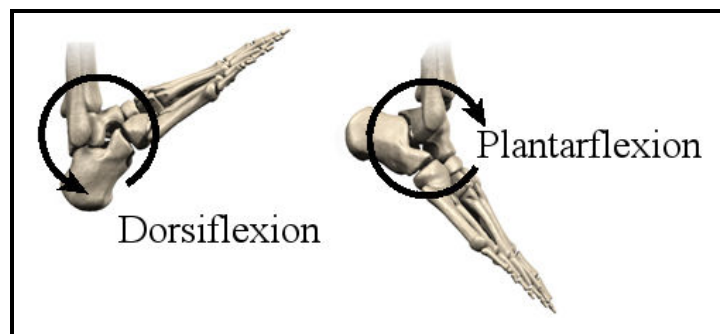

Figure 7.33. Dorsiflexion and plantarflexion.
(Source: MMG, 2010)

Another important joint of the posterior portion of the foot is the one degree of freedom subtalar joint. It is created by the connections of the talus and the calcaneus bones and allows the foot to make its inversion and eversion motions, (Figure 7.34).
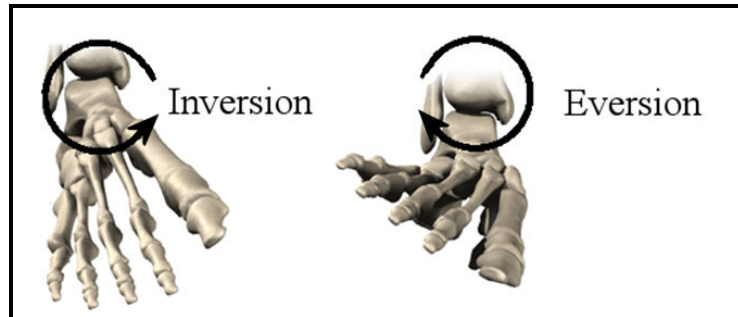

Figure 7.34. Inversion and eversion.
(Source: MMG, 2010)

Due to the similarity in motion with the wrist complex, the posterior region of the human foot can be modeled by two DoF serial chain. As seen in Figure 7.35, the axes of two revolute joints of the modeled serial mechanism should be perpendicular to each other to achieve both dorsiflexion – plantarflexion and inversion – eversion motion couples. The actuation of the revolute joints can be given actively by distinct rotational motors, passively by adding RPR shock absorber structural groups to the appropriate positions or using both active and passive options in one configuration, Figure 7.35. The all passive case has been usually used in the medical prosthesis, where the joints are passively positioned with respect to the type of ground contact and lower
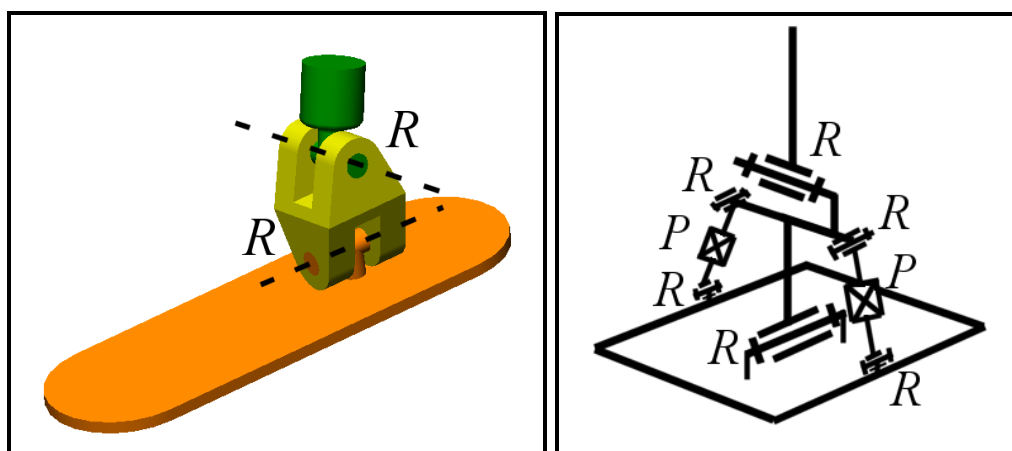

Figure 7.35. Two DoF hindfoot mechanisms.

leg position during activities by the help of prismatic shock absorbers. When the prosthesis ankle is free from external forces, all the shock absorbers as well as the joints will return to their neutral positions. It should also be noted that, if the linear actuators of the orientation platform in Figure 7.12 are changed with the prismatic shock absorbers and the mid spherical joint that connects the two platforms is changed with the spherical with finger joint so that the axial z rotation become constrained, the resulting two DoF parallel manipulator (Figure 7.36) can be also used as a passive ankle prosthesis instead of serial ones.

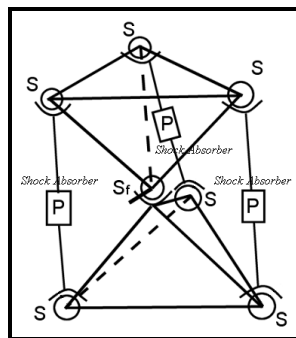Figure 7.36. Two DoF parallel manipulator with passive shock absorbers.

7.6.2. Midfoot

As seen in Figure 7.37, the mid foot is composed of five tarsal bones in various sizes. Although these bones do not contribute to the mobility of the human foot directly, they act as shock absorbers in the connection between the forefoot and the hindfoot.
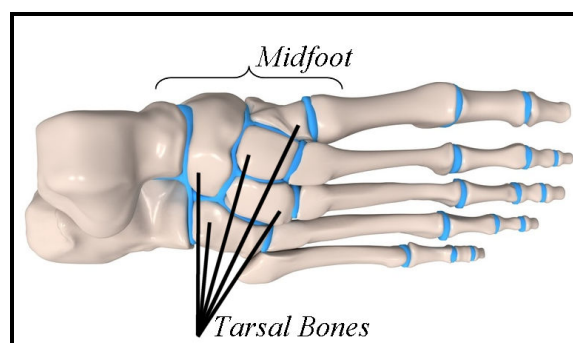

Figure 7.37. Tarsal bones of the midfoot.
(Source: PaddocksHealthcare, 2010)

7.6.3. Forefoot

The structure of the forefoot is composed of two different bone types, metatarsals and phalanges (Figure 7.38). As there are five toes in human foot, many joints exist in the complex. The connection of metatarsals with the tarsal bones creates tarsometatarsal joints. Each of the metatarsal bones are articulated with one or more tarsal bones in these joints. However, these joints do not permit a wide range workspace motions. Instead the mobility is limited to slide gliding motions between the tarsal ends
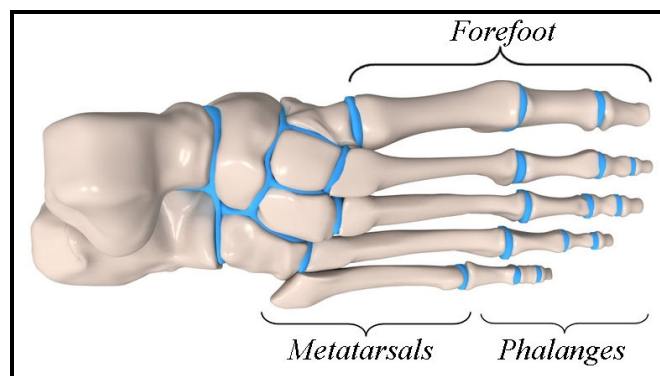

Figure 7.38. Bones of the forefoot.
(Source: PaddocksHealthcare, 2010)

and the base of the metatarsal bones. Transition to the phalange zone begins with the metatarsophalangeal joints between the metatarsal ends and the first phalanges. Similar with the metacarpophalangeal joints in the fingers, these joints also permits flexion - extension and abduction – adduction motion couples. Each of the four phalanges consists of three small bones and two joints while the big toe or hallux has two small bones and one joint. The joints between these small bones of phalanges act as a regular one degree of freedom revolute joint and allow the flexion rotation of toes as is the case in fingers. In the light of this, similar serial chains in Figure 7.27 can be used to model the structure. On the other hand, as the most of the flexor muscles that are responsible for the phalange flexion are shared through the five toes, individual mobility of the toes are restricted unlike the case in finger phalanges. Due to this property, the mentioned flexion occurs simultaneously in five of the toes and the grasping ability of the foot with its toes is weak. This simultaneous rotation can be easily simulated or simply modeled by a one degree of freedom revolute joint (Figure 7.39), and this joint can be passively

actuated by using simple mechanisms including torsional springs or prismatic shock absorbers (Figure 7.39).
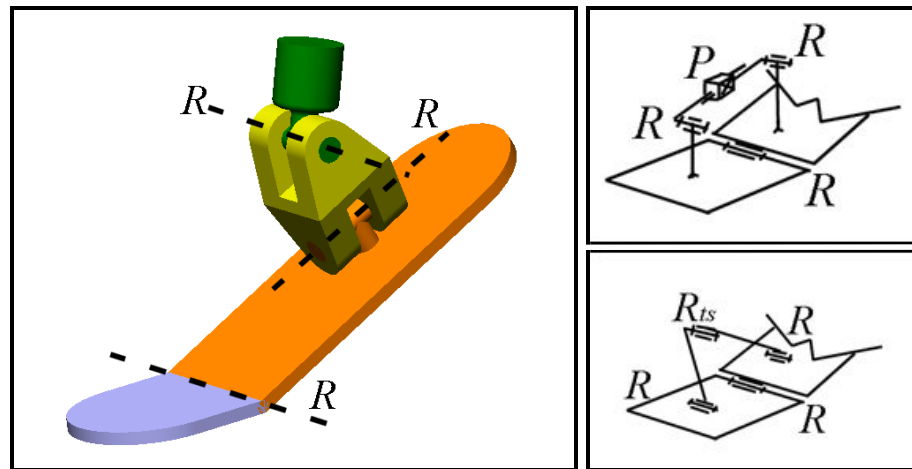
Figure 7.39. One DoF simplified forefoot mechanisms.

7.7. Human Skull

The normal adult human skull (Figure 7.40) consists of 22 bones that are connected each other by immovable joints except the mandible that forms the human jaw by the connection with the temporal bone. These immovable joints, also referred as sutures, are a type of fibrous joints that permits only a slight movement for both the elasticity and the compliance of the skull.

Figure 7.40. Human skull.
(Source: Wikipedia, 2010)

7.7.1. Human Jaw

As mentioned earlier, human jaw is formed by the connection between mandible and the temporal bone with the help of two temporomandibular joints (Figure 7.41).

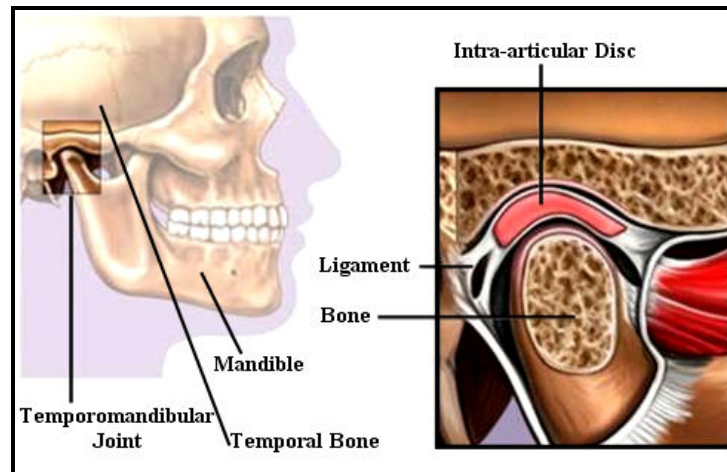Figure 7.41. Temporomandibular joint.
(Source: One with Nature, 2010)

Although the temporomandibular joints seem to give the mandible simple motion characteristics that can be modeled by common joints such as revolute and spherical, a detailed investigation will reveal that human jaw has complex motions during mastication (chewing) and speech formation so that this kind modeling will lead to incorrect results. As the study of Koolstra (2002) clearly states, this complexity is the results of both the large number of muscles of various shapes and sizes throughout the system and the incongruent articular surfaces of the temporomandibular joints, where the lower and the upper surfaces of joint formation have different shapes. While this difference results in higher motion capability in the joint, it reduces the joint stability due to relatively small joint contact areas.

Actually, similar to a rigid body moving freely in space, human jaw has capable of six DoF including three rotations around and three translations along the Cartesian axes (Figure 7.42). On the other hand the workspaces of these motions are limited. Also, as the movements of the mandible is constrained by two temporomandibular joints, at some extends the various motions may become dependent to others as is the case in overconstrained manipulators.
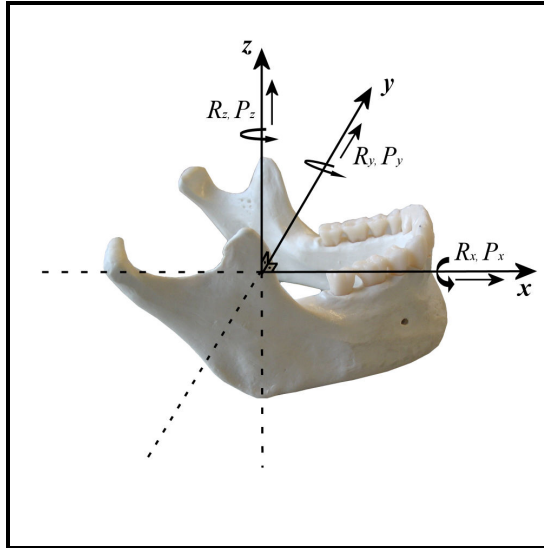
Figure 7.42. 6 DoF human jaw movements.
(Source: Wikipedia, 2010)

Despite of the fact that the system might be modeled by simplified concepts by using reduced DoF, the dynamics of the human jaw can be totally simulated by using suitable six DoF parallel platform manipulators (Figure 7.43) due to their higher precision in relatively small workspaces when compared with the serial manipulators. However it should be noted that, as the DoF increases, control of the manipulator will be more complex.

Figure 7.43. 6 DoF Euclidean parallel platform manipulator.

7.8. Human Vertebral Column

Vertebral or spinal column (Figure 7.44) can be categorized as one of the most important structures in human body. It extends from the human skull up to the pelvis and consists of 33 small b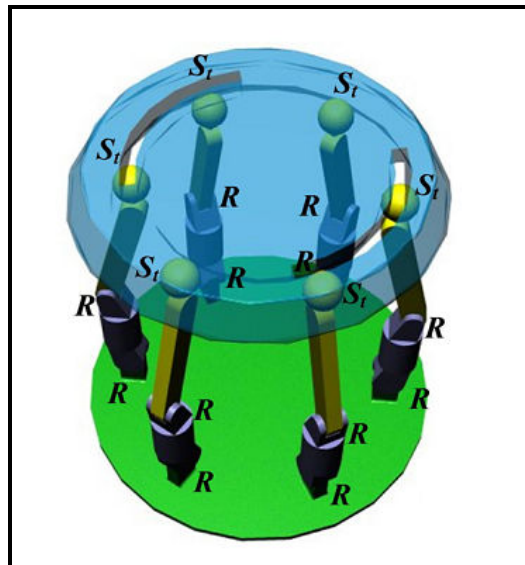ones that are stacked on top of each other. These small bones are called vertebrae and shows different characteristics throughout the four regions of the vertebral column.
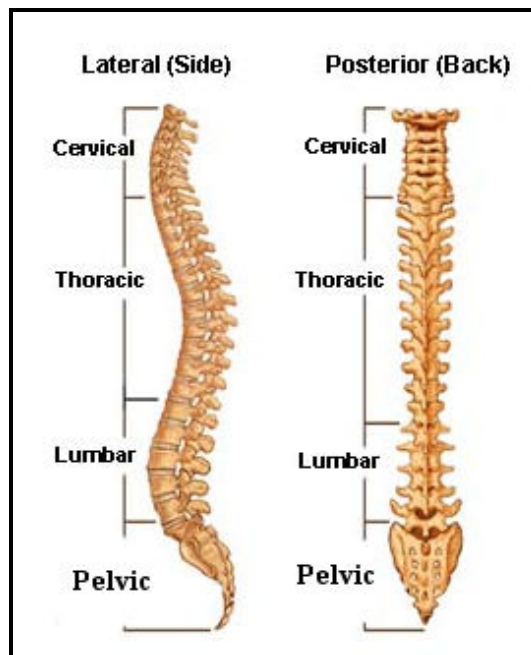
Figure 7.44. Human vertebral column and its regions.
(Source: Spine Universe, 2010)

The importance of the vertebral column comes from the vital functions of the system. The vertebral column protects the spinal cords, nerve roots and internal organs while it maintains its structural support for the body parts and creates a base for the attachment points of the muscles, tendons and ligaments of the body structures. Due to its relatively complex structure, vertebral column coarsely gives flexible mobility to the human body as flexion, extension, side bending and rotation around the vertical body axis. However, it should be noted that these motions are in reality more complex and generated by the combination of motions and workspaces of the individual parts of the system.

The cervical region (Figure 7.45) of the vertebral column is located at the neck area of the body and it includes seven unique shaped vertebrae (Figure 7.45).
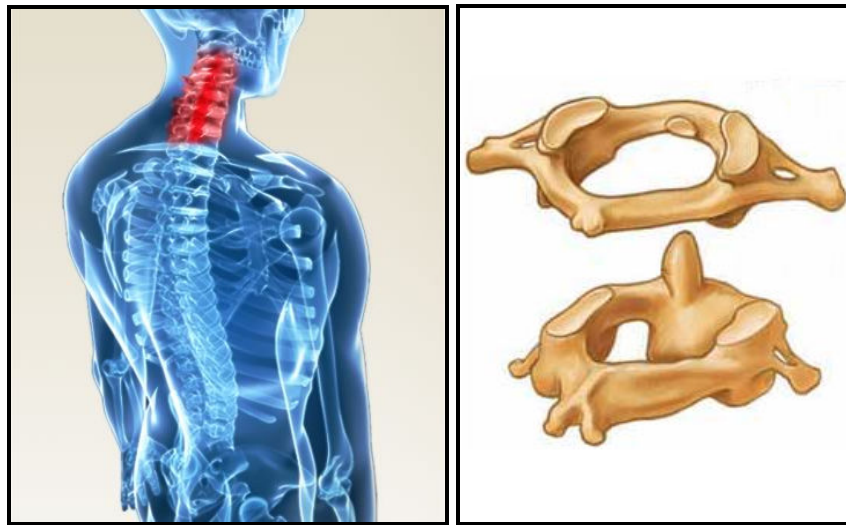
Figure 7.45. Cervicle region.
(Source: Texas Back Institute, Spine Universe, 2010)

This section gives the neck its three DoF motion capability of rotation, extension, flexion and lateral bending (Figure 7.46).
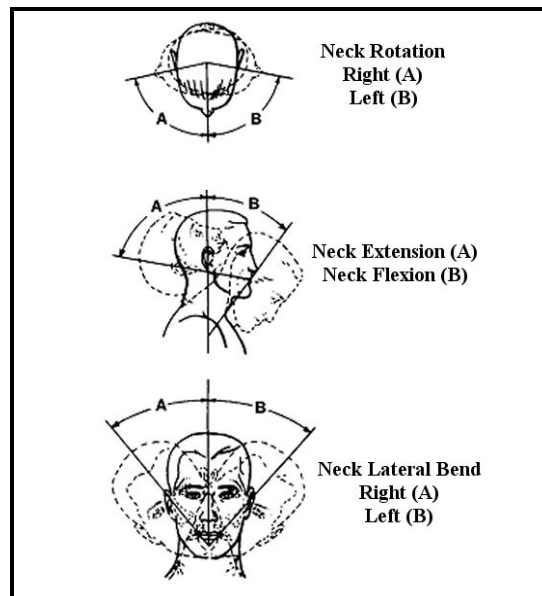
Figure 7.46. Neck motions.
(Source: NASA, 2010)

The thoracic region (Figure 7.47) of the vertebral column is located at the chest area of the body and it includes twelve unique shaped vertebrae (Figure 7.47).
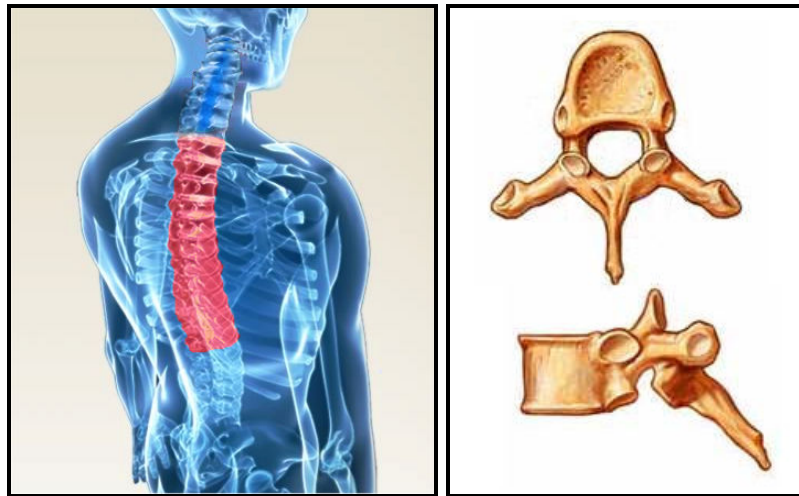
Figure 7.47. Thoracic region.
(Source: Texas Back Institute, Spine Universe, 2010)

Due to the fact that the rib cage of the human body is joined to thoracic region and there are relatively high numbers of connections on the region vertebrae, the mobility of the thoracic portion of the vertebral column is limited.

The lumbar region (Figure 7.48) of the vertebral column is located at the low back portion of the body and it includes five unique shaped vertebrae (Figure 7.48).
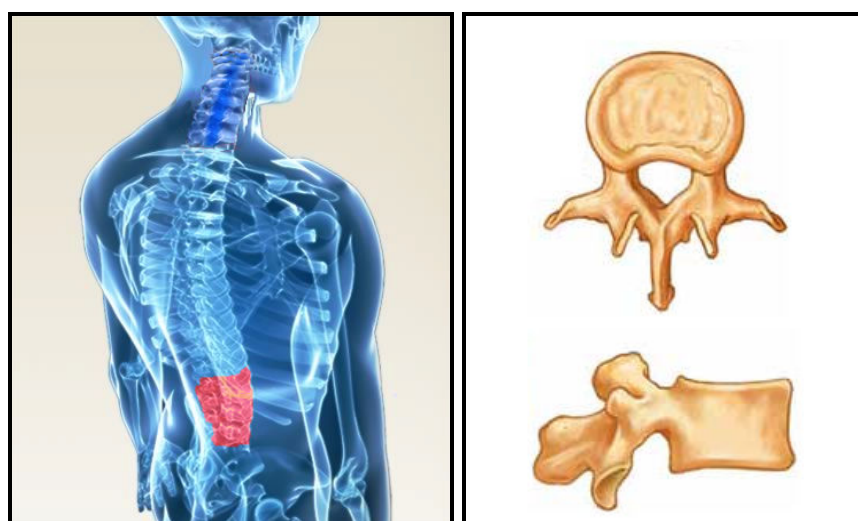

Figure 7.48. Lumbar region.
(Source: Texas Back Institute, Spine Universe, 2010)

This section of the vertebral column carries most of the body weight, and mechanical stresses so that the shapes and the structures of the vertebrae are adapted in order to sustain structural support. When compared with the other regions of the vertebral column, lumbar region has the highest mobility. On the other hand the motion characteristics are similar with other sections. Lumbar region gives the human waist three DoF including rotation, extension, flexion and lateral bending (Figure 7.49).
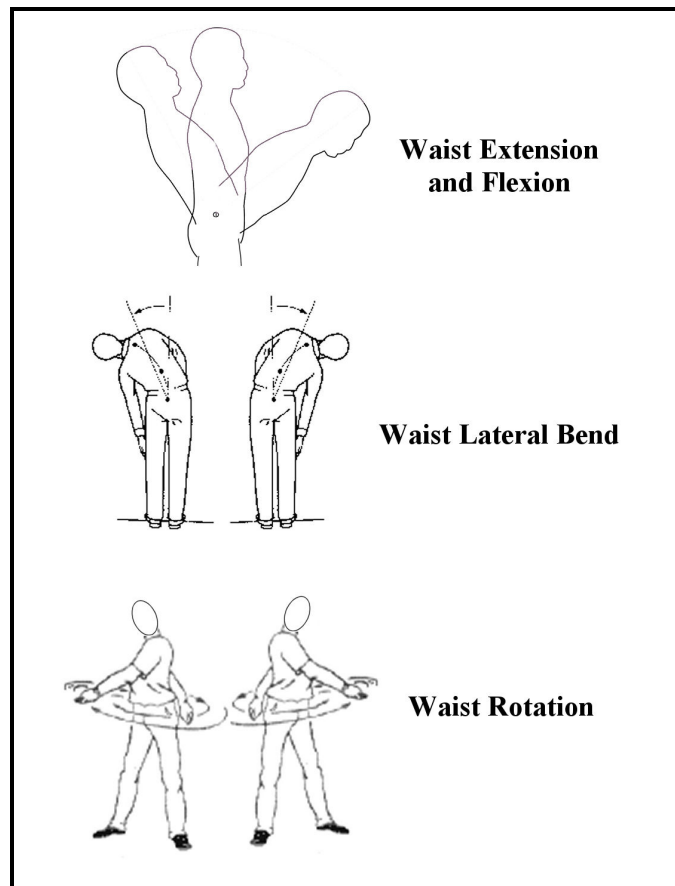

Figure 7.49. Waist motions.
(Source: Chris Adams, CRM, Spinal Soothers, 2010)

The last portion of the vertebral column is the pelvic region that can be divided into two sub regions as sacrum and coccyx (tailbone). This region is composed of nine vertebrae where the five sacrum vertebrae in adults are fused and connected with the hip bones.

As it can be seen clearly when the mobility of vertebral column regions are analyzed, it will be revealed that the motion characteristics have similarities. In fact, the overall mobility of the system is determined by the individual movements that occurred

in each of the vertebral segments (Figure 7.50) and the total workspace of the vertebral column is determined by their coupled motions.
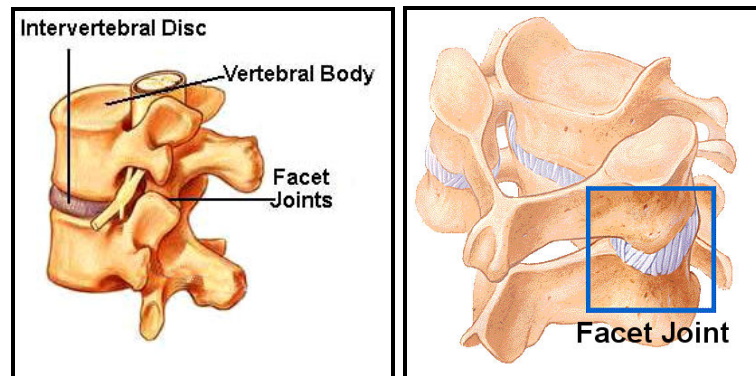
Figure 7.50. Two vertebral segments.
(Source: Spine Universe, Texas SJH, 2010)

Vertebral bodies are connected to each other by an intervertebral disc and two joints called facet joints. Throughout the system, facet joints guide the motions of the vertebral segments while they limit the excessive shear, rotation and flexion of the vertebrae, and intervertebral discs act as shock absorbers. The facet joints are actually synovial joints (Figure 7.50) filled with synovial fluid and they also responsible for the flexibility of the vertebral column. The intervertebral discs have two regions including a strong outer ring (annulus fibrosus) that connects each vertebral segment while protecting the center and a soft inner ring (nucleus pulposus) that acts as the main shock absorber (Figure 7.51).
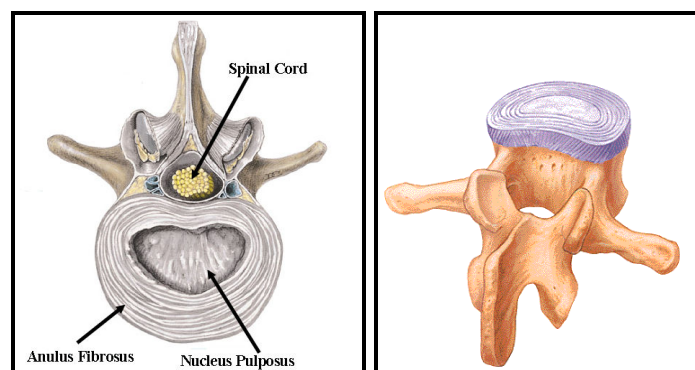
Figure 7.51. Intervertebral disc.
(Source: Stephan Lahr, Texas SJH, 2010)

Although, the workspace of the motion in each vertebral segment couple is small, the system workspace is increased by the addition of another couple. As a result of this characteristic, the modularity of the system should be considered in order to propose a mechanism or manipulator for the whole structure. Due to the fact that motion capabilities of the vertebral sections and segments are similar including rotation, bending and flexion-extension, three DoF orientation manipulator (Figure 7.52) that is presented in the clavicle rotations section would also be a good model for the vertebral segments.
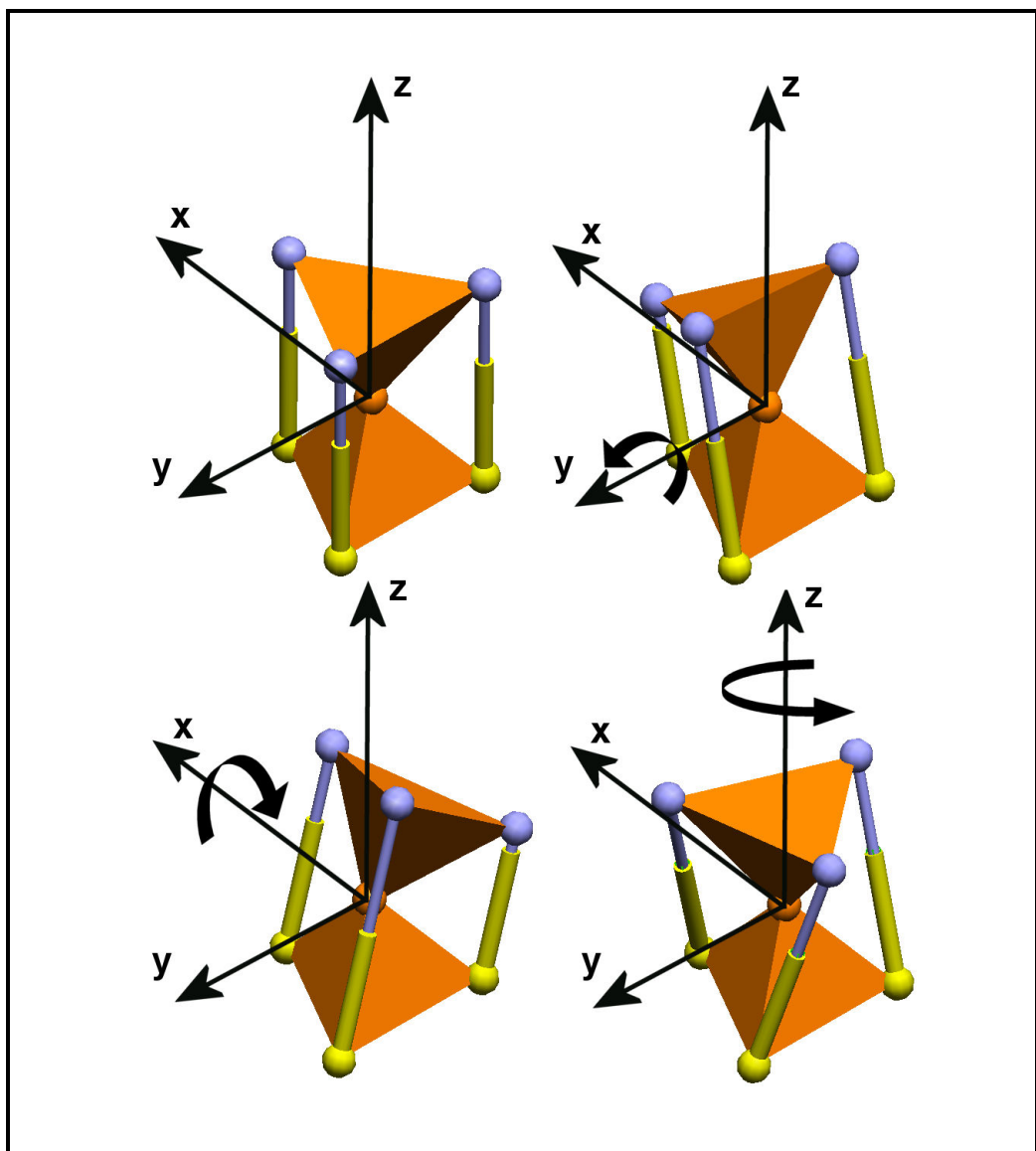
Figure 7.52. Rotational motions of 3 DoF orientation platform.

As seen in Figure 7.53, the orientation platforms can also be easily combined to form a modular manipulator system, where it is able to simulate the whole motion characteristics of the vertebral column. On the other hand, the structure of the platforms could be modified for a better model. If the spherical joints between the two platforms of the manipulator are replaced by an elastic region of suitable geometry, not only the workspace of each segment will be restricted but also the system will gain a shock absorber similar to the intervertebral discs and become more flexible.
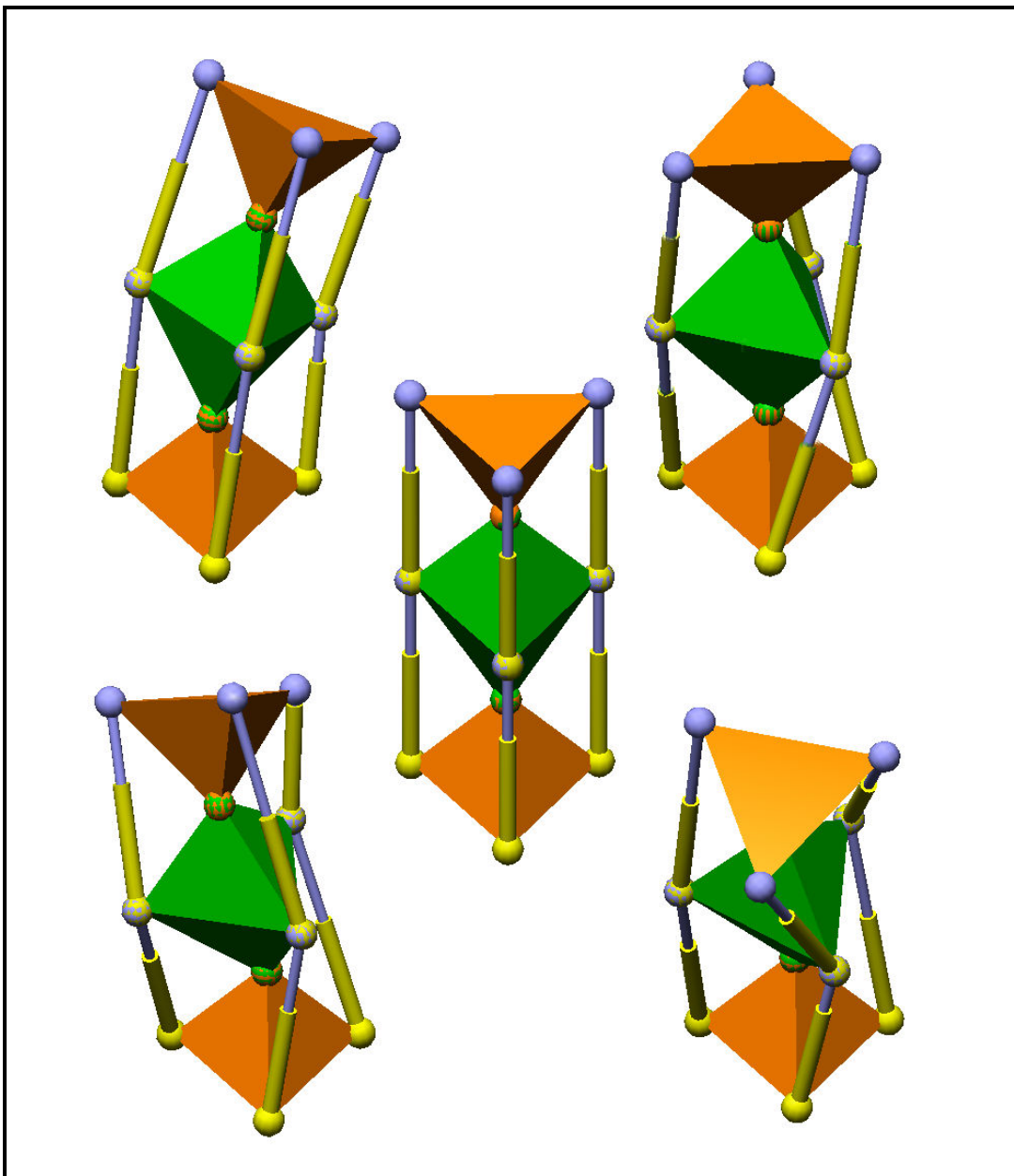
Figure 7.53. Modularity of 3 DoF orientation platform.

7.8.1. Geometrical Analysis of Spatial 3-DoF Orientation Mechanism

Throughout the chapter, three DoF orientation platform is referred as models of various kinematic joints or systems in the human body. As a result it would be suitable to carry out its geometrical analysis in order to gain wider information about the manipulator.

Equation (7.3) shows the simple equation of a sphere with radius "r" whose centre is fixed at the origin (Figure 7.54) and Equation (7.4) shows the case when the centre is positioned away from the origin (x_1, y_1, z_1) (Figure 7.55).

$$x^2 + y^2 + z^2 = r^2 \qquad (7.3)$$

$$(x - x_1)^2 + (y - y_1)^2 + (z - z_1)^2 = r^2 \qquad (7.4)$$
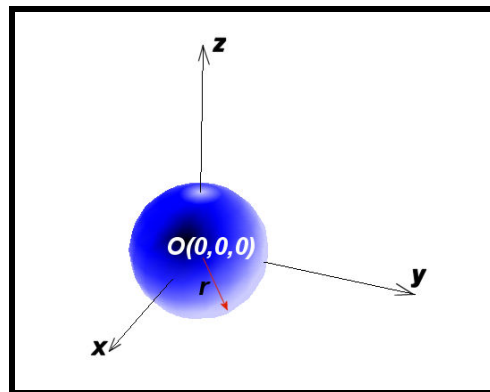
Figure 7.54. Sphere with radius "r" whose centre is fixed at the origin
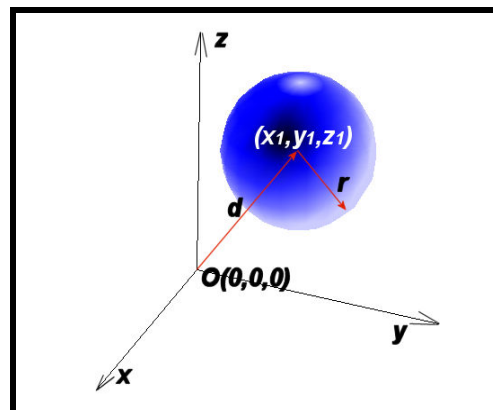
Figure 7.55. Sphere with radius "r" whose centre is away from the origin

112

If the generalized orientation platform in Figure 7.56 is considered and the origin point of the Cartesian coordinate system is placed to the rotation centre of the mechanism, where z axis is perpendicular to the upper platform in the initial configuration, workspace of the first point D_1 can be analysed by drawing a vector from the origin to the point D_1. From this point the workspace of $\mathbf{r_1}$ will be described as sphere "A" whose equation becomes,

$$x_{D_1}^{\ 2} + y_{D_1}^{\ 2} + z_{D_1}^{\ 2} = r_1^{\ 2} \tag{7.5}$$

Due to the limitation of leg d_1 the workspace of its vector will be the volume between the spheres B and C. As the coordinates of O_1 (x_1, y_1, z_1) can be easily found by using constructional parameters, the workspace of the vector $\mathbf{d_1}$ will be,

$$(x_{D_1} - x_1)^2 + (y_{D_1} - y_1)^2 + (z_{D_1} - z_1)^2 = d_1^{\ 2}$$
$$d_1 = d_{1\min} \rightarrow d_{1\max} \tag{7.6}$$

Using the same analogy, equations for other legs can be described as,

$$x_{D_2}^{\ 2} + y_{D_2}^{\ 2} + z_{D_2}^{\ 2} = r_2^{\ 2}$$
$$(x_{D_2} - x_2)^2 + (y_{D_2} - y_2)^2 + (z_{D_2} - z_2)^2 = d_2^{\ 2}$$
$$d_2 = d_{2\min} \rightarrow d_{2\max}$$
$$x_{D_3}^{\ 2} + y_{D_3}^{\ 2} + z_{D_3}^{\ 2} = r_3^{\ 2} \tag{7.7}$$
$$(x_{D_3} - x_3)^2 + (y_{D_3} - y_3)^2 + (z_{D_3} - z_3)^2 = d_3^{\ 2}$$
$$d_3 = d_{3\min} \rightarrow d_{3\max}$$

As there are six equations (Equations 7.5-7,7) with nine unknowns, remaining three equations can be written by using the construction parameters of the upper platform (Figure 7.57).

Figure 7.56. Generalized orientation platform

Figure 7.57. Construction parameters of upper platform (a, b, and c).

Using the fixed lengths, a, b, and c, remaining equations can be described as,

$$(x_{D_1} - x_{D_2})^2 + (y_{D_1} - y_{D_2})^2 + (z_{D_1} - z_{D_2})^2 = a^2$$
$$(x_{D_1} - x_{D_3})^2 + (y_{D_1} - y_{D_3})^2 + (z_{D_1} - z_{D_3})^2 = b^2 \qquad (7.8)$$
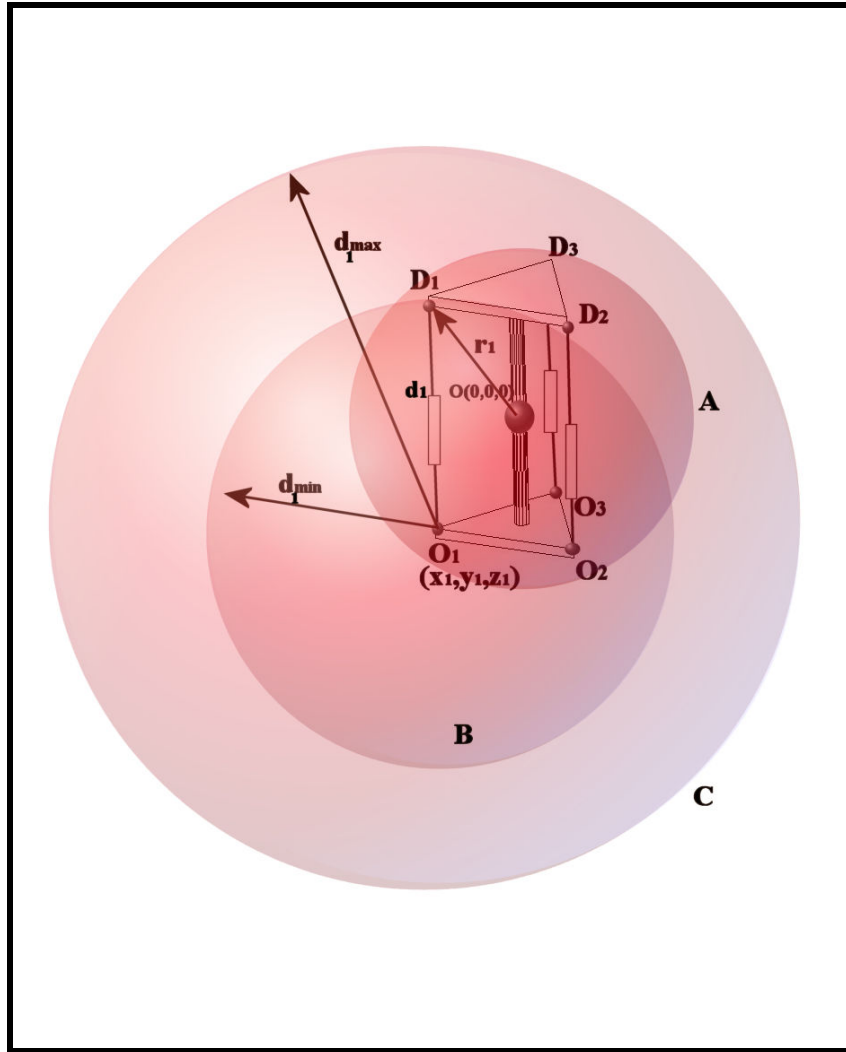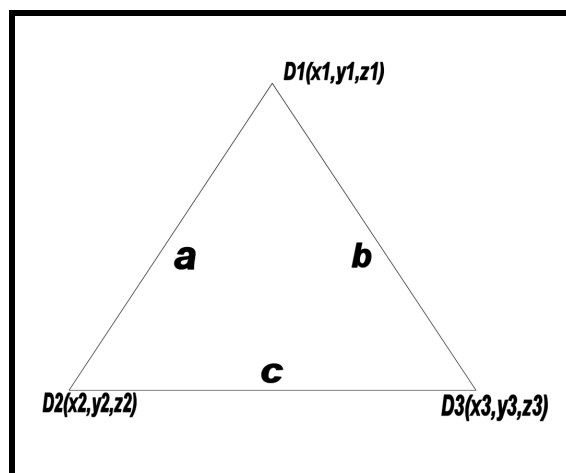$$(x_{D_2} - x_{D_3})^2 + (y_{D_2} - y_{D_3})^2 + (z_{D_2} - z_{D_3})^2 = c^2$$

After some modifications on nine equations and using new representations $x_{D_i} = \tilde{x}_i$, $y_{D_i} = \tilde{y}_i$, $z_{D_i} = \tilde{z}_i$, those equations will be reduced to six equations with six unknowns as,

$$\tilde{x}_1^2(-z_1^2 - x_1^2) + \tilde{y}_1^2(-z_1^2 - y_1^2) + \tilde{x}_1(2px_1) + \tilde{y}_1(2py_1)$$
$$+ \tilde{x}_1\tilde{y}_1(-2x_1y_1) = p^2 - z_1^2 r_1^2$$

$$\tilde{x}_2^2(-z_2^2 - x_2^2) + \tilde{y}_2^2(-z_2^2 - y_2^2) + \tilde{x}_2(2qx_2) + \tilde{y}_2(2qy_2)$$
$$+ \tilde{x}_2\tilde{y}_2(-2x_2y_2) = q^2 - z_2^2 r_2^2$$

$$\tilde{x}_3^2(-z_3^2 - x_3^2) + \tilde{y}_3^2(-z_3^2 - y_3^2) + \tilde{x}_3(2tx_3) + \tilde{y}_3(2ty_3)$$
$$+ \tilde{x}_3\tilde{y}_3(-2x_3y_3) = t^2 - z_3^2 r_3^2$$

$$\quad (7.9)$$

$$\tilde{x}_1^2(-r_2^2) + \tilde{y}_1^2(-r_2^2) + \tilde{x}_2^2(-r_1^2) + \tilde{y}_2^2(-r_1^2) + \tilde{x}_1^2\tilde{y}_2^2 + \tilde{y}_1^2\tilde{x}_2^2 + \tilde{x}_1\tilde{x}_2(2s_1) + \tilde{y}_1\tilde{y}_2(2s_1)$$
$$+ \tilde{x}_1\tilde{x}_2\tilde{y}_1\tilde{y}_2(-2) = s_1^2 - r_1^2 r_2^2$$

$$\tilde{x}_1^2(-r_3^2) + \tilde{y}_1^2(-r_3^2) + \tilde{x}_3^2(-r_1^2) + \tilde{y}_3^2(-r_1^2) + \tilde{x}_1^2\tilde{y}_3^2 + \tilde{y}_1^2\tilde{x}_3^2 + \tilde{x}_1\tilde{x}_3(2s_1) + \tilde{y}_1\tilde{y}_3(2s_1)$$
$$+ \tilde{x}_1\tilde{x}_3\tilde{y}_1\tilde{y}_3(-2) = s_2^2 - r_1^2 r_3^2$$

$$\tilde{x}_2^2(-r_3^2) + \tilde{y}_2^2(-r_3^2) + \tilde{x}_3^2(-r_2^2) + \tilde{y}_3^2(-r_2^2) + \tilde{x}_2^2\tilde{y}_3^2 + \tilde{y}_2^2\tilde{x}_3^2 + \tilde{x}_2\tilde{x}_3(2s_1) + \tilde{y}_2\tilde{y}_3(2s_2)$$
$$+ \tilde{x}_2\tilde{x}_3\tilde{y}_2\tilde{y}_3(-2) = s_2^2 - r_2^2 r_3^2$$

As there are six independent equations and six unknowns (Equation 7.9), there exists a unique solution for the position of the platform with respect to the given parameters. So that, solving Equation (7.9) by numerical methods and get the positions of the corners, any position and orientation of the centre of the orientation platform can be found by using the input parameters.

CHAPTER 8

CONCLUSION

Due to the fact that, visualization of the subspace motions of the rigid bodies is difficult and hard to comprehend, this study has introduced a novel method called "*Method of Intersections*", where simple geometric shapes representing revolute (*R*) and prismatic (*P*) joint motions are intersected by means of desired space or subspace requirements to create specific rigid body geometries in predefined octahedral fixed frame. Presented methodical approach is able to visualize space and subspace motions clearly by the help of resulting geometrical entities that have physical constraints with respect to the fixed working volume. Also, it has been proved by an example that, this new method can be used to design novel mechanisms in various subspaces.

This study has introduced the transformation unit screw equations to the literature, where it has been shown that any third screw $(\$_k)$ can be calculated, if the components of first and second screws $(\$_i, \$_j)$ are known along with the short distance and the angle between the first and the third screws. Also, by using recurrent screws and transformation unit screw equations, physical representations and kinematic representations of both lower and higher kinematic pairs are given and the method for calculating their mathematical models is presented. Moreover, novel universal mobility formulations based on screw theory for both kinematic pairs and robot manipulators are introduced and examples are given throughout the related chapters.

In the synthesis part of the study, function generation synthesis of the spherical four bar mechanism for the six precision points is carried out by using quaternion algebra. Three different techniques, as interpolation approximation, least squares approximation and Chebyshev approximation are used in the synthesis process. After the calculations, results are compared and Chebyshev approximation is proved to give the best results with respect to fitting errors as it is expected. It should also be noted that, during the consecutive trials in Chebyshev approximation, a new approach is used to renew the precision points. Furthermore, the possible usage of the dual quaternions is shown in various synthesis procedures of different mechanisms. Also, a new idea is

presented for the one degree of freedom mechanism with subspace five, where the function generation and body guidance synthesis can be carried out simultaneously.

Following mostly the theoretical studies, this study has investigated the biokinematics of human body. The most important sections of the human skeletal system and body including human eyes, arm complex, hand complex, leg complex, foot complex, skull and vertebral column are introduced in terms of their kinematical structure and DoF. Various manipulators are proposed for the body parts that have capabilities to mimic the dedicated body system. In this thesis, the aim was to extract all possible information about the biokinematics of human body into one reference that can be used for further studies in the area of medicine to design advanced prosthetics and robotics to design advanced humanoid robots for various tasks.

REFERENCES

Admiraal, M. A. et al. (2004). Modelling kinematics and dynamics of human arm movements. *Motor Control*, 8, 312-338.

Alizade, R. (1994). Synthesis of four-bar spherical mechanism on five parameters. J. Mech. Eng., Russian Academy of Science, 6 (in Russian).

Alizade, R., Bayram, C. (2004). Structural synthesis of parallel manipulators. *Mech. Mach. Theory*, 39(8), 857-870.

Alizade, R., Kilit, O. (2005). Analytic synthesis of function generating spherical four-bar mechanism for the five precision points. *Mech. Mach. Theory*, 40(7), 863–878.

Alizade, R., Bayram, C., Gezgin, E. (2007). Structural synthesis of serial platform manipulators. *Mech. Mach. Theory*, 42(5), 580-599.

Alizade, R., Can, F. C., Gezgin, E. (2008). Structural synthesis of Euclidean platform robot manipulators with variable general constraints. *Mech. Mach. Theory*, 43(11), 1431-1449.

Angales, J. (1988). Rational Kinematics. *Springer Verlag*, New York.

Angeles, J., Gosselin, C. (1988). Determination du degree de liberte des chaines cinematiques. *Trans. CSME*, 12(4), 219-226.

Barshan, B., Tunçel, O., Altun, K. (2009). Classifying human leg motions with uniaxial piezoelectric gyroscopes. *Sensors*, 9, 8508-8546.

Benjelloun, M. et al. (2007). Vertebral mobility analysis using anterior faces detection. *ACIVS 2007, LNCS 4678*, 897-908.

Benjelloun, M., Mahmoudi, S. (2007). Spine localization and vertebral mobility analysis using faces contours detection. *29th Annual International Conference of the IEEE EMBS Lyon, France*, 6557-6560.

Breazeal, C. (2003). Emotion and sociable humanoid robots. *Int. J. Human-Computer Studies*, 59, 119-155.

Buschmann, T., Lohmeiner, S., Ulbrich, H. (2009). Humanoid robot LOLA: Design and walking control. *Journal of Physiology-Paris*, 103, 141-148.

Celledoni, E., Saftsröm, N. (2010). A Hamiltonian and multi-symplectic formulation of a rod model using quaternions. *Computer Methods in Applied Mechanics and Engineering*, doi: 10.1016/j.cma.2010.04.017.

Chevallier, D. P. (1991). Lie algebras, modules, dual quaternions and algebraic methods in kinematics. *Mech. Mach. Theory*, 26(6), 613-627.

Collins, C. L., McCarthy, J. M. (1998). The quartic singularity surfaces of planar platforms in the Clifford algebra of the projective plane. *Mech. Mach. Theory*, 33(7), 931–944.

Dai, S. J. (2006). An historical review of the theoretical development of rigid body displacements from Rodrigues parameters to the finite twist. *Mech. Mach. Theory*, 41, 41–52.

Fang, Y., Tsai, L. W. (2002). Structure synthesis of a class of 4-dof and 5-dof parallel manipulators with identical limb structures. *The International Journal of Robotic Research*, 21(9), 799-810.

Fang, Y., Tsai, L. W. (2004). Analytical identification of limb structures for translational parallel manipulators. *Journal of Robotic Systems*, 21(5), 209-218.

Fang, Y., Tsai, L. W. (2004). Structure synthesis of a class of 3-dof rotational parallel manipulators. *IEEE Transactions on Robotics and Automation*, 20(1), 117-121.

Farhang, K., Midha, A., Bajaj, A. K. (1988). Synthesis of harmonic motion generation linkages Part-I, Function generation. *ASME, J. Mech. Transm. Automat. Design*, 110(1), 16–21.

Farhang, K. Zargar, Y. S. (1999). Design of spherical 4R mechanisms: function generation for the entire motion cycle. *ASME, J. Mech. Design*, 121, 521–528.

Gogu, G. (2005). Mobility of mechanisms: a critical review. *Mech. Mach. Theory*, 40(9), 1068-1097.

Gosselin, C. (1994). The agile eye: A high performance 3DoF camera orienting device. *Proceedings of the IEEE International Conference on Robotics and Automation, San Diego, CA*, 781-786.

Gupta, K. C., Beloiu, A. S. (1998). Branch and circuit defect elimination in spherical four-bar linkages. *Mech. Mach. Theory*, 33(5), 491–504.

Hamilton, W.R. (1866).Elements of Quaternions. *London*.

Hartenberg, R. S., Denavit, J. (1964). Kinematic synthesis of linkages. *McGraw-Hill, New York*.

Haslwanter, T. (2004). Mathematics of three dimensional eye rotations. *Vision Res.*, 35(12), 1727-1739.

Herve, J. M. (1999). The Lie group of rigid body displacements, a fundamental tool for mechanism design. *Mech. Mach. Theory*, 34(5), 719-730.

Huang, Z., Li, Q. C. (2002). General methodology for type synthesis of symmetrical lower-mobility parallel manipulators and several novel manipulators. *The International Journal of Robotic Research*, 21(2), 131-145.

Huang, Z., Li, Q. C. (2002). On the type synthesis of lower-mobility parallel manipulators. *Proceedings of the workshop on Fundamental Issues and Future Research Directions for Parallel mechanisms and manipulators Quebec, Canada*, 272-283.

Huang, Z., Li, Q. C. (2003). Type synthesis of 4-dof parallel manipulators. *Proceedings of the 2003 IEEE International Conference on Robotics & Automation, Taipei, Taiwan*, 755-760.

Huang, Z., Li, Q. C. (2003). Type synthesis of 5-dof parallel manipulators. *Proceedings of the 2003 IEEE International Conference on Robotics & Automation, Taipei, Taiwan*, 1203-1208.

Jenkin, M., Milios, E., Tsotsos, J. (1993). Design and performance of TRISH, a binocular robot head with torsional eye movements. *International Journal of Pattern Recognition and Artificial Intelligence*, 7(1), 51-68.

Jesus Cervantes-Sanchez, J. et al. (2009). Some improvements on the exact kinematic synthesis of spherical 4R function generators. *Mech. Mach. Theory*, 44, 103–121.

Jin, Y., Chen, I. M., Yang, G. (2004). Structure synthesis and singularity analysis of a parallel manipulator based on selective actuation. *Proceedings of the IEEE International Conference on Robotics and Automation*, 4533-4538.

Banavar, N. R. et al. (2010). Design and analysis of a spherical mobile robot. *Mech. Mach. Theory*, 45, 130–136.

Kazerounian, K., Solecki, R. (1993). Mobility analysis of general bi-modal four-bar linkages based on their transmission angle. *Mech. Mach. Theory*, 28(3), 437–445.

Kong, X., Gosselin, C. M. (2001). Generation of parallel manipulators with three translational degrees of freedom based on screw theory. *Proceedings of CCToMM Symposium on Mechanisms, Machines and Mechatronics, Montreal, Canada*.

Kong, X., Gosselin, C. M. (2004). Type synthesis of 3T1R 4-DoF parallel manipulators based on screw theory. *IEEE Transactions on Robotics and Automation*, 20(2), 181-190.

Kong, X., Gosselin, C. M. (2006). Type synthesis of 4-DoF SP-equivalent parallel manipulators: A virtual chain approach. *Mech. Mach. Theory*, 41, 1306-1319.

Kong, X., Gosselin, C. M. (2007). Type synthesis of parallel mechanisms. *Springer*.

Koolstra, J. H. (2002). Dynamics of the human masticatory system. *Crit Rev Oral Biol Med*, 366-376.

Larochelle, P., (2000). Approximate motion synthesis via parametric constraint manifold fitting. *Advances in Robot Kinematics*, *Kluwer Acad. Publ., Dordrecht*.

Liao, Q. et al. (2010). Inverse kinematic analysis of the general 6R serial manipulators based on double quaternions. *Mech. Mach. Theory*, 45, 193-199.

Ludewig, P. M. et al. (2004). Three dimensional clavicular motion during arm elevation: reliability and descriptive data. *J Orthop Sports Phys Ther*, 34(3), 140-9.

Martinez, J. M., Gallardo-Alvarado, J. (2000). A simple method for the determination of angular velocity and acceleration of a spherical motion through quaternions. *Nederlands, Meccanica*, 35, 111-118.

McCarthy, J. M., Perez-Gracia, A. (2006). Kinematic synthesis of spatial serial chains using Clifford algebra exponentials. *Proc. ImechE, 220, Part C: J. Mechanical Engineering Science*, 953-968.

Moeslund, T. B., Granum, E. (2001). Pose estimation of a human arm using kinematic constraints. *Proc. 12th Scandinavian conference on image analysis, Bergen, Norway*, 1-8.

Mohan Rao, A. V., Sandor, G. N., Kohli, D., Soni, A. H. (1973). Closed form synthesis of spatial function generating mechanism for the maximum number of precision points. *J. Eng. Industry*, 95, 725–736.

Mruthyunjaya, T. S. (2003). Kinematic structure of mechanisms revisited. *Mech. Mach. Theory*, 38(4), 279-320.

Murray, A. P., McCarthy, J. M. (1995). A linkage map for spherical four position synthesis. *ASME Tech. Conf. Boston. MA*, 833–844.

Müller, A. (2009). Generic mobility of rigid body mechanisms. *Mech. Mach. Theory*, 44(6), 1240-1255.

Nixravesh, R.A., Wehage & Kwan, O. K. (1985). Euler Parameters in Computational Kinematics and Dynamics, Part 1. *ASME J. Mech. Trans., Aut. Des.*, 107, 358-365.

Oswald, D. et al. (2004). Integrating a flexible anthropomorphic, robot hand into the control, system of a humanoid robot. *Robotics and Autonomous Systems*, 48, 213-221.

Peck, C. C., Hannam, G. A. (2007). Human jaw and muscle modeling. *Archieves of Oral Biology*, 52(4), 300-304.

Pennestri, E., Valentini, P. P. (2009). Dual quaternions as a tool for rigid body motion analysis: a tutorial with an application to biomechanics. *MULTIBODY DYNAMICS 2009, ECCOMAS Thematic Conference K. Arczewski, J. Fr ̨aczek, M. Wojtyra (eds.) Warsaw, Poland*, 1-17.

Pileicikiene, G., Surna, A. (2004). The human masticatory system from a biomechanical perspective: a review. *Stomatologija, Baltic Dental and Maxillofacial Journal*, 6, 81-84.

Porteous, I.R. (1921). Topological Geometry. *Cambridge University Press*, Cambridge, U.K.

Raabe, D., Alemzadeh, K., Harrison, AJL., Ireland, AJ. (2009). The chewing robot: a new biologically-inspired way to evaluate dental restorative materials. *31st Annual International Conference of the IEEE EMBS Minneapolis, Minnesota, USA*, 6050-6053.

Roy, D., Ghosh, S. (2008). Consistent quaternion interpolation for objective finite element approximation of geometrically exact beam. *Comput. Methods Appl. Mech. Engrg*, 198, 555–571.

Sancibrian, R., De-Juan, A., Garcia, P., Fernandez, A., Viadero, F. (2007). Optimal synthesis of function generating spherical and RSSR mechanisms. *12th IFToMM World Congress, Besançon (France), June*, 18-21.

Wu. G. et al. (2004). ISB recommendation on definitions of joint coordinate systems of various joints for the reporting of human joint motion-Part II: shoulder, elbow, wrist and hand. *Journal of Biomechanics*, 38, 981-992.

Zhang, Y. et al. (2008). Design and kinematic analysis of a novel humanoid robot eye using pneumatic artificial muscles. *Journal of Bionic Engineering*, 5, 264-270.

Zhao, J. S., Feng, J. Z., Dong, J. X. (2006). Computation of the configuration degree of freedom of a spatial parallel mechanism by using reciprocal screw theory. *Mech. Mach. Theory*, 41(12), 1486-1504.

Zimmerman, J. R. (1967). Four-precision synthesis of the spherical four-bar function generator. *Mech. Mach. Theory*, 2, 133–139.

Zupan, D., Saje, M., Zupan, E. (2009). The quaternion-based three-dimensional beam theory. *Computer Methods in Applied Mechanics and Engineering*, 198(49-52), 3944-3956.

VITA

Personal Information: Name: Erkin GEZGİN, **Date of Birth:** 15th July 1981, **Place of Birth:** Izmir, Turkey, **Nationality:** Turkey, **E-Mail:** erkingezgin@hotmail.com

Education: • **2006-2010** PhD. in Mechanical Engineering Department, Izmir Institute of Technology. (CGPA: 4,0 / 4,0) **Thesis:** Biokinematic Analysis of Human Body. • **2004-2006** MSc. in Mechanical Engineering Department, Izmir Institute of Technology. (CGPA: 4,0 / 4,0) **Thesis:** Biokinematic Analysis of Human Arm • **2000-2004** BSc. in Mechanical Engineering Department, Izmir Institute of Technology. (CGPA: 3,9 / 4,0)

Honors: • Graduate Achievement Award for PhD. Studies, Izmir Institute of Technology. • Graduate Achievement Award for MSc. Studies, Izmir Institute of Technology. • Turkey 2nd National Robot Design Contest 2004, Honorable Mention by Waste Collector Robot. • 1st Place in BSc. Graduation Degree, Izmir Institute of Technology. • 2003-2004 Fall & Spring High Honour Certificates. • 2002-2003 Fall & Spring High Honour Certificates. • 2001-2002 Fall & Spring High Honour Certificates. • 2000-2001 Fall & Spring High Honour Certificates.

Academic Experience: 2004-2011 Research Assistant in Mechanical Engineering Department, Izmir Institute of Technology.

Research Areas: • Theory of Machines & Mechanisms. • Spatial & Overconstraint Robot Manipulators. • Robotics. • Mechatronics. • Biokinematics. • Biorobotics. • Nano & Micro Mechanisms

Languages: • **Native Language:** Turkish. • Good Command of English in all Writing, Reading and Speaking Skills KPDS: 95/100, UDS: 90/100. • German (Beginner Level)

Publications: ***SCI Journal Papers*** • Rasim Alizade, Erkin Gezgin, "*Synthesis of Function Generating Spherical Four Bar Mechanism for the Six Independent Parameters*", Mechanism and Machine Theory, (in print, 2011). • Erkin Gezgin, Serhan Ozdemir, "*Classification of Manipulators of the Same Origin by Virtue of Compactness and Complexity*", Mechanism and Machine Theory, (in print, 2011). • Rasim Alizade, Ozgun Selvi, Erkin Gezgin, "*Structural Synthesis of Parallel Manipulators with General Constraint One*", Mechanism and Machine Theory, Volume 45, Issue 1, January 2010, pp: 1-14. • Rasim Alizade, Fatih Cemal Can, Erkin Gezgin, "*Structural Synthesis of Euclidean Robot Manipulators with Variable General Constraints*", Mechanism and Machine Theory, Volume 43, Issue 11, November 2008, pp: 1431-1449. • Rasim Alizade, Cagdas Bayram, Erkin Gezgin, "*Structural Synthesis of Serial Platform Manipulators*", Mechanism and Machine Theory, Volume 42, Issue 5, May 2007, pp: 580-599. ***SCI EXP Journal Papers*** • Gokmen Tayfur, Hakki Erhan Sevil, Erkin Gezgin, Serhan Ozdemir, "*Trait-Based Heterogeneous Populations Plus (TbHP+) Genetic Algorithm*", Mathematical and Computer Modelling, Volume 49, Issues 3-4, February 2009, pp: 709-720. ***International Conference Papers*** • R. Alizade, O. Selvi, E. Gezgin, "*Structural Synthesis of Multiloop Manipulators with General Constraint One*", Proceedings of the International Symposium of Mechanism and Machine Science, October 5-8, 2010, Izmir, Turkey, pp: 78-84. • E. Gezgin, "*Survey of Rigid Body Motions in Space and Subspaces by Using Method of Intersections*", Proceedings of the International Symposium of Mechanism and Machine Science, October 5-8, 2010, Izmir, Turkey, pp: 92-95. • F. C. Can, E. Gezgin, "*Structural Synthesis of Novel Parallel Manipulators*", Proceedings of the International Symposium of Mechanism and Machine Science, October 5-8, 2010, Izmir, Turkey, pp: 96-101. • T. Bilgincan, E. Gezgin, C. Dede, "*Integration of the Hybrid-Structure Haptic Interface: HIPHAD v1.0*", Proceedings of the International Symposium of Mechanism and Machine Science, October 5-8, 2010, Izmir, Turkey, pp: 267-284. • R. Alizade, F.C. Can, E. Gezgin, O. Selvi, "*Structural Synthesis of New Parallel and Serial Platform Manipulators*", 12th World Congress in Mechanism and Machine Science, June 18-21, 2007. Besancon, France, paper#: 853. • Rasim Alizade, Erkin Gezgin, Ozgür Kilit, "*Computational Kinematics of a Spherical Wrist Motion through Quaternions*", International Workshop on Computational Kinematics, CK2005, 4-6 May, 2005, Cassino, Italy paper#:32. • Gezgin E., Sevil H.E., Ozdemir S., "*The Effects of Bias, Population, Migration, and Credit Assignment in Optimizing Trait-Based Heterogeneous Populations*", International Conference on Artificial Intelligence, ICAI2005, June 27-30, 2005, Las Vegas, Nevada, USA, pp: 747-753. ***National Conference Papers*** • Sevil H.E., Gezgin E., Ozdemir S.,"*Enhanced Convergence Properties of Populations through Aging, Immunity, and Instinct*", Turkish Symposium on Artificial Intelligence and Neural Networks, TAINN2005, June 16-17, 2005, Izmir, Turkey, pp: 234-238.

Important Activities: • Member of Organizing Committee Assistants in "X. National Spectroscopy Congress 2007" Izmir Institute of Technology. • Coordinator of "AzC IFToMM International Symposium on Mechanism and Machine Science 2010" Izmir Institute of Technology.